

CHAPTER IV

RESULTS AND DISCUSSION

1. Film preparation by powder casting method I

Prior to powder casting, each powder component after sieving was evaluated for their flowability due to possibly impact on the casting of powder blend onto a mold. Compressibility index (%) and Hausner ratio were calculated from bulk and tapped density of each powder and their results are demonstrated in **Table IV-1**. Compressibility index (%) were 14.4518 ± 0.5989 , 19.7818 ± 0.2174 , 20.3027 ± 1.0869 , 28.4155 ± 1.2615 , 32.1139 ± 1.4515 , 33.2979 ± 1.5671 , and 33.9140 ± 3.2710 of EL, S, PEG, HE, C, HK, and EE, respectively, ranging from low to high value, correspondingly, their Hausner ratios showed similar results. Their flow characters were interpreted in accordance to USP35 (145) by ranging from good flow to very poor flow that $EL > S > PEG > HE > C \approx HK \approx EE$.

This result can be explained by morphology and size of each polymer (160, 161). Generally, spherical powder showed a better flow than plate- or needle-shaped. Comparison among EL, HE, and C, EL which is spray-dried powder form of Eudragit[®] L30 D-55 with spherical shape had better flowability than HE and C, which powder morphology are fibrous and flakes, respectively (143, 162). Additionally, the more size decrement, the less is the flowability (161). Approximate size of EL is reported to be less than 250 micron. When this polymer has passed sieved # 80, its size is less than 180 micron, while size of EE is reported to be less than 50 micron (163).





Table IV-1 Bulk density, tapped density, compressibility index, and Hausner ratio of polymers used.

Sieved powder	W ₀ (g)	V ₀ (ml)	V _t (ml)	ρ _{bulk} (g/ml)	ρ _{tapped} (g/ml)	Compressibility index (%) (Mean±SD)	Hausner ratio (Mean±SD)	Flow character
S	20.0644	46.0	37.0	0.4362	0.5423	19.7818±0.2174	1.2466±0.0034	Fair
	20.0134	45.5	36.5	0.4399	0.5483			
	20.0265	45.0	36.0	0.4450	0.5563			
HK	14.0116	47.0	32.0	0.2981	0.4379	33.2979±1.5671	1.4998±0.0355	Very poor
	14.0082	47.0	31.5	0.2980	0.4447			
	14.0668	50.0	32.5	0.2813	0.4328			
C	20.0363	42.0	34.0	0.4771	0.5893	32.1139±1.4515	1.4735±0.0313	Very poor
	20.0826	43.0	34.0	0.4670	0.5907			
	20.0484	43.0	34.0	0.4662	0.5897			
EE	20.0168	59.0	41.0	0.3393	0.4882	33.9140±3.2710	1.5156±0.0729	Very poor
	20.0193	60.0	40.5	0.3337	0.4943			
	20.0295	60.0	40.0	0.3338	0.5007			
EL	20.0768	73.0	51.0	0.2750	0.3937	14.4518±0.5989	1.1690±0.0082	Good
	20.0244	81.0	51.0	0.2472	0.3851			
	20.0118	81.0	52.0	0.2471	0.3848			
HE	20.0167	42.0	36.0	0.4766	0.5560	28.4155±1.2615	1.3972±0.0245	Poor
	20.0425	43.0	36.5	0.4661	0.5491			
	20.0495	43.0	37.0	0.4663	0.5419			
PEG	20.0420	48.0	35.0	0.4175	0.5726	20.3027±1.0869	1.2549±0.0170	Fair to Passable
	20.0196	49.0	35.0	0.4086	0.5720			
	20.0145	49.0	34.5	0.4085	0.5801			

After flowability evaluation, the matrix films were prepared after that their film characteristics were physically and visually determined. As can be seen in **Figure IV-1** S formulations without PEG could not form a matrix film. With 20% w/w of PEG (S-2), small transparent flakes occurred, while brittle, transparent matrix films with pores and smooth surface were obtained with $\geq 40\%$ of PEG (S-4, S-6, S-8, and S-10). Pores occurring on a matrix film might result from assembly of air within porous particles of S powder that escaped during film formation.

Optical photographs of C formulations are also shown in **Figure IV-1**. No matrix film formed at 0% w/w of PEG (C-0). With higher percentage of PEG, the obtained samples became more fused to be enlarged with more transparent, light yellowish, and brittle flakes. Although surface of C formulation was smoother with high PEG, that of S formulation was more smoother at the same percentage of PEG.

While HE and HK formulations gave similar results (**Figure IV-1** and **Figure IV-2**), matrix films could not be formed without PEG (HE-0 and HK-0). Partially fused particles with brittle, opaque flakes were noted since 20% w/w of PEG, and HK formulations with more than 80% w/w of PEG (HK-8 and HK-10) could form brittle and opaque film. However, the film surface was not smooth.

As shown in **Figure IV-2**, the obtained samples from EE formulation were easy to embrittle and the appearance was more transparent with increasing amount of PEG (EE-2, EE-4, EE-6, EE-8, and EE-10), although formulation without PEG could not form a matrix film (EE-0). According to "Technical information of Eudragit[®] E 100, Eudragit[®] E PO and Eudragit[®] E 12,5" (163), film formation from those polymers should be a clear film. Thus disappearing of white spot on cast films indicated that there was transformation of EE powder to EE film.

From **Figure IV-2**, powder (EL-0) and flakes (EL-2) were observed in EL formulations with 0% and 20% w/w of PEG, respectively. EL-4 could not completely form a matrix film comparing to EL-6, EL-8, and EL-10, which formed sticky and transparent films.



In summary, all film forming polymers without PEG could not form a matrix film. There were two reasons for these phenomena. First, because the melting points or glass transition temperatures (T_g) of all polymers except EE ($T_g = 48\text{ }^\circ\text{C}$) were higher than the oven temperature (138, 164-166). Thus such polymers did not melt at this point, while only PEG melted (138). Second, any ingredient acting as binder might be needed to form a film. Moreover, formulations with various amount of PEG ranging from 20-100% w/w provided different matrix film characteristics as aforementioned. Comparing all film forming polymer with the same percentage of PEG, S formulation provided the best film characteristics with smoothness. It might be because S powder had the lowest glass transition temperature at about $70\text{ }^\circ\text{C}$ (164). Thus, at the oven temperature and appropriate time, S powder gradually transformed to rubbery state.



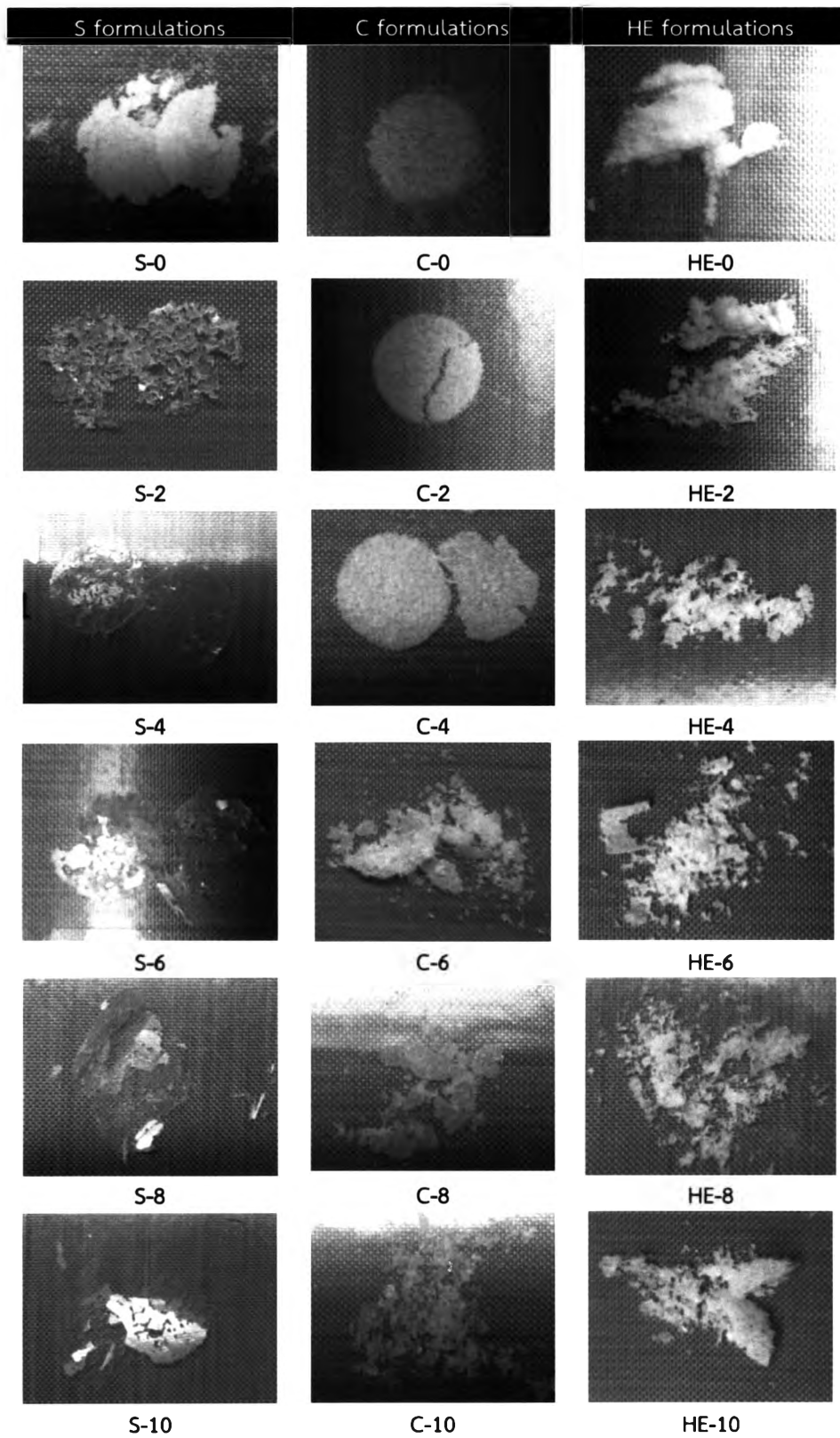


Figure IV-1 Optical photographs of S, C, and HE formulations after casting at 65°C for 12 hours.



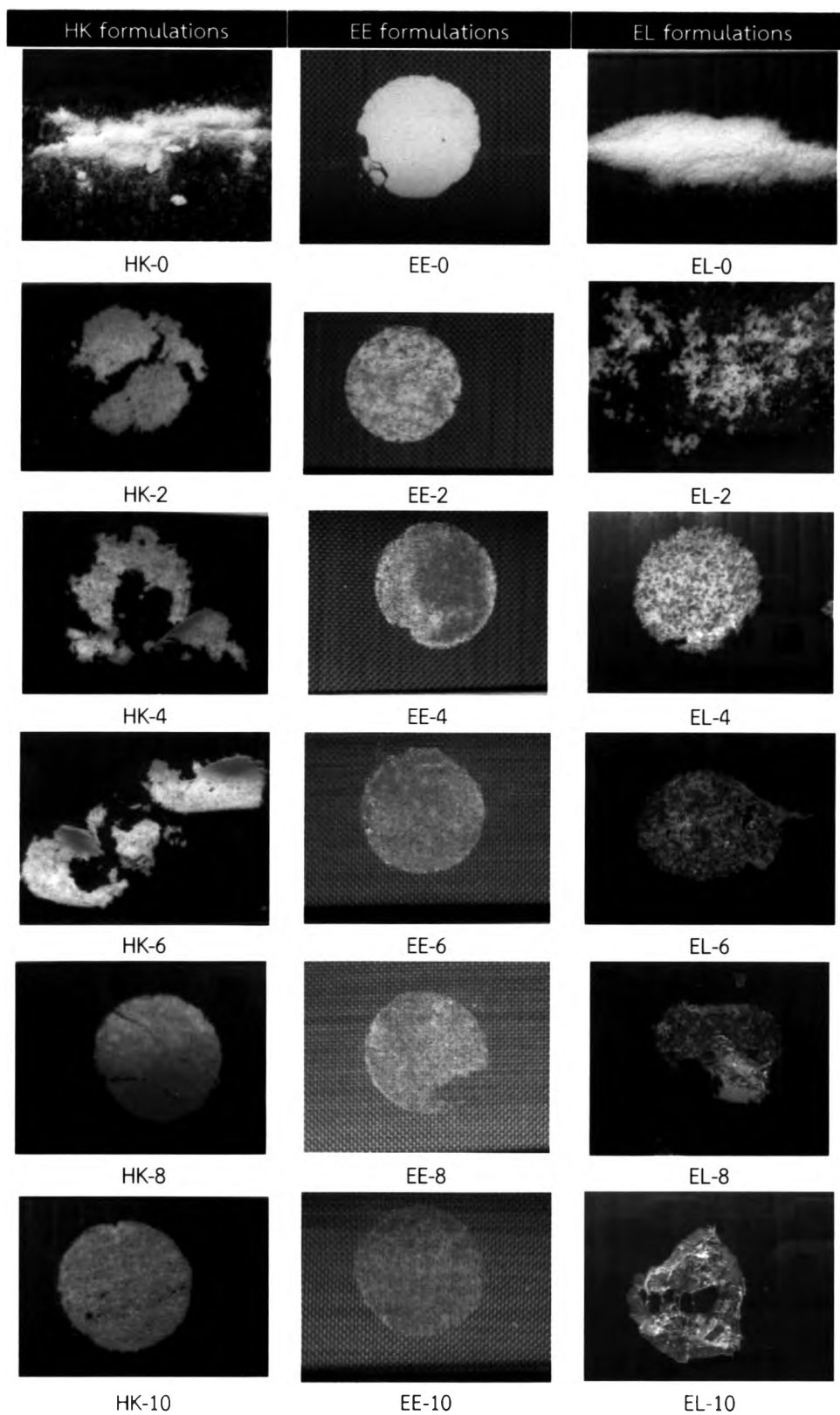


Figure IV-2 Optical photographs of HK, EE, and EL formulations after casting at 65°C for 12 hours.

1.1. Effect of weight loading on the formation of powder casting film

The result of weight loading on film characteristics of S-2 formulations was revealed in **Figure IV-3** that all obtained film characteristics were quite similar under visual detection, as well as the same film topography under SEM as illustrated in **Figure IV-4**. Therefore, these finding suggests that weight loading from 0 to 738 g on top of powder casting during film preparation may not have any effect on film characteristics.

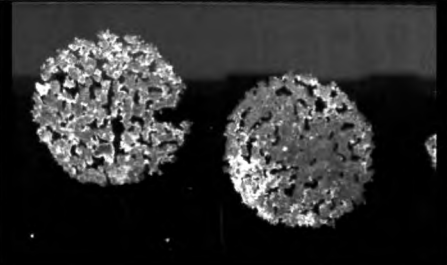
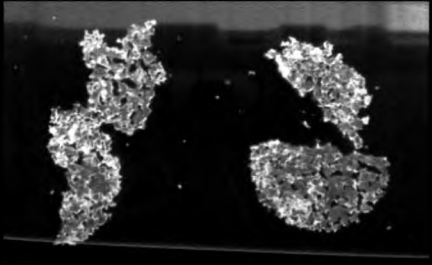
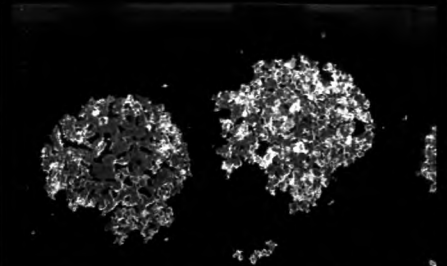
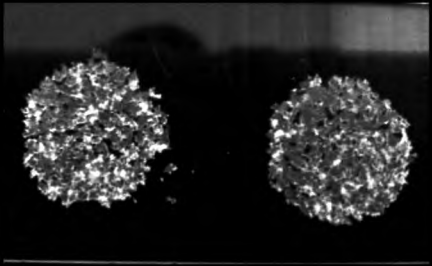
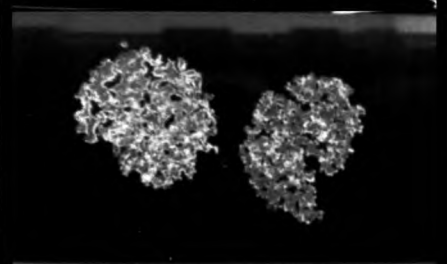
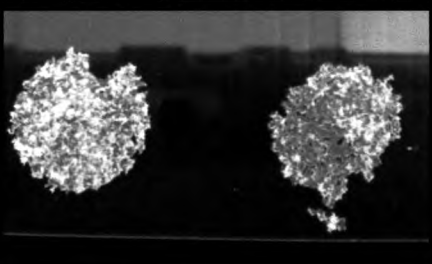
Weight loading (g)	Visual characteristics	Weight loading (g)	Visual characteristics
0		310	
105		465	
155		738	

Figure IV-3 Visual film characteristics of weight loading ranging from 0 to 738 g.



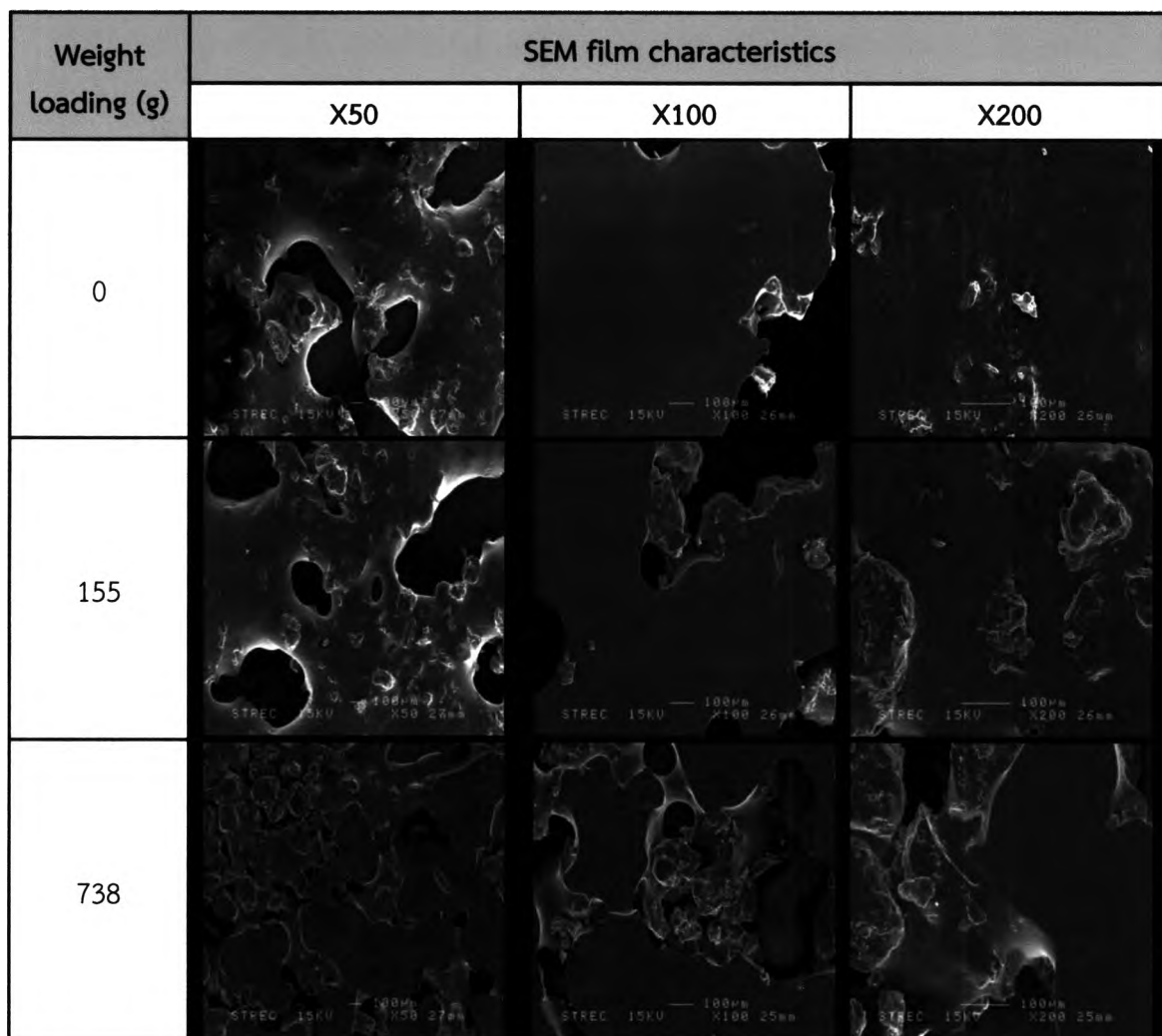


Figure IV-4 Effect of weight loading on film characteristics of S-2 formulation under SEM, model JSM6400.



1.2. Effect of glidant type

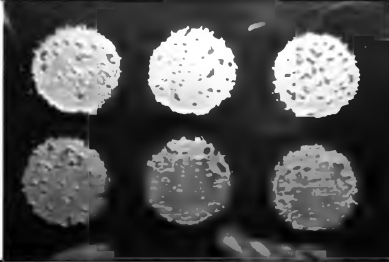

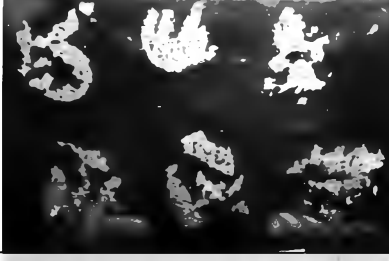

As can be seen in **Table IV-2**, matrix film of S-6 formulation with colloidal silicon dioxide (A) (formulation A) and that of formulation with talc (T) (formulation T) gave transparent and brittle matrix films, but the former formulation produced less pore with smoother surface and was easier to take off from the polytetrafluoroethylene coated sheet than the latter formulation. Moreover, formulation T was more brittle resulting in small flakes after peeling off. It might be explained that T was highly hydrophobic glidant (167), but S and P were hydrophilic substances, thus T might act as barrier in entanglement of matrix film. On the other hand, A was hydrophilic glidant (168), there was no any barrier to form an enlarged matrix film.

Furthermore, average weight per each film cast of formulation A without Brilliant Blue (BB) was 33.65 ± 2.50 mg, while that of formulation T was 25.77 ± 3.14 mg. The lower average weight per film cast of formulation T than that of formulation A was also noted in BB incorporated film. These results might be explained from different morphologies of both glidants. T is a plate-like shape, but A is sphere-like particle (138). Therefore, in a mold, particle packing of polymer blend of formulation A was more compact than that of formulation T. Although there was difference in average weight per cast film, SD of both formulations was similarly low.

For content uniformity study, it was found that percentage of BB content was 98.29 ± 4.72 and 98.05 ± 3.68 in formulation A and T, respectively, which was not significantly different ($p > 0.05$). These results indicated that T and A are comparable glidant. However, amount of A used 10 times less than that of T, and the characteristics of film was also more satisfactory. Therefore, A at 1% w/w of polymer blend was selected for further study.



Table IV-2 Film characteristics, weight uniformity, and content uniformity of formulation A and formulation T. Data are presented as the mean \pm SD of three samples.

	Film characteristics	Weight of film (mg)	Uniformity of BB* in film (%)	Figures of film w/o BB and w BB
Formulation A	Transparent and brittle film with a few pores	33.65 \pm 2.50	-	
	A blue-color and brittle film with a few pores	28.80 \pm 3.31	98.29 \pm 4.72	
Formulation T	Transparent and brittle pieces of film with more pores	25.77 \pm 3.14	-	
	A blue-color and brittle pieces of film with more pores	23.33 \pm 2.37	98.05 \pm 3.68	

Remark: BB = Brilliant Blue



1.3. Mechanism of film formation by powder casting method

From the previous study, S-4 and S-6 formulations showed good film characteristics with moderate amount of PEG which was tolerable and acceptable to mucosa (143, 144). Thus, both formulations were selected and the film formation mechanism was recorded at different time intervals. According to **Figure IV-5** and **Figure IV-6**, powder under optical photographs of S-4 formulation started to partially fuse at 15 minutes and while time was increasing, the area of fused powder enlarged as well as became clearer and smoother. The matrix film became visually clear and completely fused within only 2-3 hrs and 3-4 hrs for S-6 and S-4 formulations, respectively. When, S-6 formulation was observed under SEM, film topography became smoother with the increased heating time, as shown in **Figure IV-7**. Film topography was rough and uneven at 15, 30, and 60 minutes, and was smooth surface at 3, 6, and 12 hrs.

It was evident that polymer particles had a tendency to melt and coalesce under oven temperature with the time increased. At the time, when all particles were melted and created a smooth matrix film, increasing time would not have any influence on smoothness of film. This phenomenon was quite similar to that described in "Film formation and surface tension studied of powder coating" (169). The possible mechanism of film formation by powder casting technique may rely on the mechanism of solventless coating reviewed by Bose and Bogner (170). Three processes occur in solventless coating mechanism. First step is spreading of melted powder particles over a substrate. Second step, the melted particles are growing into one solid unit or film called coalescence. Last step is flowing and leveling of film.

Moreover, these results may also provide information about appropriate time for complete film formation that the formulation with 40% w/w of PEG spends only 4 hrs, and the formulation with 60% w/w of PEG only 3 hrs forming a smooth matrix film.



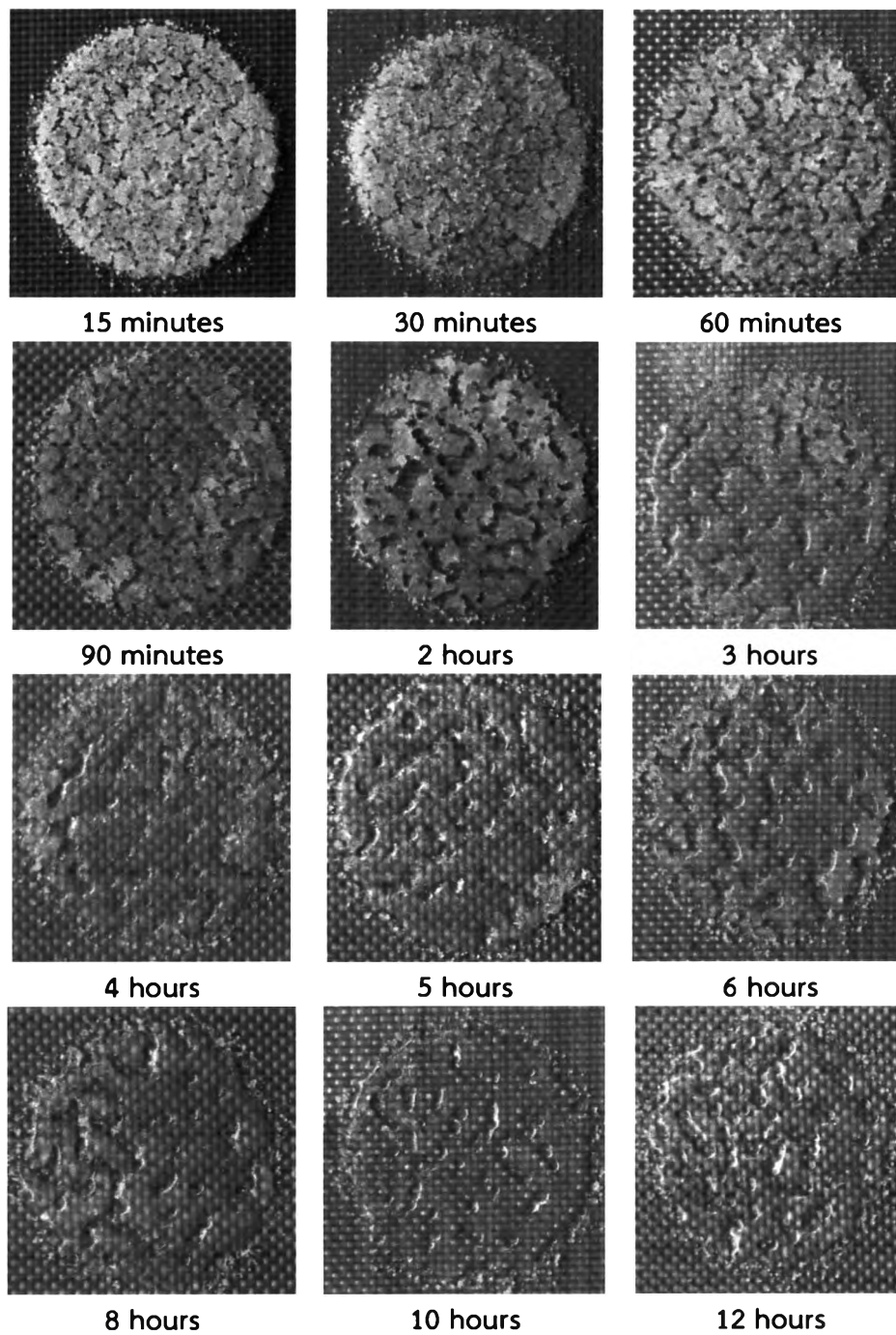


Figure IV-5 Optical micrographs of S-4 formulation at different time intervals at 65°C.

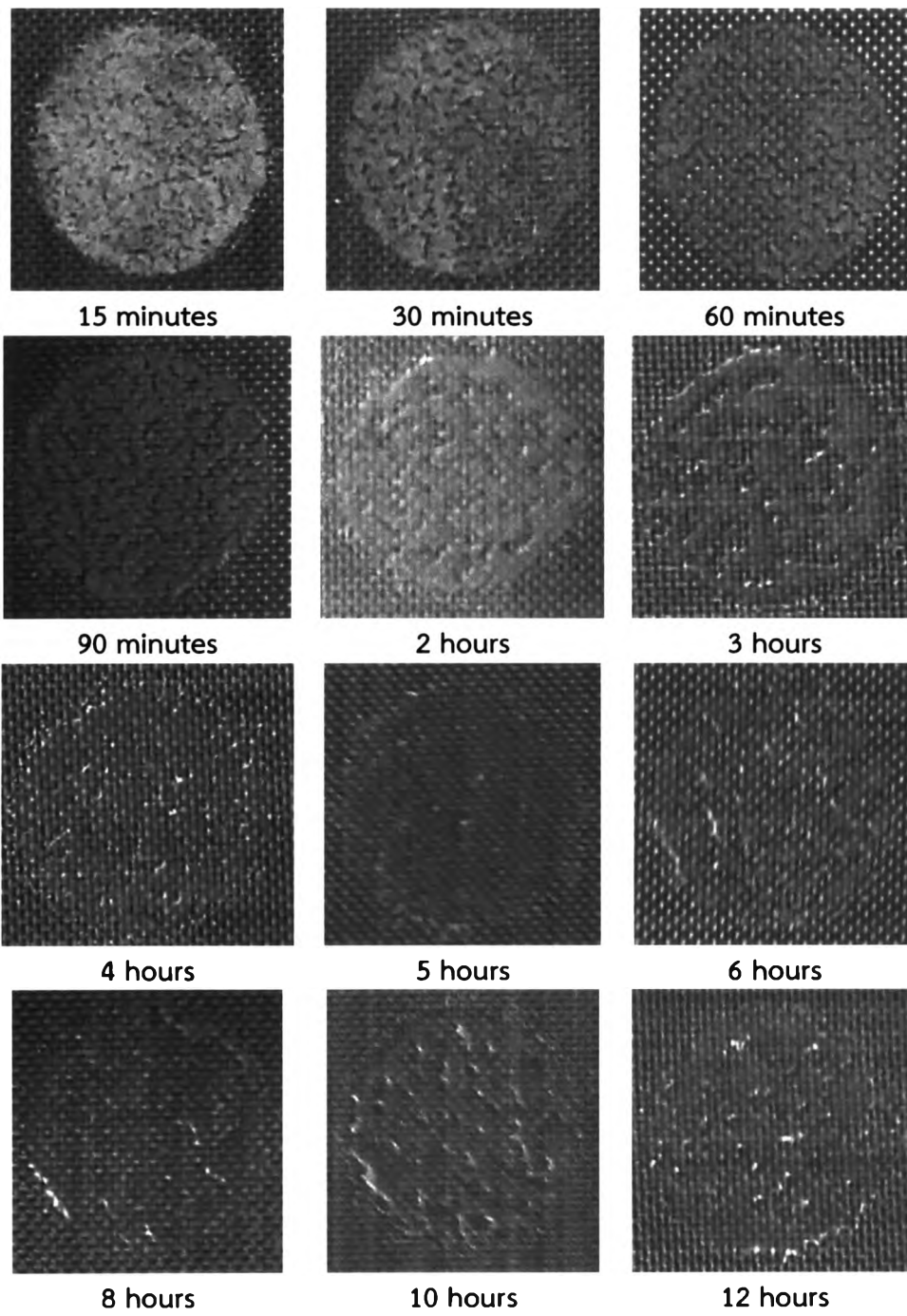


Figure IV-6 Optical micrographs of S-6 formulation at different time intervals at 65°C.

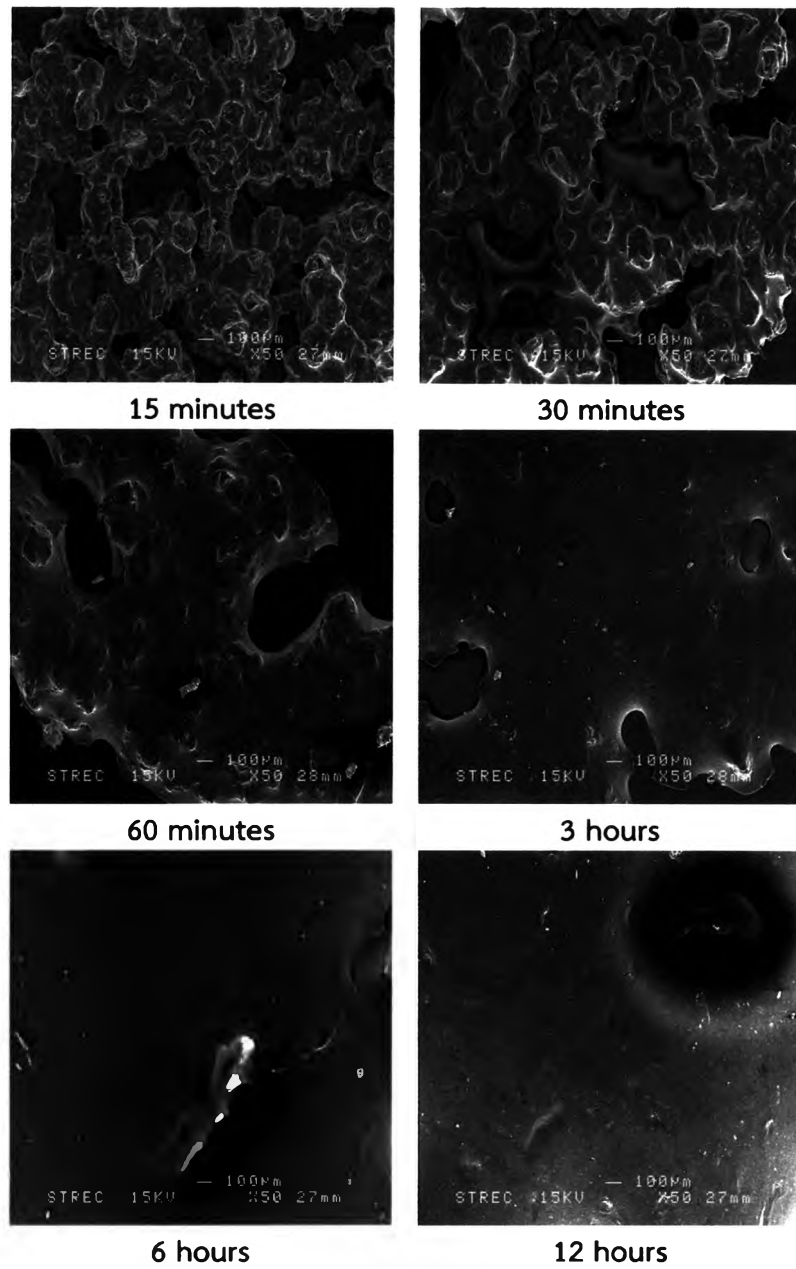


Figure IV-7 SEM micrographs of S-6 formulation at different time intervals (magnification x50).



2. Film preparation by powder casting method II

Film characteristics from combined polymer between S and C (SC formulation) are demonstrated in **Figure IV-8** and **Figure IV-9**. All formulations could form a light-yellowish, brittle matrix film with different film roughness, and the lower amount of C used, the smoother the films were. Films obtained from S_7C_3-4 and S_8C_2-4 formulations which having the ratio of S:C of equal or less than 7:3 provided smooth topographic film like the control formulation ($S_{10}C_0-4$). Such a consequence was similar to formulation composing 60% w/w of PEG.

Reasons could be that chitosan was not able to melt at 65°C (171), and too high amount of chitosan might disturb film-formation process, as well.

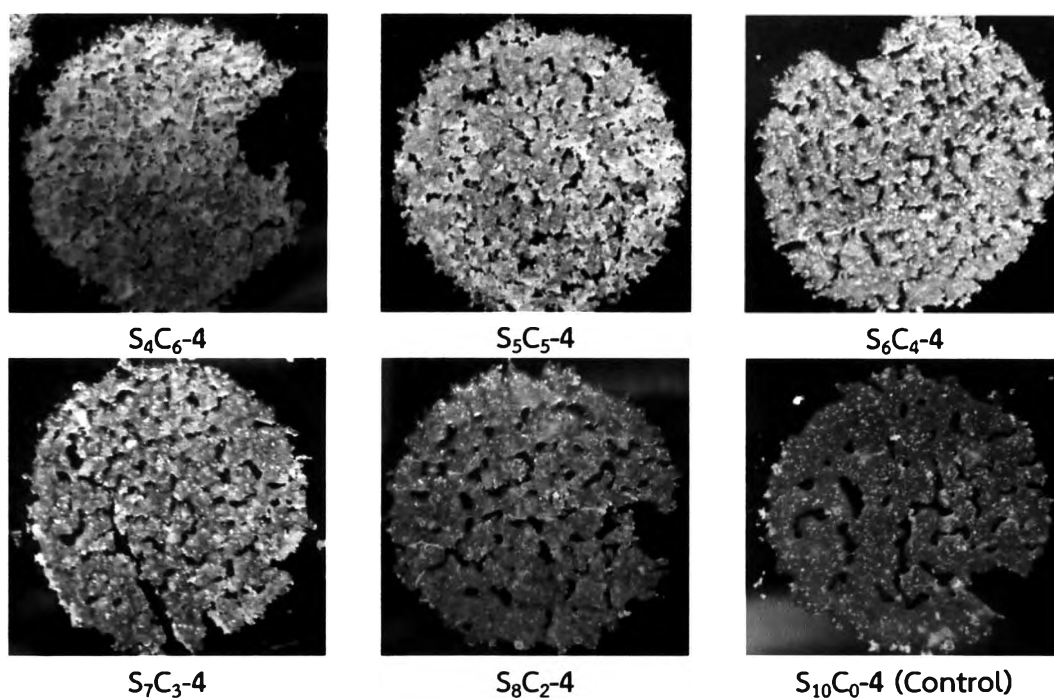


Figure IV-8 Film characteristics of SC-4 formulations containing 40% w/w of PEG.

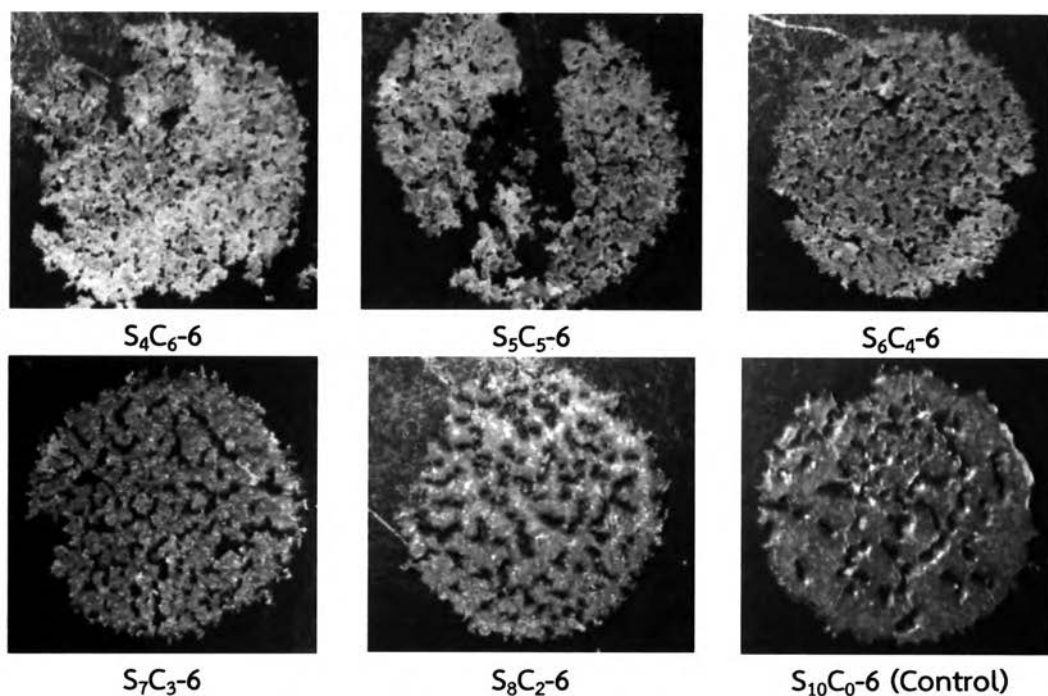


Figure IV-9 Film characteristics of SC-6 formulations containing 60% w/w of PEG.

All SEE formulations (combine polymers between S and EE) could form a brittle matrix film but smoothness and homogeneity of film were varied depending on the amount of EE (**Figure IV-10** and **Figure IV-11**). According to “Technical information of Eudragit[®] E 100, Eudragit[®] E PO and Eudragit[®] E 12,5” (163), film formation from those polymers should obtain a clear film. In case of SEE with 40% w/w of PEG, formulations comprising EE ratios equal or more than 8:2 (S_0EE_{10-4} , S_3EE_{7-4} , S_4EE_{6-4} , S_5EE_{5-4} , S_6EE_{4-4} , S_7EE_{3-4} , and S_8EE_{2-4}) provided matrix films with off-white spot which indicating that EE powder did not completely form or homogeneously melt with other ingredients. Furthermore, for SEE formulations with 60% w/w of PEG, obtained films composed of EE ratios equal or less than 7:3 (S_7EE_{3-6} , S_8EE_{2-6} , and S_9EE_{1-6}) were physically quite the same as the control ($S_{10}EE_{0-6}$).

In summary, suitable ratios of combined polymers consisting of S and C were $\leq 7:3$ in both PEG concentrations. The ratios of S and EE at $\leq 9:1$ and $\leq 7:3$ were suitable ratios for formulations composed of 40% and 60% w/w of PEG, respectively.



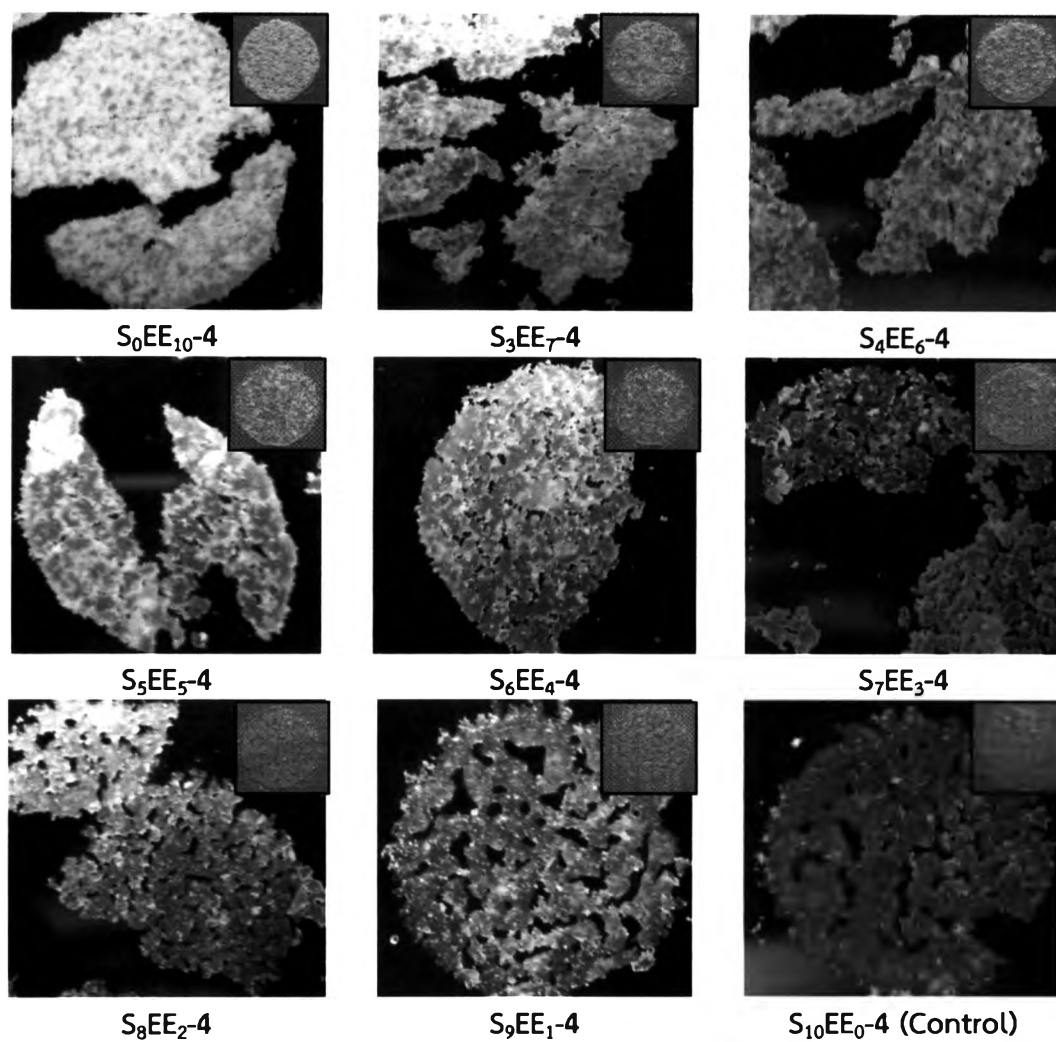


Figure IV-10 Film characteristics of SEE-4 formulations. Insert pictures were the obtained films upon the polytetrafluoroethylene coated sheet after ovened.

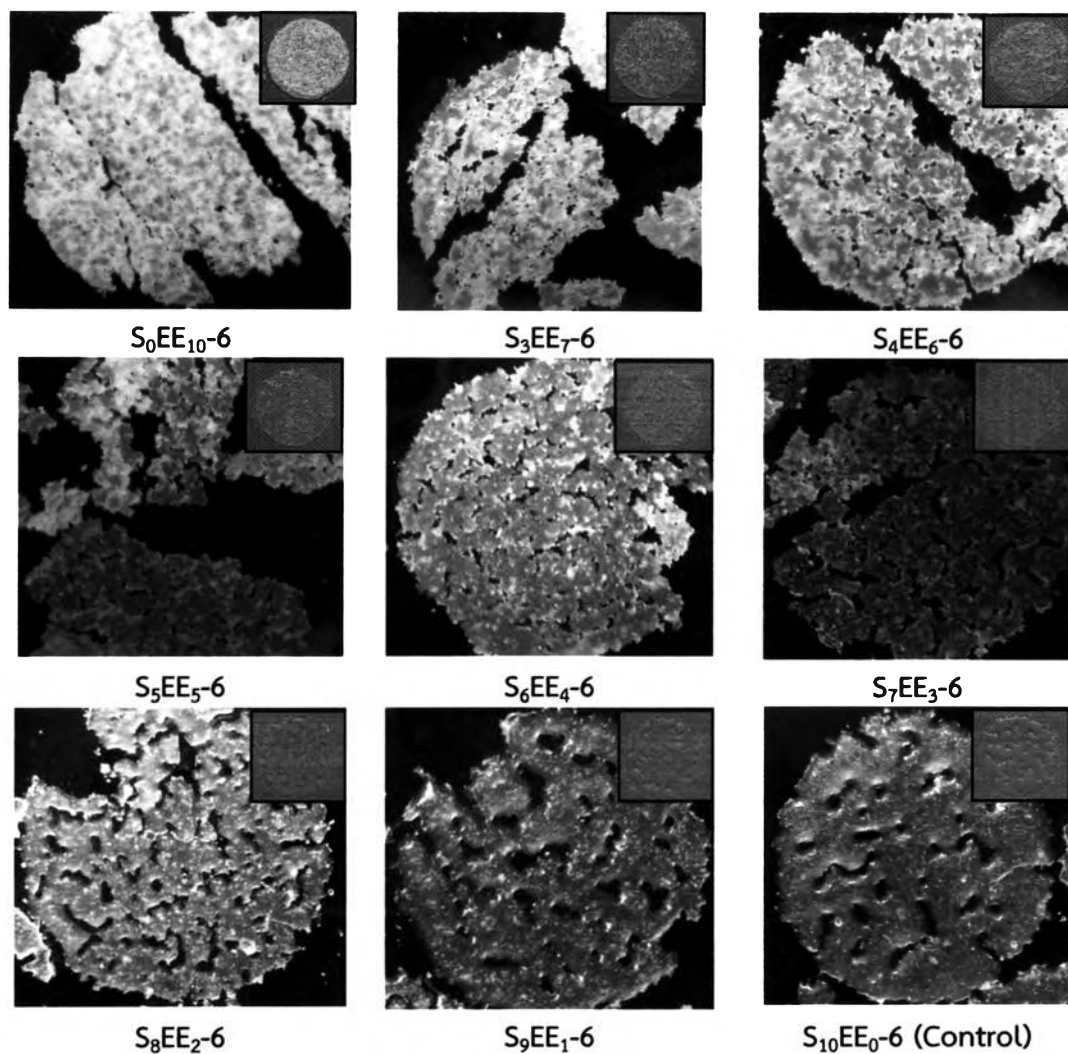


Figure IV-11 Film characteristics of SEE-6 formulations. Insert pictures were the obtained films upon the polytetrafluoroethylene coated sheet after ovened.



3. Pulverization processes

For pulverization methods, six formulations, which were selected from previous studies, consisted of S-4 (S + 40% w/w of PEG), S-6 (S + 60% w/w of PEG), S₇C₃-4 (S:C = 7:3 + 40% w/w of PEG), S₉EE₁-4 (S:EE = 9:1 + 40% w/w of PEG), S₇C₃-6 (S:C = 7:3 + 60% w/w of PEG), and S₇EE₃-6 (S:EE = 7:3 + 60% w/w of PEG). JM, PBM, and CM were chosen to grind such formulations.

Prior to comminution, polymer blends of each selected formulation were investigated their flowability. Compressibility index (%) and Hausner ratio were calculated from bulk and tapped density of each powder blend and their results are demonstrated in **Table IV-3**. Compressibility index (%) were 20.3419±0.2961, 21.4408±2.0674, 21.6593±0.8677, 23.6610±1.1893, 23.7179±1.1103, and 29.3394±0.6280 of S-6, S-4, S₇C₃-6, S₇C₃-4, S₉EE₁-4, and S₇EE₃-6, respectively, ranging from low to high value, while their Hausner ratios showed the similar results. Their flow characters were interpreted in accordance to USP35 (145). It was found that passable flowability was acquired from all formulations except S₇EE₃-6 formulation. Poor flowability of S₇EE₃-6 formulation might be accounted from the fine particles of EE in powder blend resulting in reduction of flow (172).





Table IV-3 Bulk density, tapped density, compressibility index, and Hausner ratio of polymer blends.

Polymer Blends	W ₀ (g)	V ₀ (ml)	V _t (ml)	ρ_{bulk} (g/ml)	ρ_{tapped} (g/ml)	Compressibility index (%) (Mean±SD)	Hausner ratio (Mean±SD)	Flow character
S-4	10.0120	21.0	16.0	0.4768	0.6258	21.4408±2.0674	1.2735±0.0340	Passable
	10.0105	20.0	16.0	0.5005	0.6257			
	10.0100	19.5	15.5	0.5133	0.6458			
S-6	10.0075	20.0	16.0	0.5004	0.6255	20.3419±0.2961	1.2554±0.0047	Fair to Passable
	10.0210	19.5	15.5	0.5139	0.6465			
	10.0180	19.5	15.5	0.5137	0.6463			
S ₇ C ₃ -4	10.0112	22.0	17.0	0.4551	0.5889	23.6610±1.1893	1.3102±0.0206	Passable
	10.0045	22.0	16.5	0.4548	0.6063			
	10.0153	21.5	16.5	0.4658	0.6070			
S ₉ EE ₁ -4	10.0207	20.0	15.0	0.5010	0.6680	23.7179±1.1103	1.3111±0.0192	Passable
	10.0044	19.5	15.0	0.5130	0.6670			
	10.0100	19.5	15.0	0.5133	0.6673			
S ₇ C ₃ -6	10.0063	21.5	17.0	0.4654	0.5886	21.6593±0.8677	1.2766±0.0142	Passable
	10.0184	21.0	16.5	0.4771	0.6072			
	10.0152	21.0	16.3	0.4769	0.6163			
S ₇ EE ₃ -6	10.0149	20.5	14.5	0.4885	0.6907	29.3394±0.6280	1.4153±0.0126	Poor
	10.0030	20.0	14.3	0.5002	0.7020			
	10.0051	20.0	14.0	0.5003	0.7147			

3.1. Film pulverization by jet mill (JM)

3.1.1. Effect of cycle numbers

As can be seen in **Figure IV-12**, all size distribution patterns of S-6 formulation with 1, 2, and 3 grinding cycles indicated unimodal size distribution, and all obtained particle sizes were extremely reduced from about ≤ 590 micron (coarse grinding through 30-mesh screen) with narrower size distribution. Increasing milling cycle from 1 cycle to 2 cycles resulted in about twice size reduction from 11.601 ± 0.207 micron (span value = 2.577 ± 0.104) to 6.318 ± 0.025 micron (span value = 1.286 ± 0.006), and for 3 milling cycles, 4.481 ± 0.031 micron (span value = 1.240 ± 0.055) was accomplished.

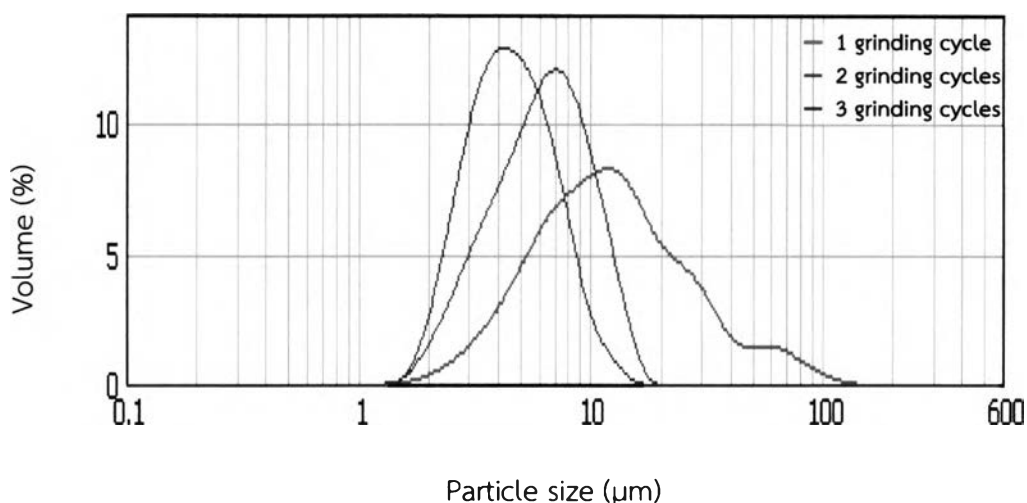


Figure IV-12 Particle size and size distribution of S-6 formulation with different JM cycles (n=6).

More grinding cycles to model formulation led to smaller size of particles could be explained that with increasing grinding cycle, initial size of feed would be smaller than that of the previous feed. However, there was a limitation of the obtained particle sizes after JM, which might be explained from two reasons. First reason was grinding limit where no more breakage could happen. Because cracks and flaws present within particles are required in advance for all comminution techniques, the possibility of those imperfection decreases when size of particle is

reduced (173, 174). Second reason was the centrifugal force. Within grinding chamber, only larger particles would stay by effect of centrifugal force, as smaller particles would stay for a short time and then move to the collecting chamber resulting in less impaction or attrition (118).

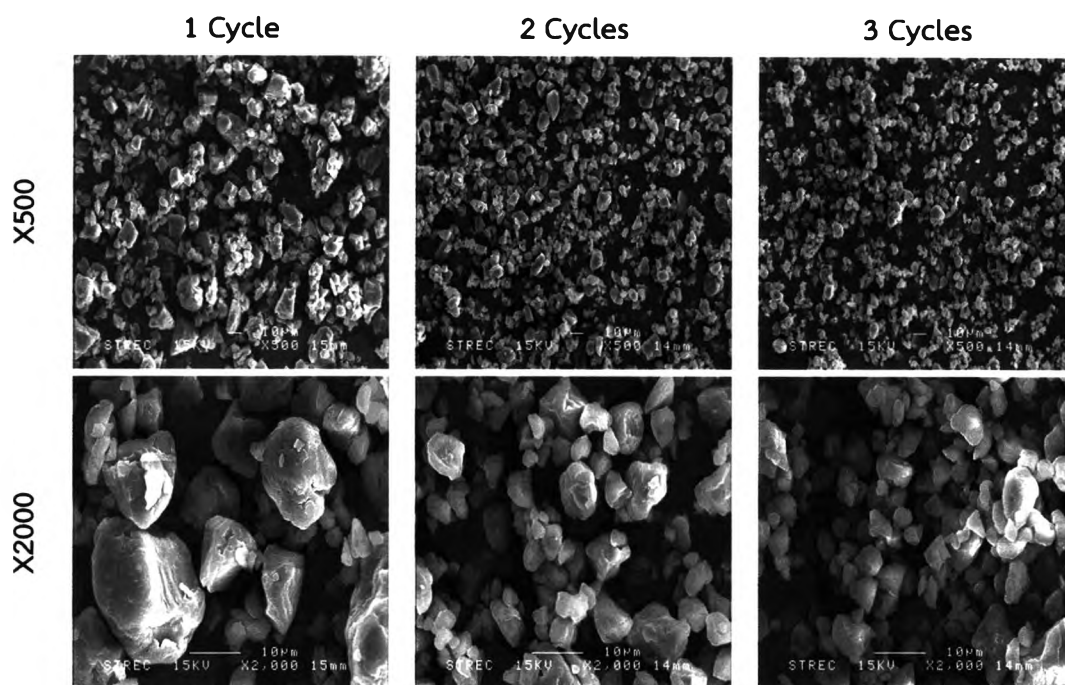


Figure IV-13 Particle morphology under SEM of S-6 formulation after JM process with different grinding cycles.

SEM micrographs of the micronized powder were to confirm the results from laser light diffraction shown in **Figure IV-13**. It was likely that particle sizes of each milling cycle complied with the results measured by laser light diffraction. JM resulted in roundish-edge particles and it seemed to be apparently rounder with more milling cycles. This result was in consistency with Ehmer's dissertation (116) that cubic crystals of insulin, lysozyme, and BSA after 1 milling cycle at 6 bars to 3 cycles at 14 bars became more rounded particles. This phenomenon is a typically common occurred after JM because impaction and attrition between particle-to-particle and particles-to-wall of the mill resulted in rounded edge morphology (175, 176).

Owing to importance of particle size to dry powder nasal drug delivery, desirable size range and narrow size distribution are required. According to draft guidance for industry on “Sinusitis: designing clinical development programs of non-antimicrobial drugs for treatment” (103) and several publications (45, 177), appropriate size of particles for nasal drug delivery should be in range about 5-120 micron due to prevent inhaling into the lung of particle less than 5 micron. Moreover, too large particle size could not reach the target site in nasal cavity but remain in the anterior part of nose resulting in limiting clinical efficacy (102). Therefore, powders obtained from 1 and 2 milling cycle were appropriate for nasal powder delivery and further development.

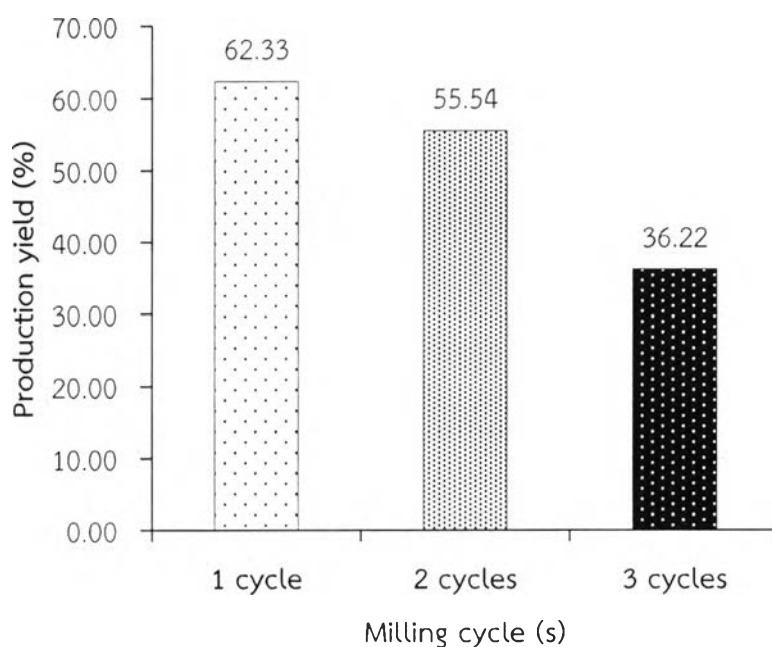


Figure IV-14 Production yield (%) of S-6 formulation after JM process with different milling cycles (n=1).

Moreover, it was found that milling cycle also had an effect on production yield. Yield of production decreased from initial of 100% to 62.33%, 55.54%, and 36.22% after 1, 2, and 3 milling cycles, respectively (**Figure IV-14**). This result was in consistence with Ehmor’s experiment about size reduction of proteins by using JM. It

was reported that yield of production decreased to 83% after 1 grinding cycle as well as reached to 40% after 3 grinding cycles (116).

From the results, one milling cycle was selected for further studies as an optimum condition, due to the capability to produce suitable particle size and size distribution, particle shape, high yield of production comparing to more milling cycles, and economical reasons.

3.1.2. Effect of feeding amounts

The result of different amounts of feed on production yield revealed in **Figure IV-15** that approximate 150 g of feeding amount could provide production yield (%) reaching up to 80%. On the contrary, about 50% of production yield was achieved from approximate 40 g of feeding amount. These results can be implied that the higher amount of feed introduced, the higher production yield obtained.

There were two reasons for explaining low production yield of JM process. First reason was loss of production in grinding chamber by filling in void space in that chamber. Second reason was loss of powder in the other parts of the machine by electrostatic charges of small particles obtained. From two possible root causes, there was fixed amount of product losing during milling process, regardless of the feeding amount introduced.



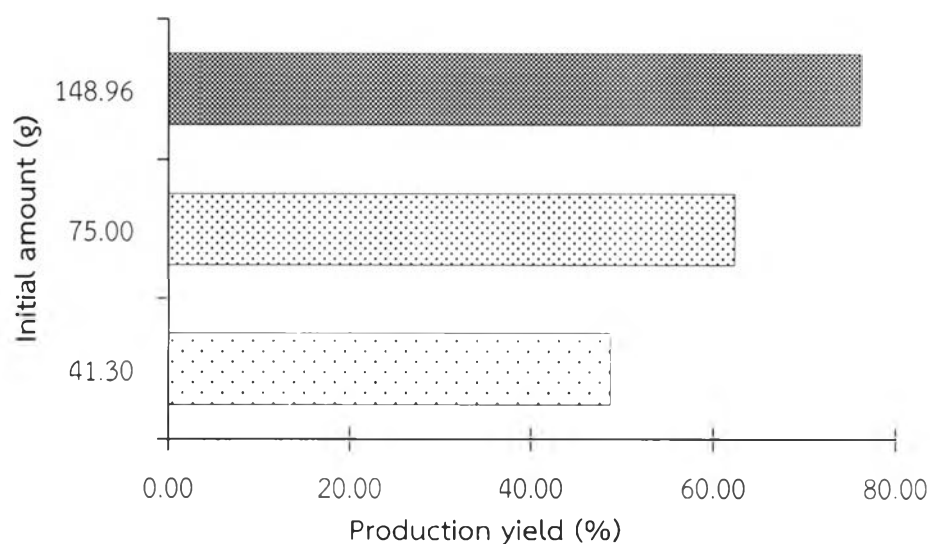


Figure IV-15 Production yield (%) of S-6 formulation after milling of 1 cycle by JM with different initial feeding amounts (n=1).

After optimized condition for JM process was accomplished, all selected formulations; S-4, S-6, S₇C₃-4, S₉EE₁-4, S₇C₃-6, and S₇EE₃-6, were pulverized following such a condition. Median particle sizes (d(v,0.5)) of all formulations ranged from 6.4-9.4 micron, and their span values were between 1.24 and 2.22, as shown in **Figure IV-16**. S₉EE₁-4 formulation had the smallest particle sizes, 6.407±0.020 micron, which was close to the size obtained from S₇EE₃-6 formulation of 6.561±0.103 micron with statistical insignificance (p>0.05). S₇C₃-4 formulation had the largest particle size of 9.391±0.050 micron while 9.297±0.141 micron was from S-4 formulation, which were non-statistically significant (p>0.05). These results indicated that all obtained powders were in appropriate range from nasal powder delivery as aforementioned.

Moreover, to verify their shape, SEM micrographs were taken and shown in **Figure IV-17**. It was clear that all resulting powders had similar morphology with round edge after micronization.

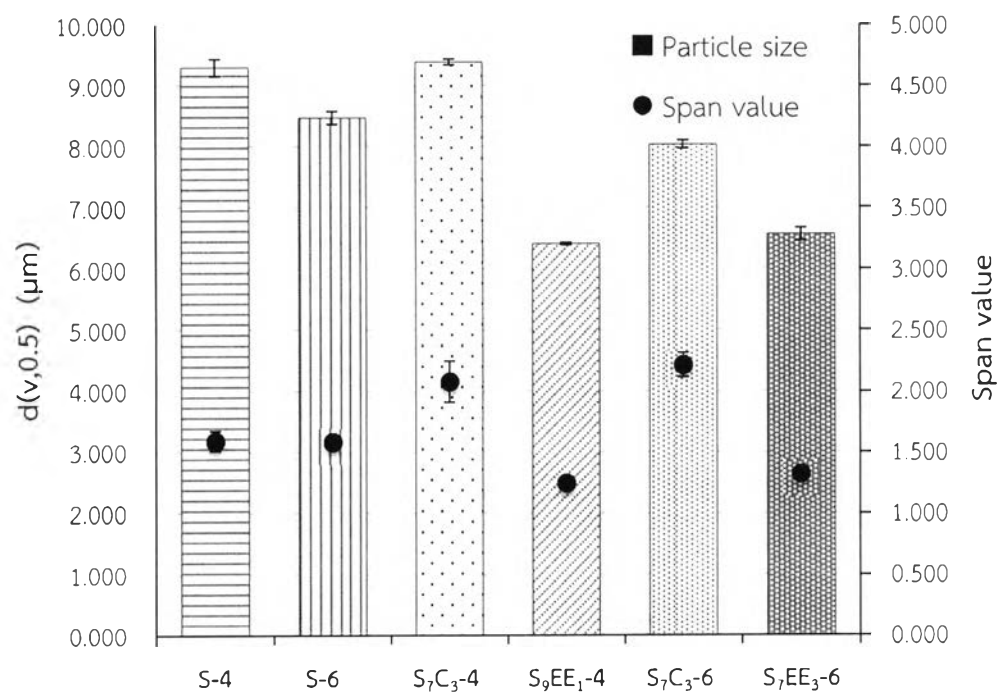


Figure IV-16 Particle sizes and span values of 6 selected formulations after 1 milling cycle of JM process. The vertical bar represented the mean \pm SD of results from triplicate measurements.



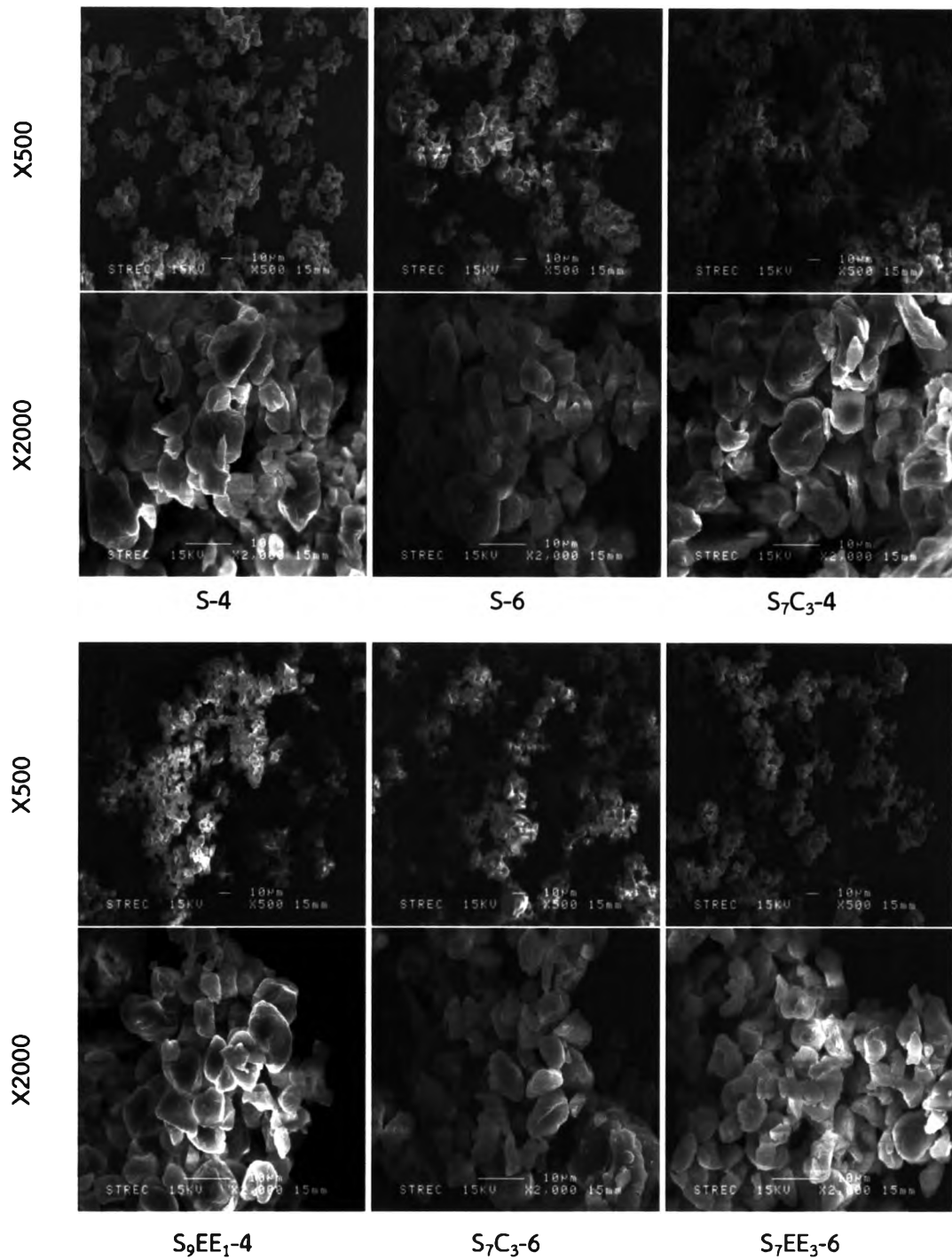


Figure IV-17 SEM micrographs of powder formulations after JM process of S-4, S-6, S7C3-4, S9EE1-4, S7C3-6, and S7EE3-6 formulations.



Furthermore, flow characteristics of pulverized powder were determined and demonstrated in **Table IV-4** by presenting in compressibility index and Hausner ratio, which were calculated from bulk and tapped density of each pulverized powder. Compressibility index (%) were 23.2241 ± 5.6126 , 25.7200 ± 3.7251 , 25.8686 ± 1.4597 , 26.0973 ± 1.1223 , 27.7414 ± 3.2938 and 28.3760 ± 2.3834 for S-4, S₉EE₁-4, S-6, S₇EE₃-6, S₇C₃-6, and S₇C₃-4, respectively, ranging from low to high value, while their Hausner ratios showed the same results. According to USP35 (145), their flow characters were interpreted and it was found that S-4 pulverized powder was the best (passable), as S₇C₃-4 had the worst flowability. When comparing to polymer blends before casting, almost all powders after JM had a tendency of poorer flow characteristics because of the increased compressibility index and Hausner ratios. The explanation of these results may be because particle size of powder which was smaller led to agglomeration of particles as illustrated in **Figure IV-17** and then exhibited tackiness and stickiness (178).





Table IV-4 Bulk density, tapped density, compressibility index, and Hausner ratio of pulverized powders.

Pulverized powder	W ₀ (g)	V ₀ (ml)	V _t (ml)	ρ _{bulk} (g/ml)	ρ _{tapped} (g/ml)	Compressibility index (%) (Mean±SD)	Hausner ratio (Mean±SD)	Flow character
S-4	10.0144	35.0	29.0	0.2861	0.3453	23.2241±5.6126	1.3071±0.0938	Passable
	10.0382	37.0	28.0	0.2713	0.3585			
	10.0383	39.0	28.0	0.2574	0.3585			
S-6	10.0418	39.0	29.5	0.2575	0.3404	25.8686±1.4597	1.3493±0.0265	Passable to Poor
	10.0022	38.5	28.5	0.2598	0.3510			
	10.0362	38.5	28.0	0.2607	0.3584			
S ₇ C ₃ -4	10.0260	43.0	31.5	0.2332	0.3183	28.3760±2.3834	1.3972±0.0474	Poor
	10.0287	44.0	32.0	0.2279	0.3134			
	10.0335	45.0	31.0	0.2230	0.3237			
S ₉ EE ₁ -4	10.0101	46.5	36.5	0.2153	0.2742	25.7200±3.7251	1.3485±0.0661	Passable to Poor
	10.0570	49.0	35.0	0.2052	0.2873			
	10.0355	48.0	35.0	0.2091	0.2867			
S ₇ C ₃ -6	10.0475	40.0	30.0	0.2512	0.3349	27.7415±3.2938	1.3859±0.0643	Poor
	10.0401	41.0	30.0	0.2449	0.3347			
	10.0185	43.0	29.5	0.2330	0.3396			
S ₇ EE ₃ -6	10.0138	41.5	31.0	0.2413	0.3230	26.0973±1.1223	1.3533±0.0207	Poor
	10.0361	41.0	30.5	0.2448	0.3291			
	10.0499	42.0	30.5	0.2393	0.3295			

3.2. Film pulverization by planetary ball mill (PBM)

Effect of milling time

The effect of grinding time of S-6 formulation in PBM can be seen in **Figure IV-18**. Particle size was apparently less than 150 micron with broad size distribution at 10 minutes of grinding time, as at 60 minutes of grinding period seem to be less than 50 micron size with apparently narrower size distribution was accomplished. Therefore, it can be assumed that size of particle was smaller with narrower size distribution when grinding time increased from 10 minutes to 60 minutes. For shape of particles, all obtained powders were irregular shape with sharp-edge. Moreover, increasing grinding time in PBM also resulted in generating more heat, so care should be taken for heat-sensitive drug (126).

In summary, a period of 60 minutes was the optimum grinding time for further studies because of providing visually finer particle size with narrower size distribution than the others.



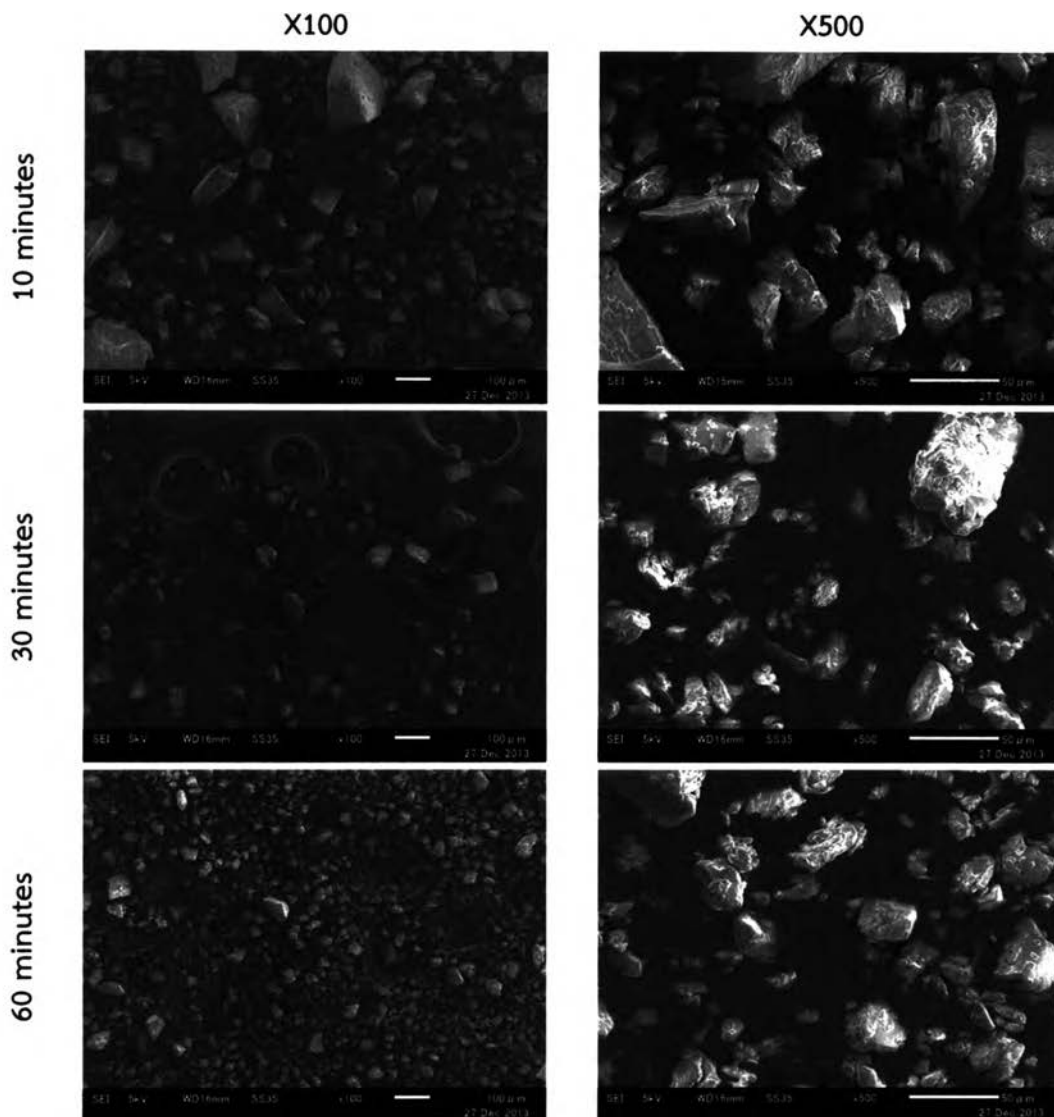


Figure IV-18 SEM micrographs of S-6 formulation after different milling time by using PBM.



3.3. Film pulverization by cryomill (CM)

Three formulations; S-6, S₇C₃-6, and S₇EE₃-6, were selected for cryogenic grinding. The morphology of obtained powders under SEM is shown in **Figure IV-19**. In S-6 formulation, the received powder was too small of less than 1 micron and likely to agglomerate to be larger particles. The other two formulations also had similar results. Although the mechanism of CM was impaction similar to PBM, the particle size was much smaller. Cryogenic condition rendered harder and more brittle material compared to ambient temperature (129, 135). Moreover, size distribution of agglomerates was not visually uniform in all formulations because of too small particles resulting in uncontrolled growth of agglomerates (179).

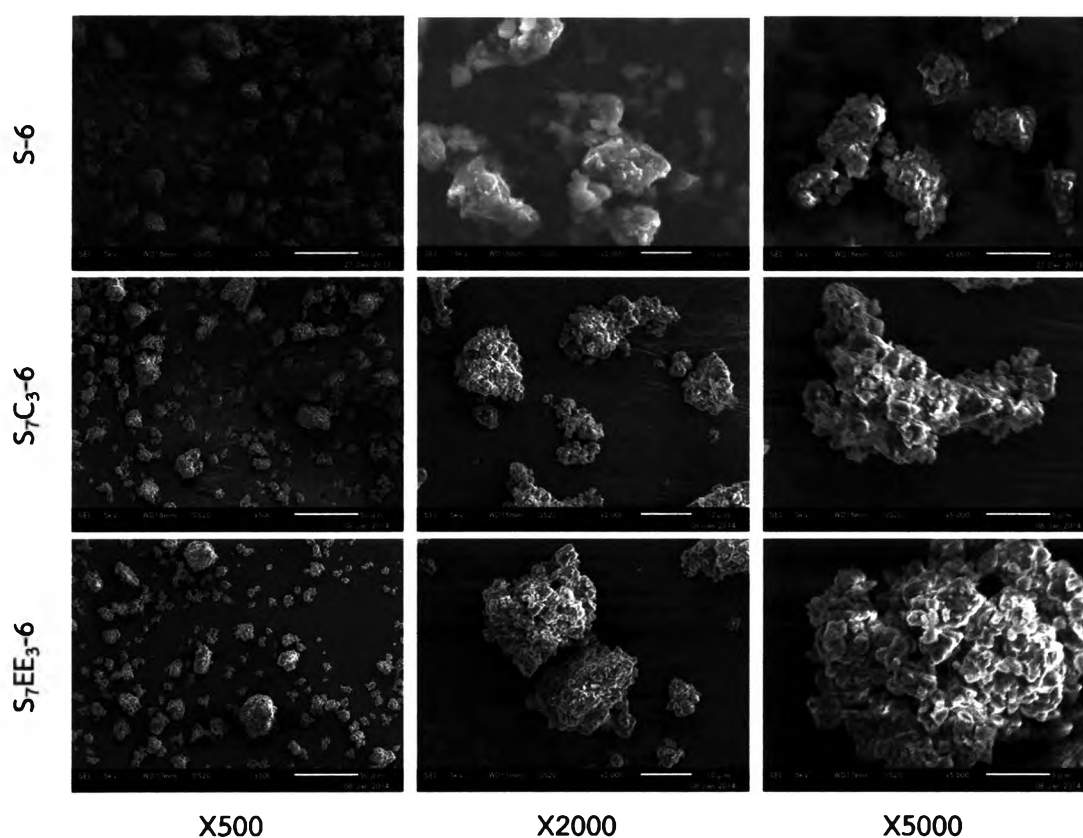


Figure IV-19 SEM micrographs of blank S-6, S₇C₃-6, and S₇EE₃-6 formulations after grinding by CM for 90 minutes.

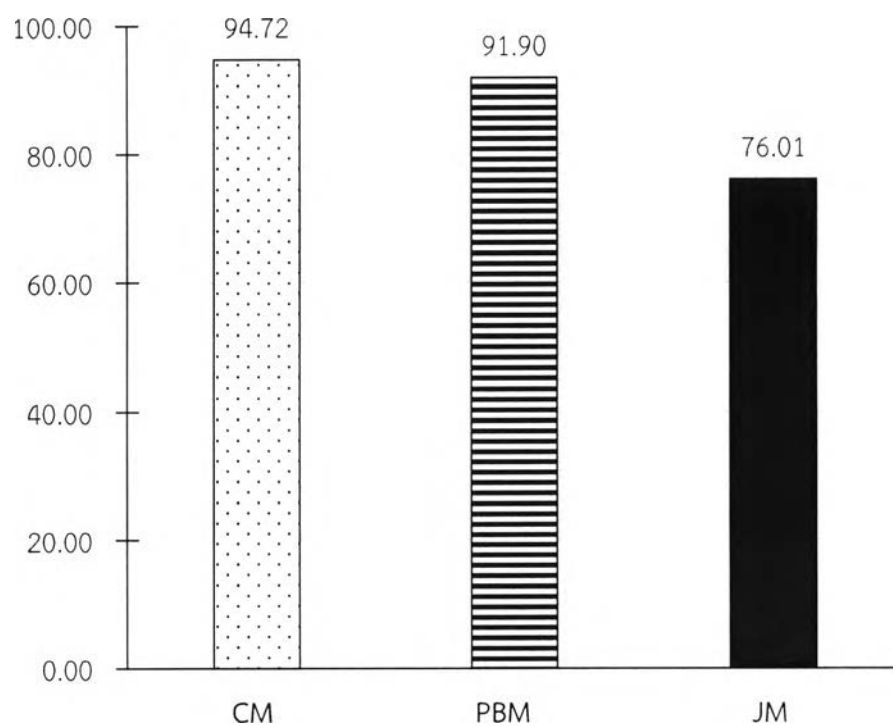


Figure IV-20 Production yield (%) of S-6 formulation after CM, PBM and JM processes (n=1).

Essentially, production yields from CM and PBM could reach more than 90%, as shown in **Figure IV-20**, while JM showed lower production yield reaching up to 80%. It might be because both CM and PBM processes were close system, and all materials were comminuted within grinding chamber with a rod or balls. Thus, materials were merely lost during a grinding process.



3.4. Pulverization of BSA incorporated film formulations

S-6 (S + 60% w/w of PEG) formulation was selected in order to incorporate 10% w/w of lyophilized bovine serum albumin (BSA). Different milling processes were carried out with suitable condition by using 1 milling cycle for JM, 60 minutes milling period for PBM, and 90 minutes milling period for CM.

SEM micrographs shown in **Figure IV-21** revealed that for JM and PBM, particle size of pulverized BSA incorporated formulation was slightly smaller than blank formulation illustrated in **Figure IV-17** and **Figure IV-18** and was quite similar morphology for CM (**Figure IV-19**). One reason could be that BSA incorporated in matrix film might have an impact on a decrease in fracture toughness value of obtained film. Arencón and Velasco (180) reported that the increasing of %filler contents in polypropylene-matrix composite had an influence on decreasing of the values from Izod impact strength and drop-weight tests, which were methods for determining the impact resistance of materials. Thus under the same milling condition, BSA incorporated film formulation would be easier to breakdown than blank formulation.

Moreover, shape of pulverized powder with BSA by JM was apparently more roundish edge than that in PBM, while in CM agglomerates were obtained, which was the same as previous results of blank formulation (**Figure IV-19**).



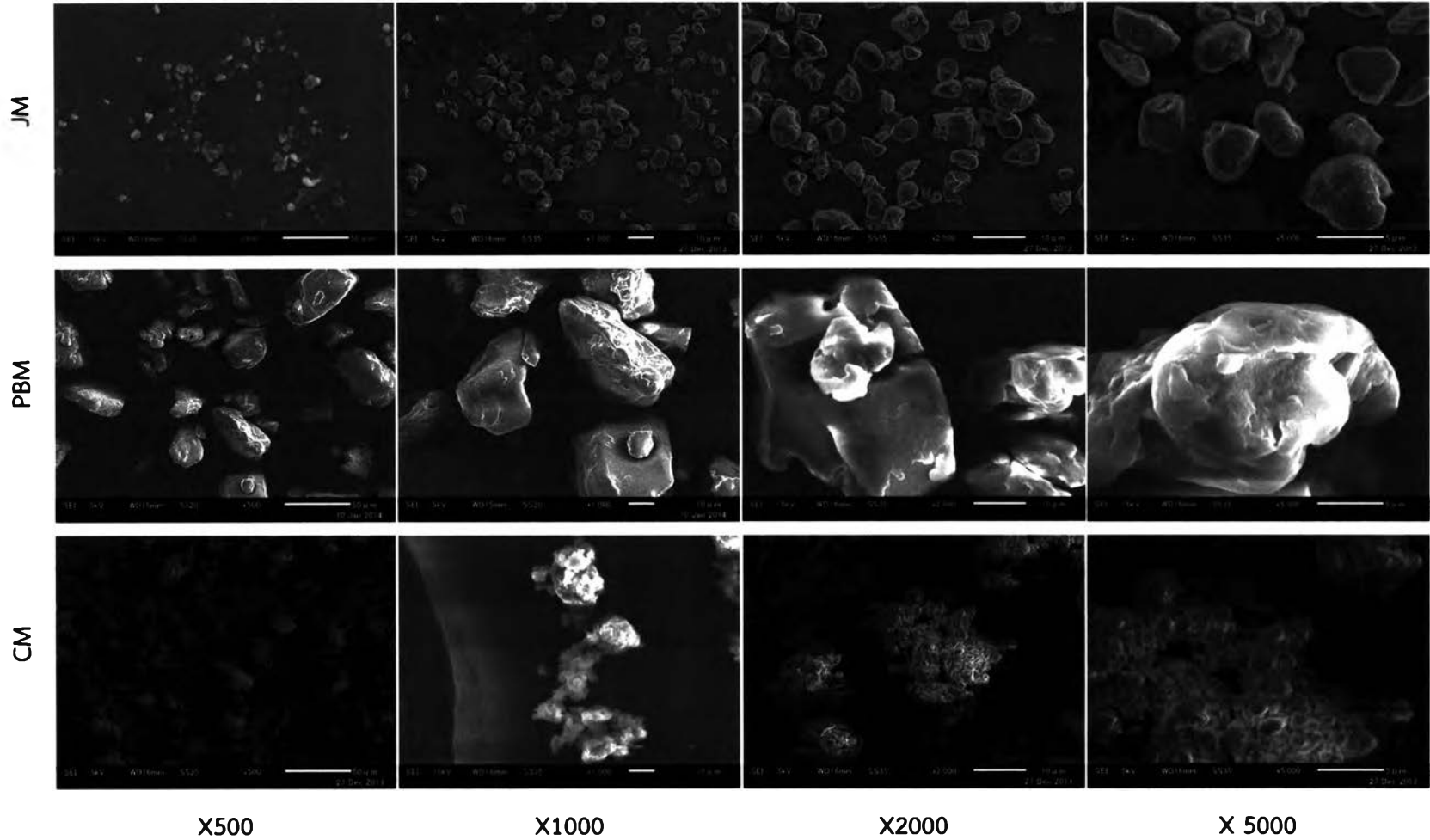


Figure IV-21 SEM micrographs of BSA S-6 formulation with different production processes.

4. Physicochemical characterization of matrix film and pulverized formulation

4.1. Moisture content by Karl Ficsher method

According to the **Figure IV-22**, % moisture contents of pulverized powders of S-6 formulation after PBM, CM and JM were 3.03 ± 0.21 , 3.03 ± 0.54 , and 3.20 ± 0.64 , respectively, which was not statistically significant differences ($p>0.05$). Such low moisture content was due to the production processes such as heating process in powdered film preparation, exposure of sample to dry and cool air during JM (181), and exposure of sample with high temperature in PBM (182).

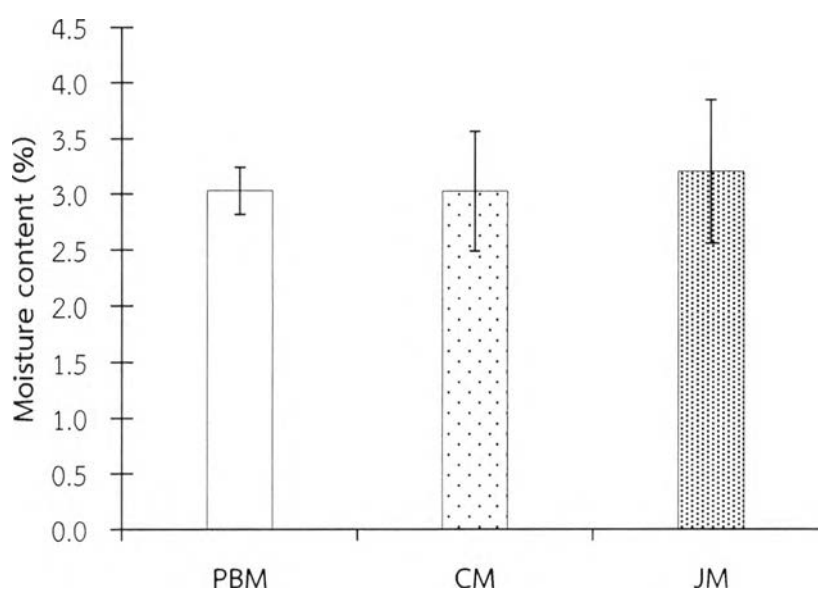


Figure IV-22 Moisture content (%) of the powder obtained from different pulverization processes. The vertical bars represented the mean \pm SD of the results from triplicate measurements.

4.2. Differential scanning calorimetry (DSC)

According to **Figure IV-23**, DSC thermogram of PEG showed a sharp endothermic peak at around 60°C, corresponding to its melting point, while that of S exhibited two broad melting endotherms at 70°C and 315°C, respectively, corresponding to the T_g (164) and its recrystallization. EE showed a small endothermic peak at around 56°C and a broad endothermic peak around 300°C. C exhibited a broad melting endotherm below 140°C indicating loss of water, and exothermic peak around 280-350°C corresponding to degradation of the polymer (183, 184). A did not display any thermal event in the examined temperature range. For a model protein, BSA showed a broad endothermic peak around 80°C which was relevant to melting point and absorbed water, and followed by protein unfolding, while bimodal endotherms at 215°C and 305°C were attributed to thermal degradation of BSA (185).

DSC thermograms of physical mix formulations (S-6, S₇C₃-6, and S₇EE₃-6) showed a sharp endothermic peak at 55-58°C which was slightly lower than native PEG of 60°C, as can be seen in **Figure IV-24**, while the peaks of the other ingredients did not display. The dilution effect was used to make an explanation about decreasing of peak intensity in physical mixtures (186) and melting point depression. Furthermore, after making a matrix film, DSC thermograms exhibited endothermic sharp peak which were slightly lower and broader than the thermograms of physical mixed formulations, as shown in **Figure IV-25**. It might be due to sample size and mass which were functions effecting to peak maximum, as well as thermal gradient occurring across a sample reflecting to broadening of the peak (187).



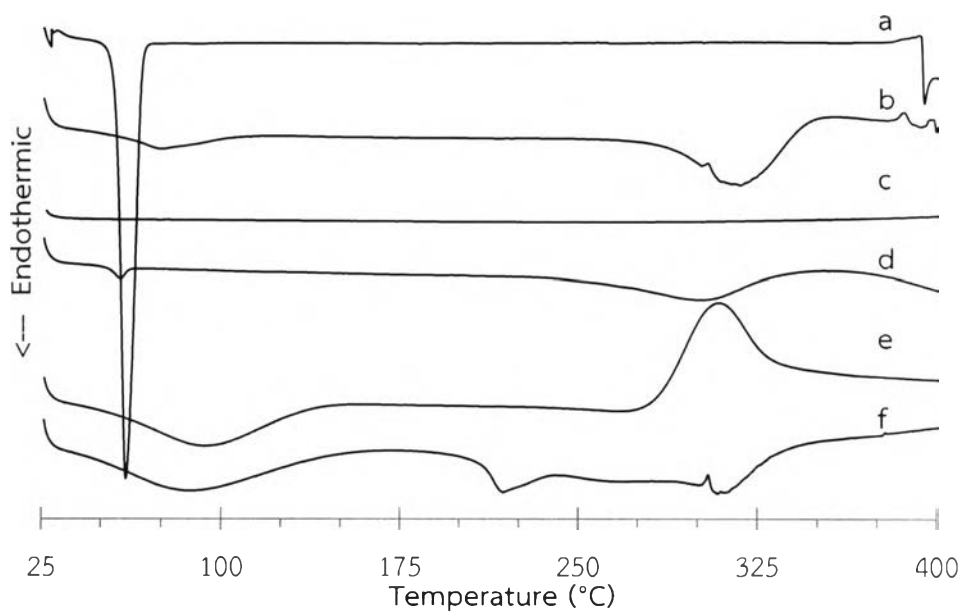


Figure IV-23 DSC thermograms of raw materials used from model DSC6200; (a) PEG, (b) S, (c) A, (d) EE, (e) C, and (f) native BSA.

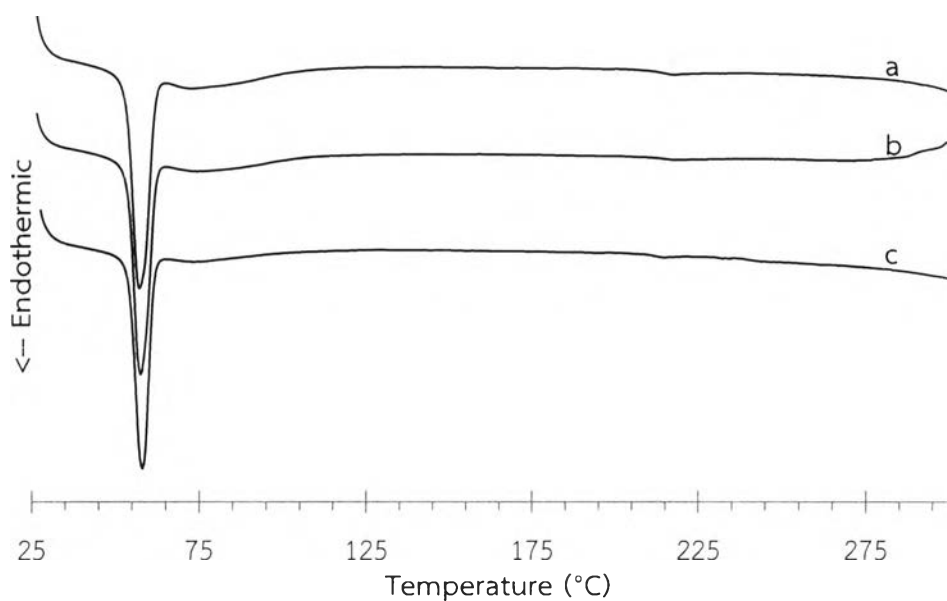


Figure IV-24 DSC thermograms of physical mixtures with BSA formulations from model DSC6200; (a) S-6, (b) S₇C₃-6, and (c) S₇EE₃-6 formulations.



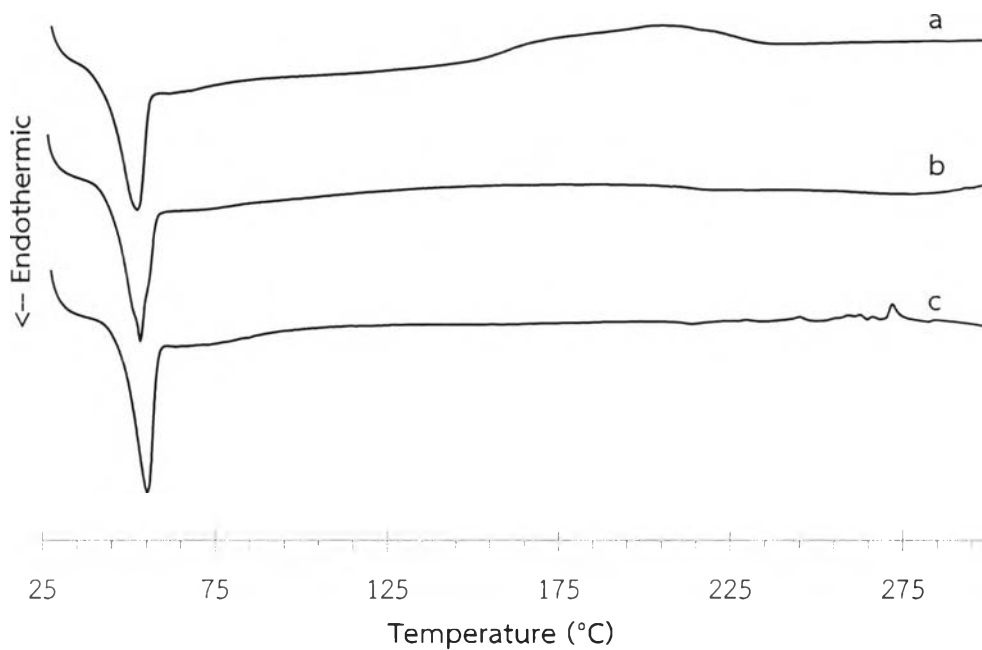


Figure IV-25 DSC thermograms of BSA-film formulations from model DSC6200; (a) S-6, (b) S₇C₃-6, and (c) S₇EE₃-6 formulations.

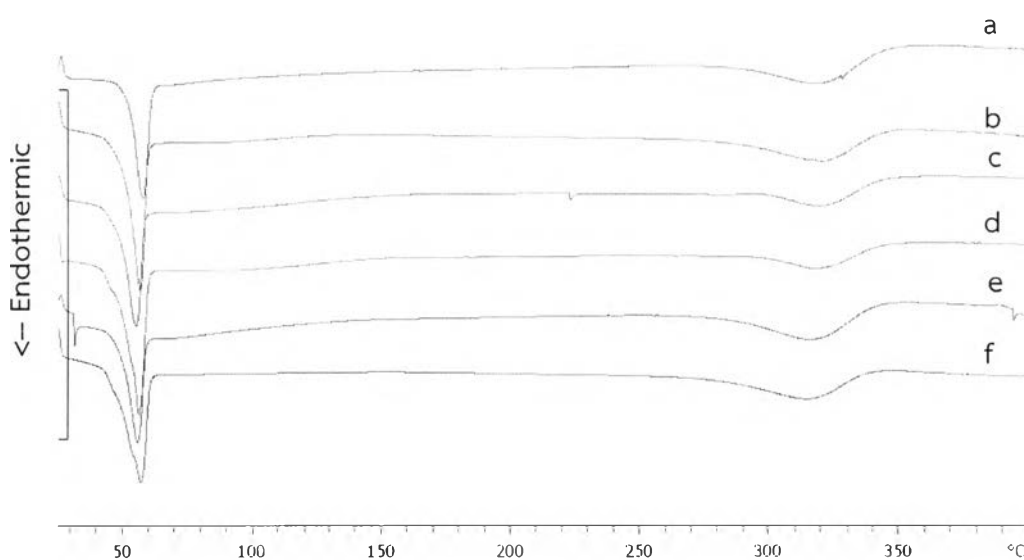


Figure IV-26 DSC thermograms of pulverized formulations (without BSA) after JM process from model DSC822^E; (a) S-4, (b) S-6, (c) S₇C₃-4, (d) S₉EE₁-4, (e) S₇C₃-6, and (f) S₇EE₃-6 formulations.



The DSC thermograms of blank pulverized formulations by JM were shown in **Figure IV-26**, and there was no significant peak shift occurring. A sharp endothermic peak at around 54-58°C and a broad one below 350°C which were exhibited melting point peak of PEG and recrystallization peak of S, respectively.

To compare whether milling processes causing physicochemical change, S-6 formulation containing BSA was used as a model. Thermograms of samples obtained from a matrix film preparation process and three milling were quite the same, especially at the sharp peak around 51-55 °C which resulted from melting peak of PEG as shown in **Figure IV-27**. Only CM had a small endothermic peak around 37-38°C on the thermogram. The thermograms, adjusting the DSC scanning rate by reducing from 10°C/min to 3°C/min as illustrated in **Figure IV-28**, also showed the similar result. Therefore, such a peak did not a result from mechanical stress of the machine. Additionally, this peak was unlikely to be peak of absorbed water because %moisture content in the S-6 formulation from different milling processes was not statistically significant ($p>0.05$) and at such temperature, water would not evaporate.



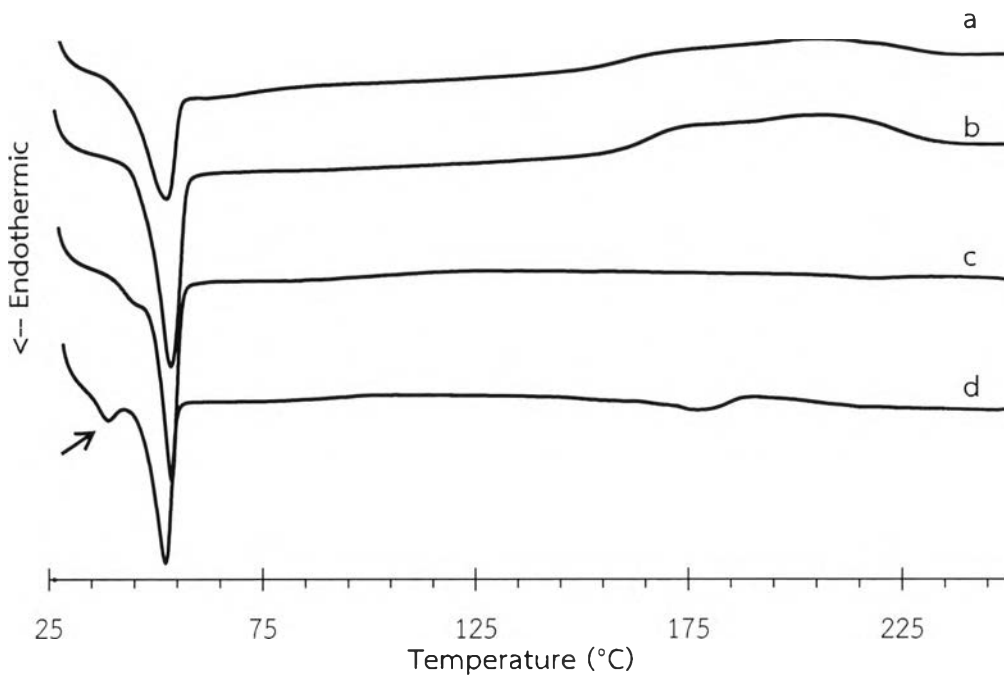


Figure IV-27 DSC thermograms from model DSC6200 of BSA incorporated S-6 formulation after making a film (a), JM (b), PBM (c), and CM (d) processes.

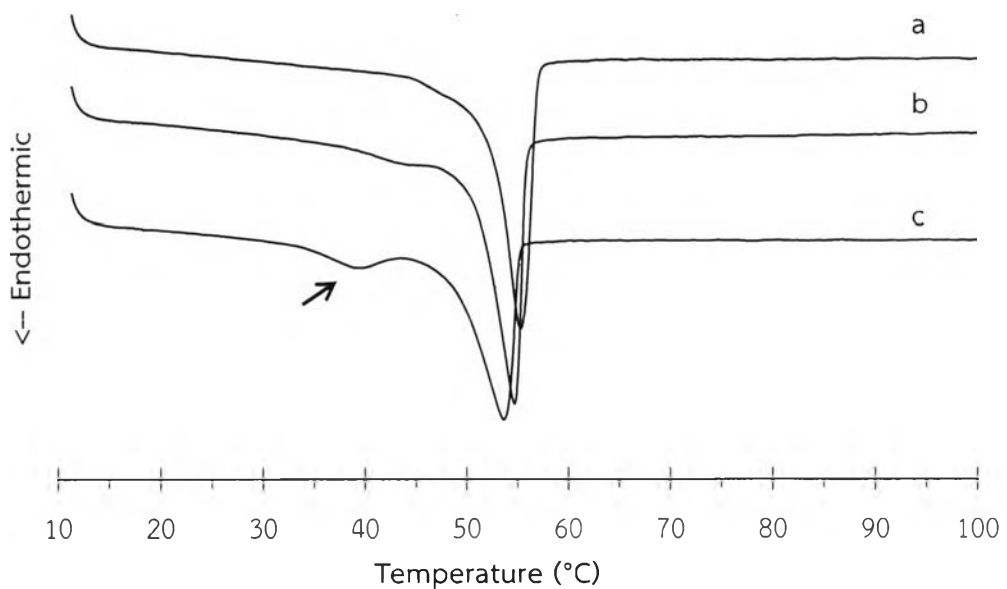


Figure IV-28 DSC thermograms of BSA incorporated S-6 formulations after pulverization with a reducing scanning rate of $3^{\circ}\text{C}\cdot\text{min}^{-1}$ from model DSC6200; (a) JM, (b) PBM, and (c) CM processes.

4.3. Fourier transform infrared (FT-IR) spectroscopy

The FT-IR spectra of BSA including raw materials used are illustrated in Figure IV-29. In FT-IR spectrum of native BSA, a broad band at 3425 cm^{-1} was attributed to N-H stretching vibration (188), and two characteristic peaks were observed at 1668 cm^{-1} (C=O stretching), 1563 cm^{-1} (in-plane N-H bending and C-N stretching of amide bond) attributed to amide I and amide II band, respectively (188, 189). Moreover, C-H stretching (CH_3) at 2976 cm^{-1} , asymmetric C-H stretching (CH_2) at 2942 cm^{-1} and 2886 cm^{-1} (190), CH_2 bending (scissor) at 1461 cm^{-1} and symmetric stretching vibration of COO^- at 1405 cm^{-1} were observed (185, 188).

FT-IR spectrum of C demonstrated the broad band at around 3450 cm^{-1} which corresponded to N-H and O-H stretching as well as inter- and extra-molecular bonding of C molecule (191). Moreover, C-H stretching (CH_2) at 2913 cm^{-1} and NH_2 bending at 1614 cm^{-1} were detected, as well as 1433 cm^{-1} ascribed to CH_2 bending and vibration of primary hydroxyl group in polysaccharides (192, 193).

Next, EE exhibited 5 characteristic peaks in FT-IR spectrum at 1154, 1245, and 1274 cm^{-1} attributed to C-O stretching, as well as C=O stretching of ester at 1736 cm^{-1} (163). Additionally, C-H vibrations were located at 1395, 1467, and 2963 cm^{-1} , as well as dimethylamino groups of EE can be discerned at 2776 and 2825 cm^{-1} (163).

A presented three specific absorption peaks at 1121, 838, and 480 cm^{-1} which were assigned to symmetric Si-O stretching, asymmetric Si-O stretching, and Si-O bending vibration of silica, respectively (194).

FT-IR spectrum of PEG displayed a broad peak at about 3454 cm^{-1} due to OH stretching, a strong peak at 2895 cm^{-1} corresponded to C-H stretching, and sharp peaks at 1470 and 1340 cm^{-1} which were assigned to C-H bending. In the spectrum, there were also a strong band for O-H and C-O-H stretching vibration located at 1283 and 1114 cm^{-1} (195).



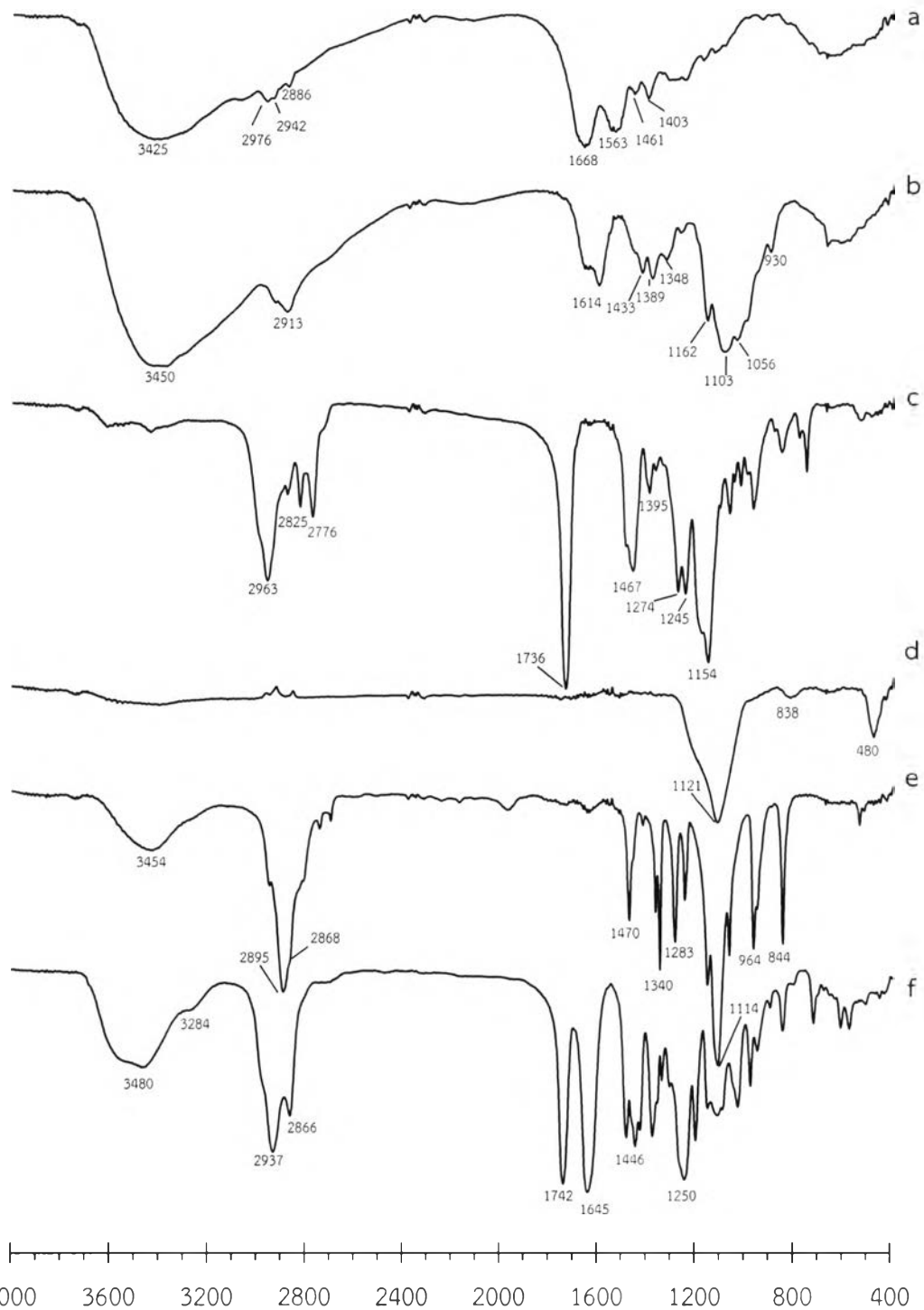


Figure IV-29 FTIR spectra of raw materials used; (a) native BSA, (b) C, (c) EE, (d) A, (e) PEG, and (f) S.



1515806291

For S powder, the FT-IR spectrum exhibited intermolecular hydrogen bond of O-H stretching at about 3480 cm^{-1} , C=O stretching of ester group at 1742 cm^{-1} , C=O stretching bond of tertiary amide at 1645 cm^{-1} , C-H₃ bending at 1446 cm^{-1} , and C-O stretching vibration at 1250 cm^{-1} (196, 197).

When physical mixtures of excipients and BSA were investigated using FT-IR spectroscopy, the specific characteristics peaks of main ingredients were presented. In S-6 spectrum (Figure IV-30a), peaks at 2949 cm^{-1} and 2896 cm^{-1} might be attributed to C-H stretching of S and PEG, respectively, while peak at 2866 cm^{-1} was either C-H stretching of S or PEG. In addition, two bands at 1746 and 1650 cm^{-1} assigning to C=O stretching of ester group were bonds from S. However, the later band was amide I bond of BSA, as well. Peaks below 1650 were probable mixture of peaks from S, PEG, and BSA.

For physical mixture of S₇C₃-6 formulation containing C, its FT-IR spectrum was not able to characterize the specific bands of C (Figure IV-30b), because these bands occurred at same region in spectrum from S.

On the other hand, spectrum of S₇EE₃-6 formulation composing of EE exhibited bands which originated from EE itself, such as bands at 2783 and 2837 cm^{-1} (Figure IV-30c). Furthermore, increasing of intensity at 1736 cm^{-1} comparing with that at 1650 cm^{-1} resulted in C=O stretching of ester in EE and S.



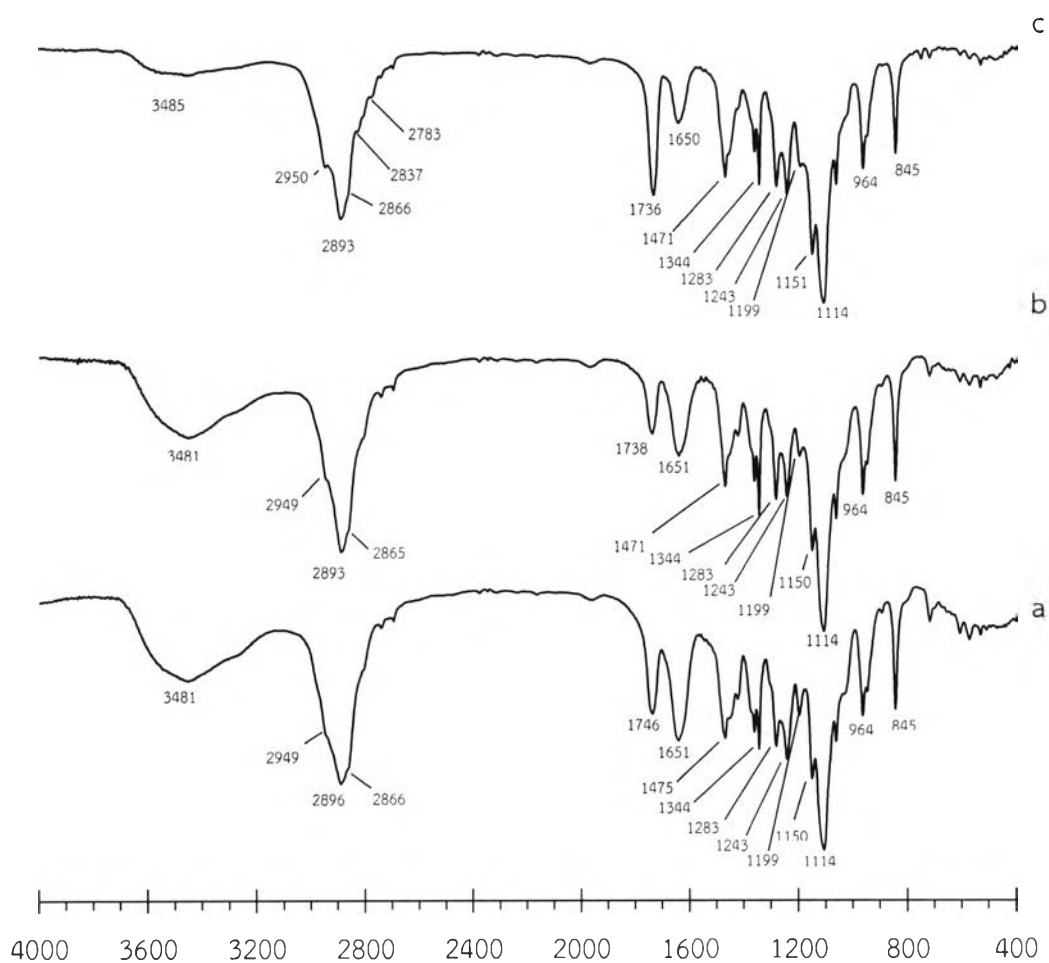


Figure IV-30 FTIR spectra of physical mixtures (with BSA); (a) S-6, (b) S₇C₃-6, and (c) S₇EE₃-6 formulations.

After being matrix film, FT-IR with ATR technique was used and the spectra of S-6, S₇C₃-6, and S₇EE₃-6 were shown in **Figure IV-31**. It was found that O-H stretching vibration at about 3480 cm⁻¹ disappeared in all three film formulations. One possible reason could be that moisture in polymer blends might evaporate during film preparation by heating in hot air oven. Additionally, changing of band intensity was observed at 1283 cm⁻¹, and decreasing the intensity might be resulted from hindrance or interaction with other ingredients when all ingredients were homogeneously melted.

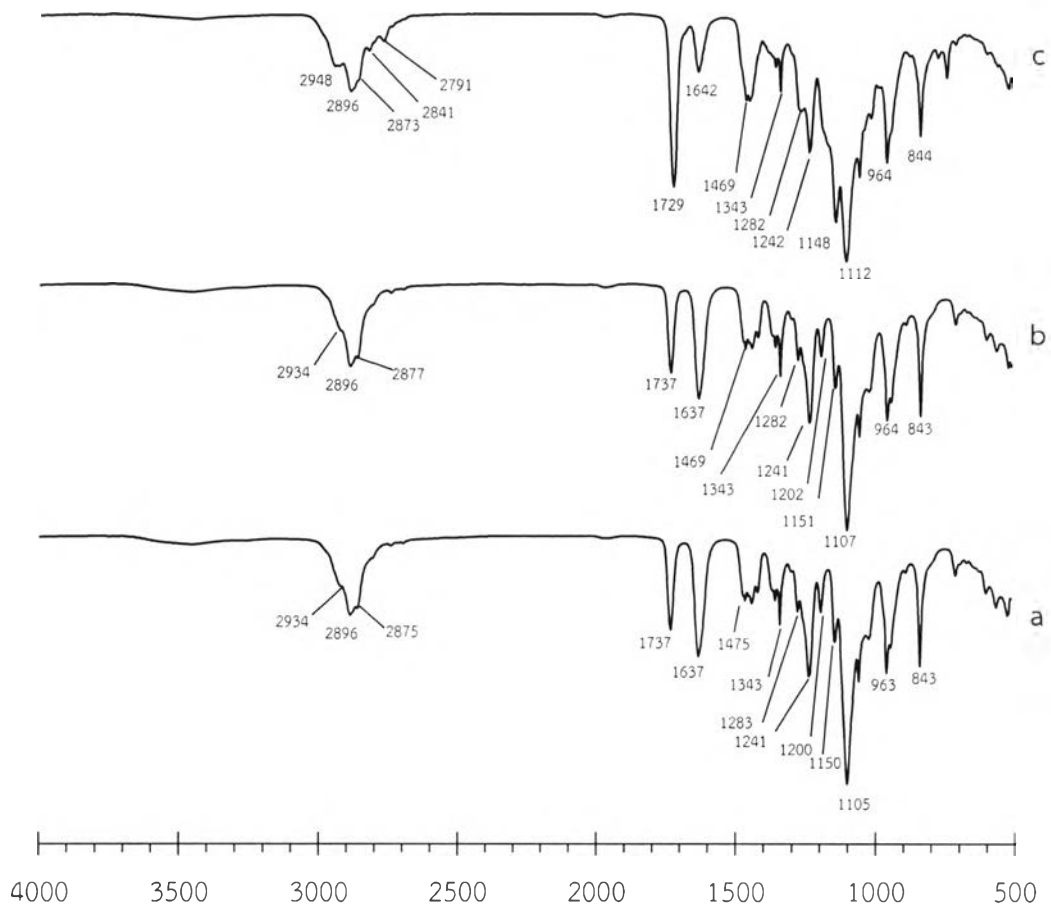


Figure IV-31 FTIR spectra of matrix film (without BSA) by using ATR technique; (a) S-6, (b) S₇C₃-6, and (c) S₇EE₃-6 formulations.

BSA incorporated formulations were finally pulverized by JM, CM, or PBM and FT-IR spectra are illustrated in **Figure IV-32**. All pulverized powders from different comminution processes demonstrated the same FT-IR spectra as the others, and such spectra were similar to spectra of film formulations. Therefore, it was likely that there was no interaction occurred on all production processes.

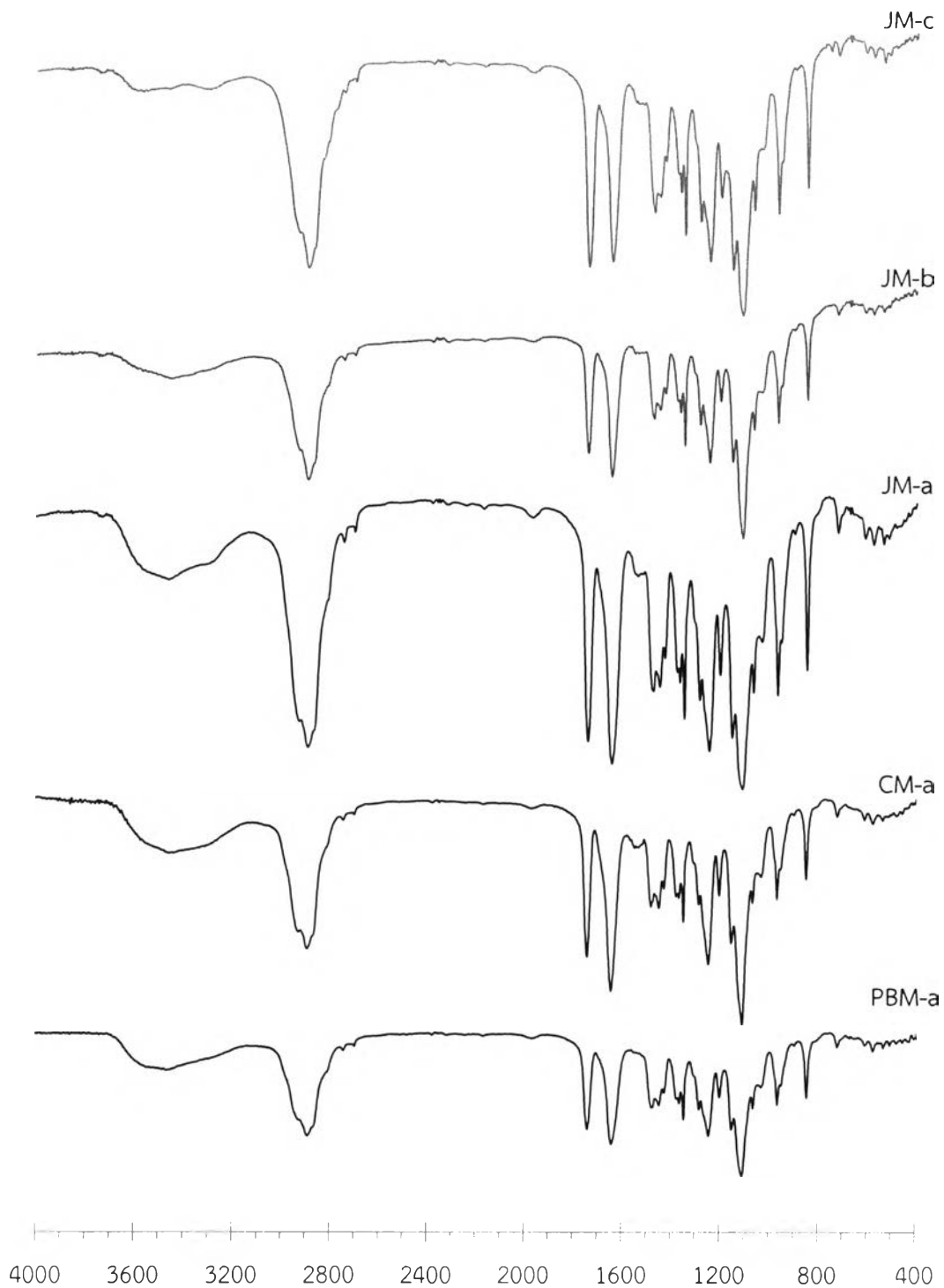


Figure IV-32 FTIR spectra of JM formulations of S-6 (JM-a), S_7C_3 -6 (JM-b), and S_7EE_3 -6 (JM-c), CM formulation of S-6 (CM-a), and PBM formulation of S-6 (PBM-a) incorporated with BSA.

4.4. X-ray powder diffractometry (XRPD)

The overlay in **Figure IV-33** demonstrates XRPD patterns of BSA and polymers used. Only PEG showed crystalline characteristics with two dominant diffraction peaks at $2\text{-theta} = 19.2^\circ$ and 23.3° (198), as the others exhibited halos. In addition, there were a few small diffraction peak at about 26.22° and 26.74° . The XRPD pattern of C exhibited halos with two broad bands at $2\text{-theta} \approx 10.6^\circ$ and 19.7° (195, 199). S and EE indicated an amorphous form (197, 200) with broad diffraction peak at $2\text{-theta} \approx 18.7^\circ$ and 17.2° , respectively. The XRPD peak of BSA also appeared an amorphous state with two broad peaks at $2\text{-theta} \approx 9.9^\circ$ and 19.3° (201).

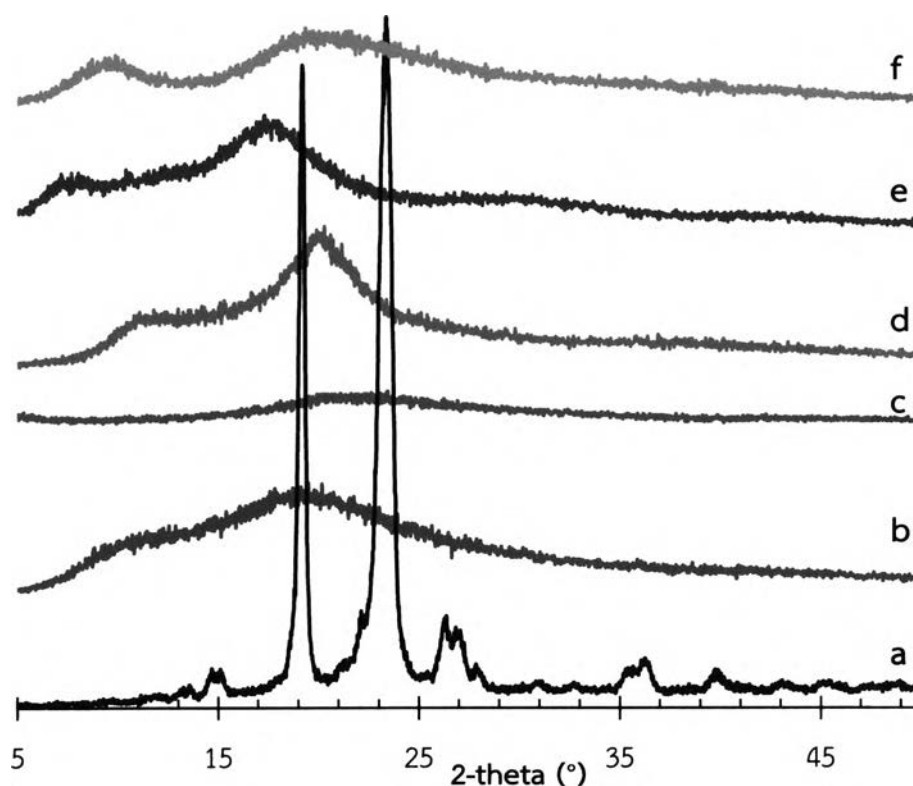


Figure IV-33 XRPD patterns of raw materials used; (a) PEG, (b) S, (c) A, (d) C, (e) EE, and (f) native BSA.

In XPRD patterns of three selected physical mixtures; S-6, S₇C₃-6, and S₇EE₃-6 formulations without BSA shown in **Figure IV-34**, the main characteristic peaks of PEG were still found with increased baseline which was resulted from summation with other polymer diffractions. At 2-theta value of around 19°, S-6, S₇C₃-6, and S₇EE₃-6 formulations exhibited different peak intensity as quite equal, lower, and slightly higher comparing to intensity at peak of 2-theta ≈ 23°, respectively.

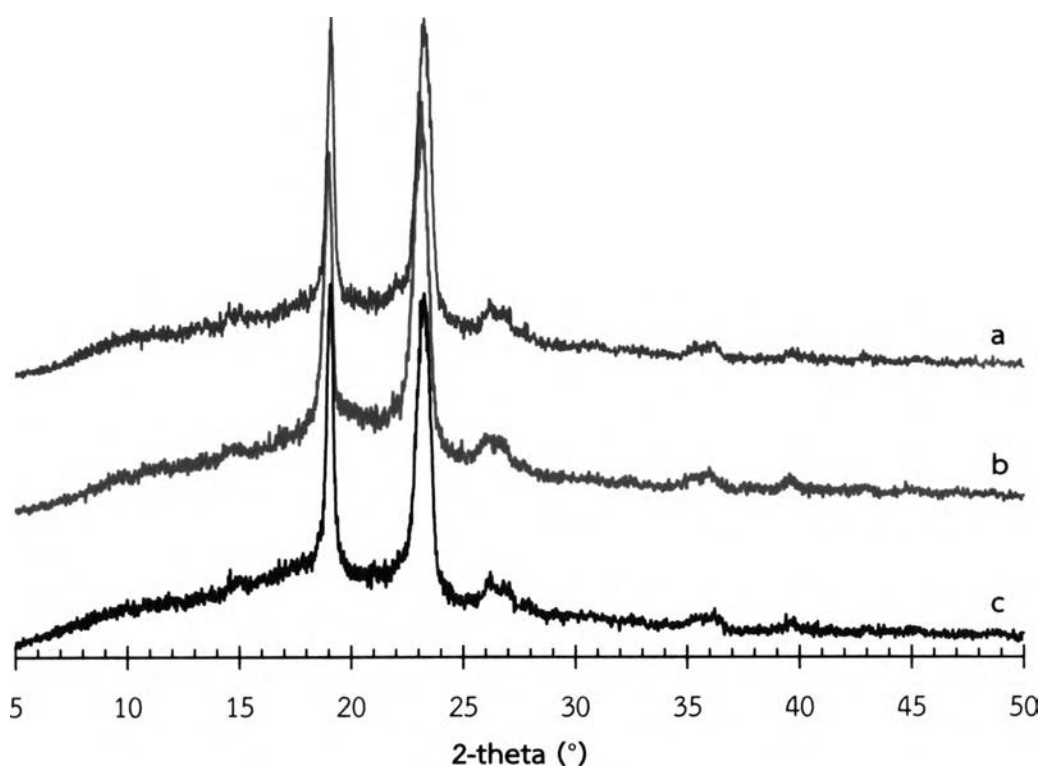


Figure IV-34 XRPD patterns of physical mixture formulations without BSA; (a) S-6, (b) S₇C₃-6, and (c) S₇EE₃-6 formulations.

After pulverization, the XRPD patterns of powders obtaining from JM process were similar to their physical mixtures (**Figure IV-35JM**) demonstrating that the crystallinity of PEG did not change by JM. On the other hand, the diffraction peak at 2-theta value of about 19° decreased when compared to diffraction patterns of physical mixtures in all S-6, S₇C₃-6, and S₇EE₃-6 powders after CM and PBM (**Figure IV-35CM** and **Figure IV-35PBM**). In addition, only of CM powder, two diffraction peaks around 2-theta $\approx 26^\circ$ seemed to be absent and became a small broad peak. It was possible that crystallinity of polymer may partially change to amorphous state under milling. This is consistent with the previous studies that pulverized chitosans undertaken by PBM or high energy nano ball mill exhibited amorphous state comparing to non-milled chitosan, indicating crystalline-amorphous transformation (191, 202). Furthermore, under CM in which temperature was much lower than the T_g of corresponding liquid, crystalline powder was readily transformed to amorphous one (203). Adrjanowicz and colleagues (135) reported that degree of crystallinity of furosemide decreased from 100% to 12% and 2% after 30 and 60 minutes under CM, respectively, and the XRPD diffraction peaks exhibited significant broadening peaks and considerably decreased intensity.

Together with XRPD pattern, the previous DSC results of CM powder could be speculated that the small endotherms emerging around 38°C was possibly the T_g of polymer resulting from partially transformation of crystalline PEG to amorphous state.



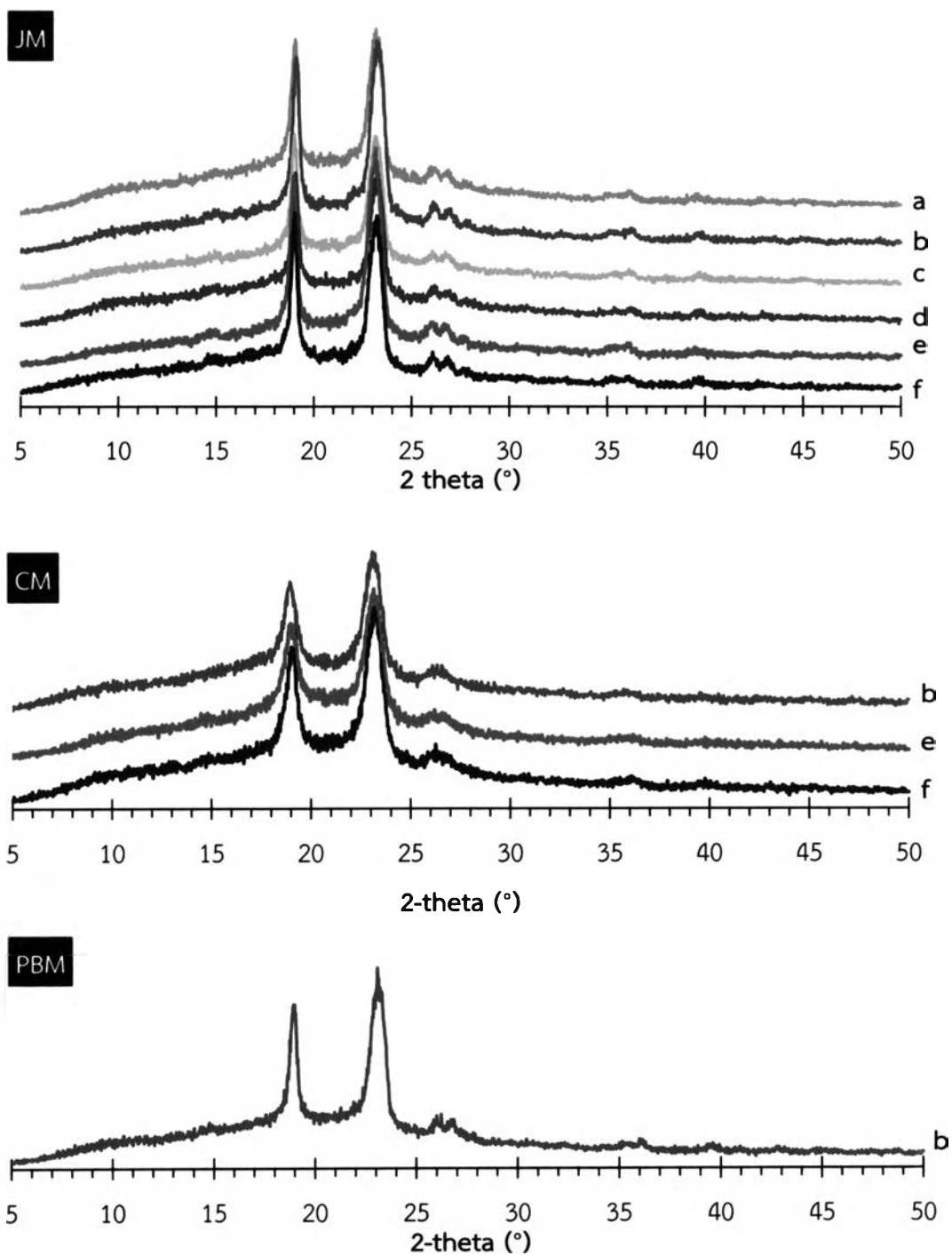


Figure IV-35 XRPD patterns of powder formulations without BSA which processed under different milling machines; JM, CM, and PBM of (a) S-4, (b) S-6, (c) S₇C₃-4, (d) S₉EE₁-4, (e) S₇C₃-6, and (f) S₇EE₃-6 formulations.

Additionally, in order to clarify the previous results, S-6 formulation incorporated with BSA was chosen. Overlaying XRPD diffractions of all ingredients used including BSA, physical mixture, and pulverized formulation receiving from JM, CM, and PBM were presented, as in **Figure IV-36**. Similar results were preserved.

In summary, it can be concluded that JM micronization may have no effect on polymorphic state of formulation, as CM and PBM have an influence on crystalline-amorphous transformation of polymer.



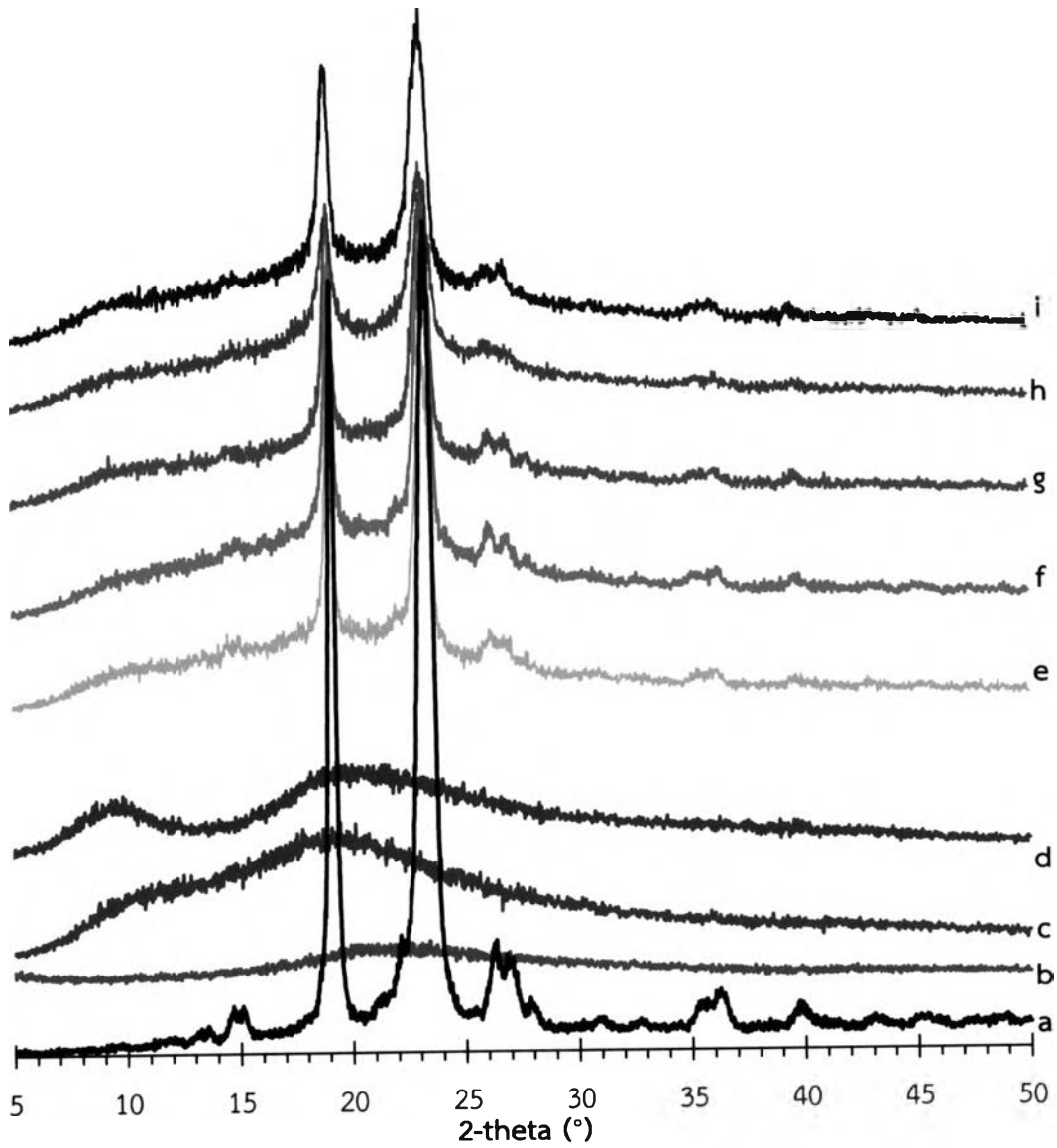


Figure IV-36 XRPD patterns of ingredients used and S-6 formulation containing BSA with different production processes; (a) PEG, (b) A, (c) S, (d) native BSA, (e) physical mixed, (f) JM (without BSA), (g) JM, (h) CM, and (i) PBM powder formulations.



5. Determination of mucoadhesive properties

5.1. *In vitro* mucoadhesive studies

As can be seen in **Figure IV-37**, by observing percentage of Brilliant Blue (BB) washed, all powder formulations could retain on the mucosa for 60 minutes except a control formulation (BB mixed with lactose powder) which could stay on the mucosa for more than 120 minutes. More than 75% of BB in all formulations was washed within 10 minutes except a control. Although there was no significant difference among control and powder formulations at any measuring time ($p>0.05$), comparing among the powder formulations, S_7C_3-4 , S_9EE_1-4 , S_7C_3-6 , and S_7EE_3-6 formulations had a tendency to better adherence to the mucosa than the others at the first 10 minutes.

Furthermore, as illustrated in **Table IV-5**, it was evident that blue color faded out with time increase in all formulations which was quite consistent with the amount of BB washed. After 120 minutes, there was still blue color stained on tissue, thus amount of BB on tissue was extracted by shaking in SNF. The results demonstrated that up to 8-13% of BB was found on the tissue after finishing the experiment which was not statistically significant ($p>0.05$) for all powder formulations.



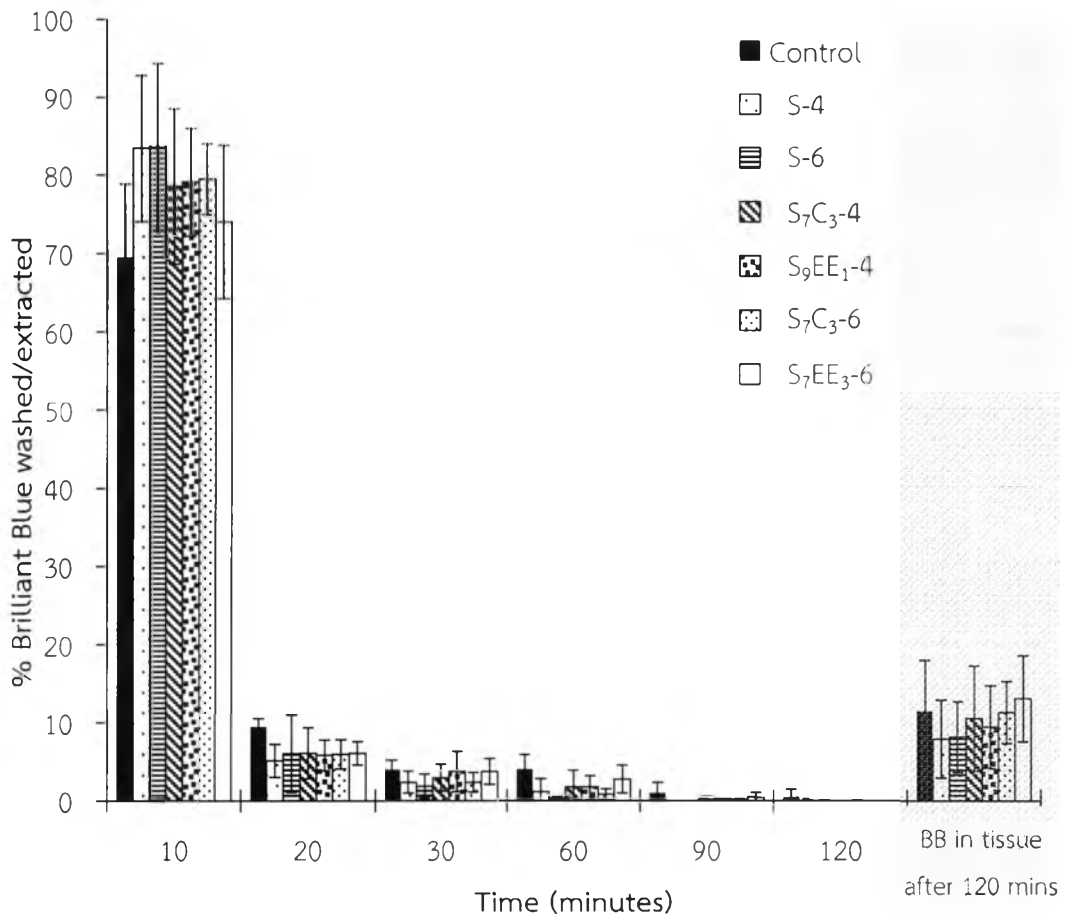
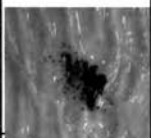
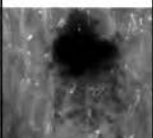
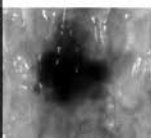
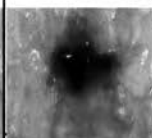
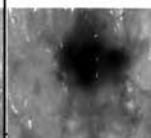
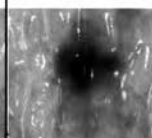
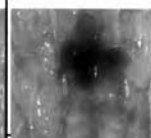
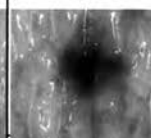
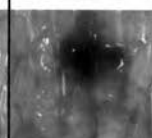
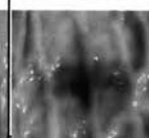
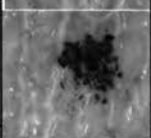

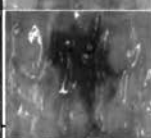
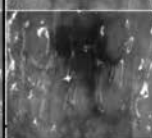
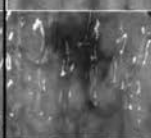
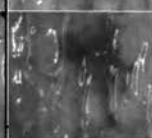
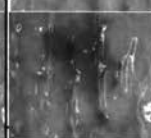
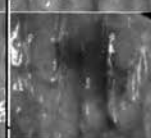
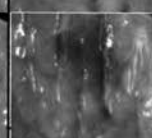
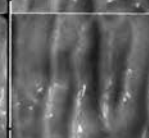
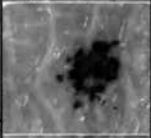

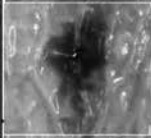
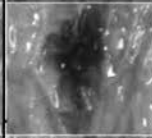
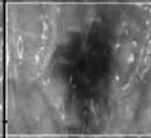
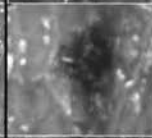
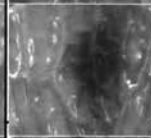
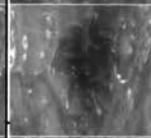
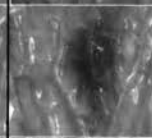
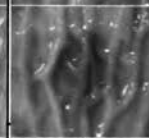
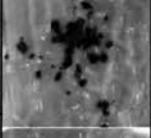


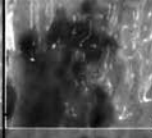

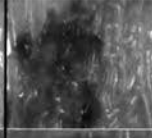
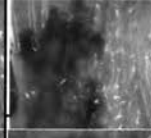
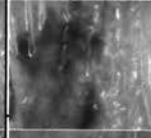
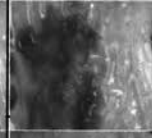
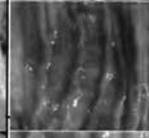
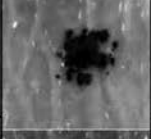



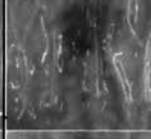
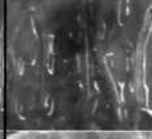
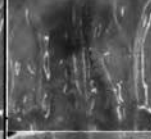
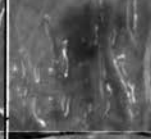
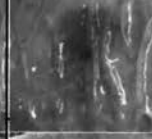
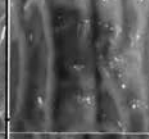
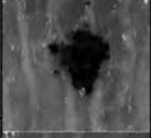

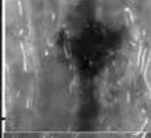

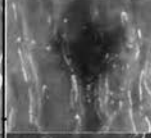

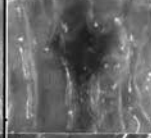
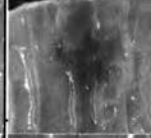
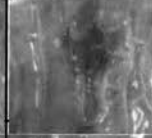
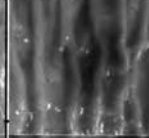
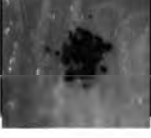
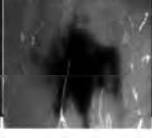
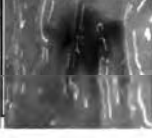
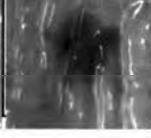
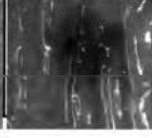
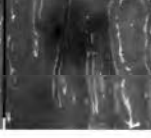
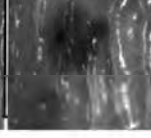
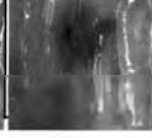
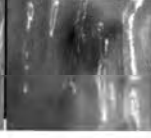
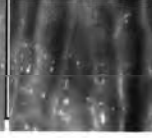


Figure IV-37 The percentage of BB in the formulations washed from porcine small intestine mucosa and extracted in tissue after 120 minutes (n=5).

Table IV-5 Mucoadhesive property of 6 powder formulations on porcine intestinal mucosa at different time intervals.

Formulation	Before incubation	After incubation	Time (minutes)							After 3 hrs. Shake
			10	20	30	45	60	90	120	
Control										
S-4										
S-6										
S ₇ C ₃ -4										
S ₉ EE ₁ -4										
S ₇ C ₃ -6										
S ₇ EE ₃ -6										

5.2. Viscosity evaluation

According to **Figure IV-38**, for SV-10 vibro viscometer, the viscosity was ranked $S_9EE_{1-4} > S_7C_3-6 > S_7C_3-4 > S-6 > S-4 > S_7EE_{3-6} > 8\%$ mucin dispersion (a control formulation). There was statistically significant between control and formulations as well as among formulations ($p < 0.05$). While for RV-1 Roto viscometer, the viscosity of $S_7C_3-4 > S_9EE_{1-4} > S-6 > S-4 > S_7C_3-6 > S_7EE_{3-6} > a$ control formulation were observed. Although the viscosity of a control group was significantly different from powder formulations ($p < 0.05$), viscosity of S-4 formulation was not statistically significant difference from S-6 and S_7C_3-6 formulations by using RV-1 Roto viscometer.

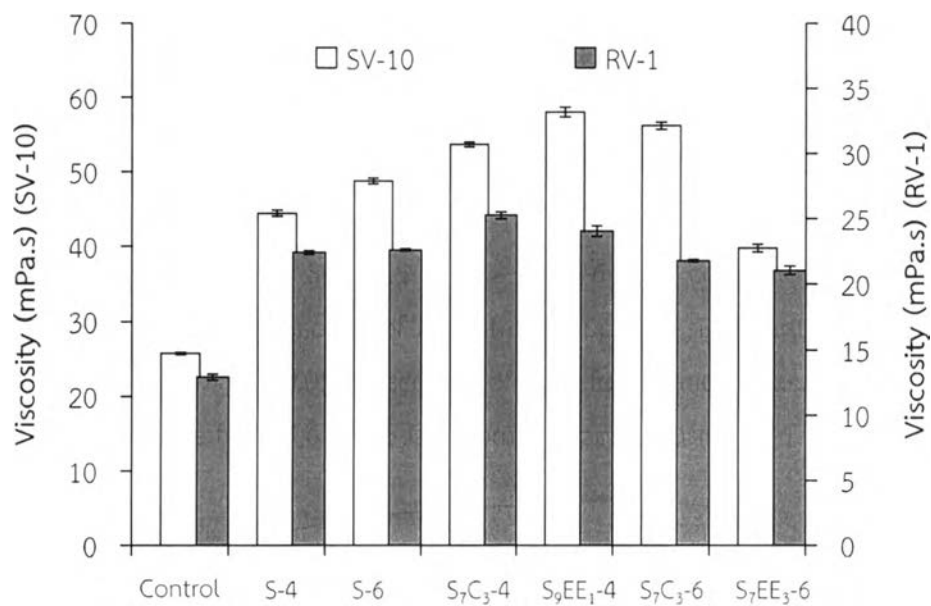


Figure IV-38 Viscosity of powders in 8% mucin dispersion by using SV-10 viscometer (□) and RV-1 Roto viscometer (■) ($n=3$).

5.3. Zeta potential evaluation

Zeta potentials, measured by Zetasizer, were -3.85, -4.54, -4.37, 2.74, -4.88, and 5.79 mV for S-4, S-6, S₇C₃-4, S₉EE₁-4, S₇C₃-6, and S₇EE₃-6 formulations in ultrapure water (dilution 1:10), respectively and then was -3.32, -3.61, -3.27, 0.42, 0.03, and 0.21 mV for 8% mucin dispersion and S-4, S-6, S₇C₃-4, S₉EE₁-4, S₇C₃-6, as well as S₇EE₃-6 formulations in 8% mucin dispersion (dilution 1:100) (Figure IV-39).

It was found that zeta potential of C containing formulations (S₇C₃-4 and S₇C₃-6) significantly increased and change to positive charge when they were dispersed in mucin dispersion compared to those in ultrapure water because of protonating and solubilizing of C in acidic medium (204, 205), while significant decreasing in zeta potential of EE containing formulations (S₉EE₁-4 and S₇EE₃-6) was observed. It might be because there was electronic charge interaction occurred between positive charge of EE and negative charge of mucin.

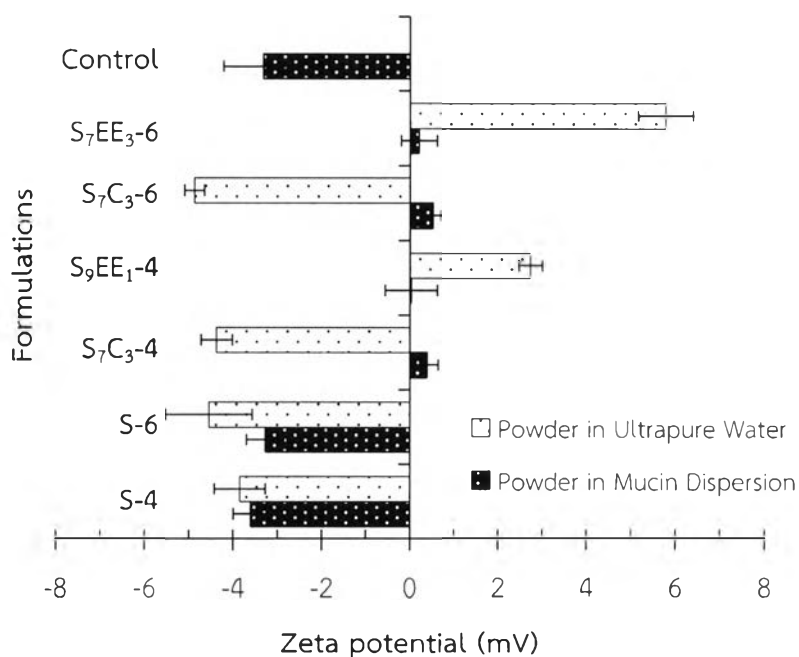


Figure IV-39 Zeta potential of formulations in ultrapure water (dilution 1:10) and in mucin dispersion (dilution 1:100) (n=5) as well as mucin dispersion used as a control (n=3).

According to the results in *in vitro* mucoadhesion, a control formulation showed the longest adhesion time on the mucosa. Such a result might make an explanation from dye's properties as well as the location where the dye was in the formulations and capability that dye could interact with mucosa. BB, a dye indicator, had a protein binding properties by sulfonate groups of dye containing negative charge that would interact with positive charge of protein (206) and stereo chemical interaction (207) as well as the binding strength was also depended on pH (208). In addition, in a control, dye was physically mixed with water soluble excipient, lactose, so it could directly and well interact with mucosa, while in test formulations, direct contact with mucosa less possibly occurred which resulted from dye incorporated in polymer matrix. Thus, the results from control group may not be reasonable to use in order to compare with other powder formulations. This limitation suggests that BB may not be an appropriate indicator for *in vitro* mucoadhesive test, and the other substance which is not binding to protein may be more suitable.

Additionally, better tendency to adhesion on mucosae from S_7C_3-4 , S_9EE_1-4 , S_7C_3-6 , and S_7EE_3-6 formulations comparing to S-4 and S-6 formulations may be resulted from C and EE polymer via ionic interaction. For C containing formulations, these results were also confirmed by viscosity evaluation and zeta potential which significantly increased comparing to a control, 8% mucin dispersion. There were repeatedly, collectively reported in literatures that positively-charged amino group of chitosan bond via ionic interaction with negatively-charged sialic acid and sulphonic acid of mucus (142).

On the other hand, in case of EE especially S_7EE_3-6 formulation, which contained 30% of EE demonstrated a better result in mucoadhesion, but decreased value in viscosity determination. Such decreased value when mixed with mucin dispersion may be explained by hydrogen bond formation. EE has tertiary amine group (166) which does not form hydrogen bond with itself but can form hydrogen bond with the other molecules by using lone pair electron on the nitrogen atom. When comparing to primary amine and secondary amine, tertiary amine exhibits weaker hydrogen bond. It was a review that hydrogen bond played an important role



in bringing polymers together, so viscosity of polymer dramatically decreased due to lessening of hydrogen bonding (209). Therefore, it may be assumed that ionic interaction from positive charge of EE and negative charge of mucin may be one of the mucoadhesive mechanisms but decreasing of viscosity was an influence of hydrogen bond formation.

In conclusion, powder formulations showed a promising mucoadhesion time up to 60 minutes, and one of the mechanisms of action may be ionic interaction.



6. Protein Integrity study

Proteins are complex macromolecule with specific functions which depend on the protein's structure. Changing or denaturation of the structure may have an influence on protein functions, so protein structural integrity is very essential. Several factors including method of preparing BSA or any proteins such as coacervation (210), lyophilization (211), spray drying (212), or milling (116) may affect protein stability. In the powder preparation, BSA was exposed to heat and mechanical stress which might cause denaturation of protein structure.

6.1. Sodium dodecyl sulfate polyacrylamide gel electrophoresis (SDS-PAGE) study

SDS-PAGE technique was utilized to determine the primary structure of protein by providing information related to molecular weight. The difference of protein molecular size has an influence on protein mobility in polyacrylamide gel (213). The protein with small molecular size faster mobilizes than larger molecular size.

The SDS-PAGE results demonstrated reference markers including BSA, native BSA, BSA incorporated film, and powder formulations, as well as blank powder formulations, as illustrated in **Figure IV-40** and **Figure IV-41**. The band in standard BSA solution, film formulations, and pulverized formulations showed in the same position with the BSA band in reference markers. Moreover, SDS-PAGE lane of BSA in powder formulations exhibited no additional or new bands that might assign to the aggregation or fragmentation. Therefore, it could be implied that the primary structure of BSA loaded in film and obtained after JM was generally maintained.



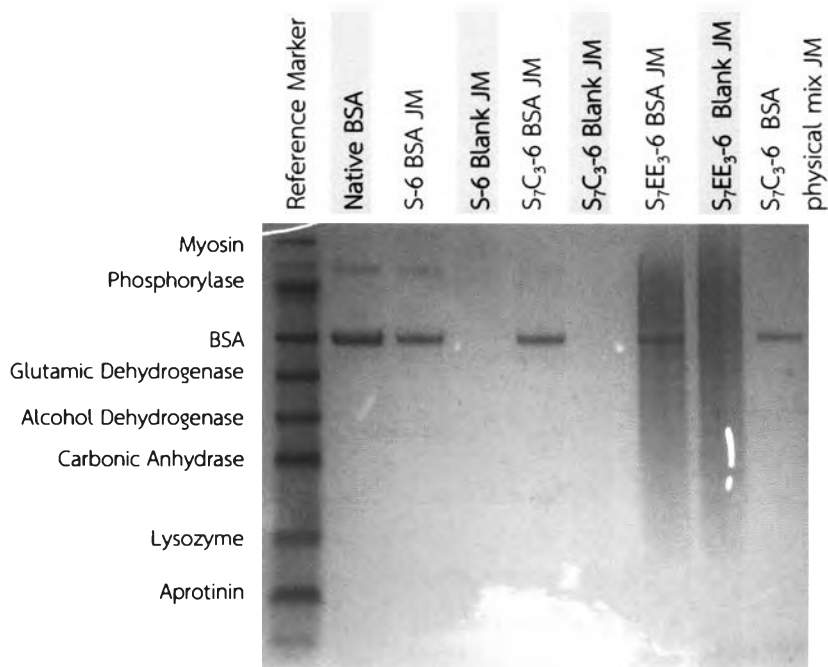


Figure IV-40 SDS-PAGE of reference marker, native BSA, and BSA incorporated as well as blank JM formulations.

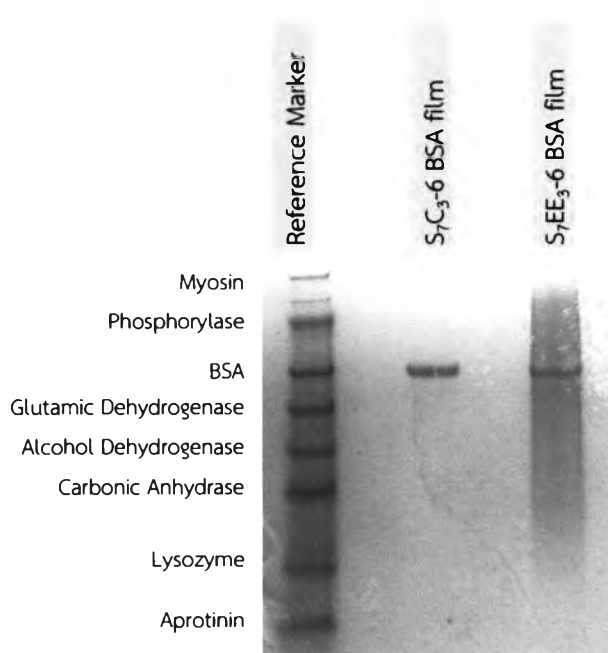


Figure IV-41 SDS-PAGE of reference marker and BSA incorporated film formulations.

6.2. BSA secondary structure determinations

In order to determine the conformational change of BSA under production processes, those CD spectra were compared with the native BSA. In this study, however, the tertiary structure in near-UV region (320-260 nm) was not observed due to high BSA concentration required (151). **Figure IV-42A** showed CD spectrum of native BSA solution with two negative valleys at 208 and 222 nm as well as a positive valley at 192 nm. These were assigned to α -helical structure of protein (212, 214). Moreover, almost all of the CD spectra of BSA in formulations after JM were shifted comparing to native BSA, except BSA in S-6 formulation (**Figure IV-42B**). These changes indicated secondary structural change of protein. However, CD spectrum of S-6 was not too similar to that of native BSA, but its spectrum below 220 nm was quite turbulent as shown in **Figure IV-42B**. It could be explained that turbulent spectra below 220 nm resulted from excipients used. The spectra of blank formulations shown in **Figure IV-42A** revealed turbulent valleys below 220 nm and there were reports that S and PEG could absorb UV light at < 260 nm (215) and < 200 nm (216), respectively.

Therefore, it can be concluded that only S-6 formulation was able to preserve secondary conformation of BSA, as the others could not under JM process.



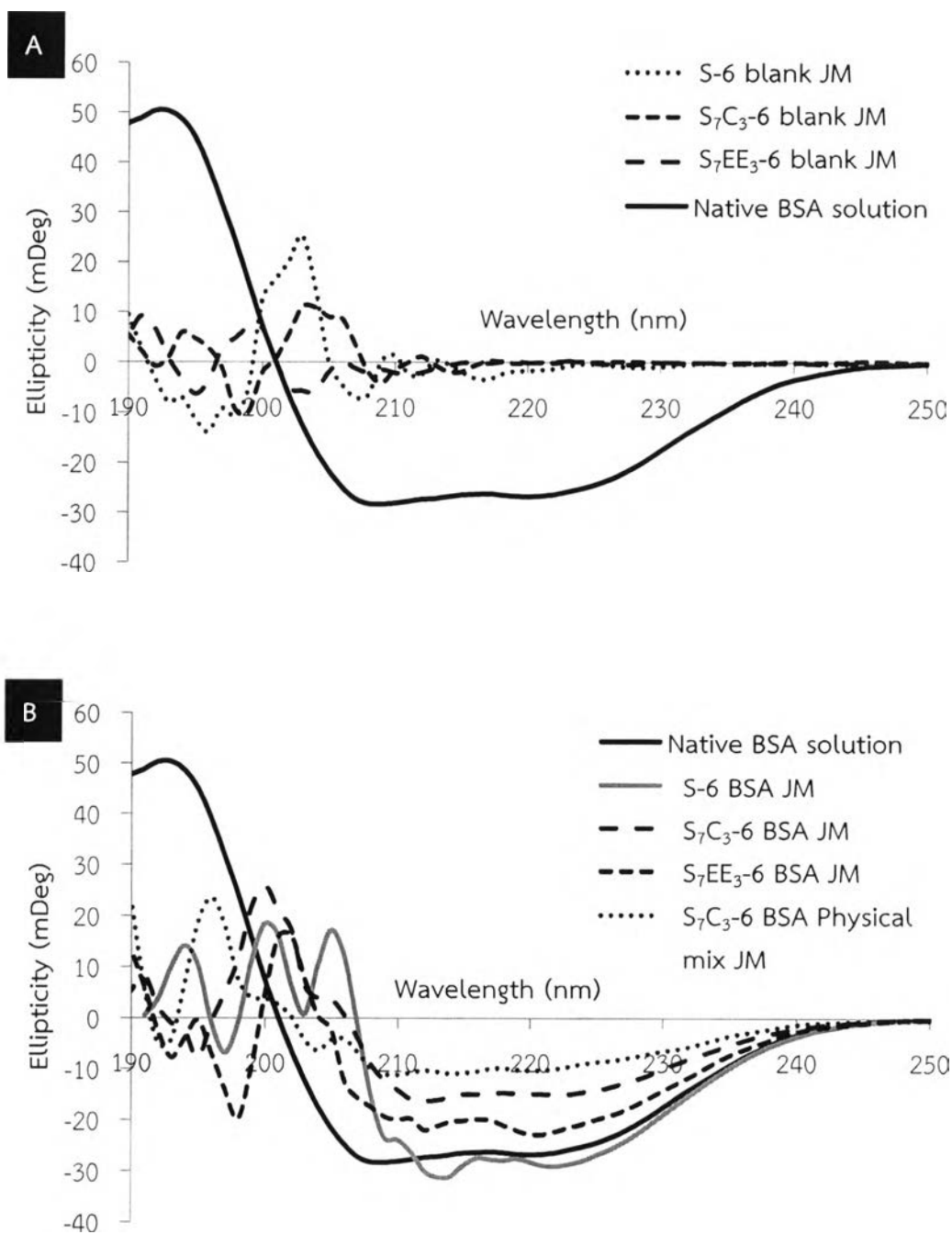


Figure IV-42 CD spectra of native BSA solution with blank formulations (A) and with BSA incorporated formulations (B) after JM process.

To compare the influence of production processes with different milling techniques, BSA incorporated S-6 formulation was selected as a model. As can be seen in **Figure IV-43**, CD spectra of film formulation and powders obtained from three milling techniques were quite the same as that of native BSA solution. These results indicated that production processes including milling techniques may not have any influence on secondary conformational change of BSA in S-6 formulation.

In summary, low energy process have no influence on protein integrity both primary and secondary structure at all, while micronization by milling have a potential effect on secondary structure except only S-6 formulation that could maintain secondary conformation of protein under millings.

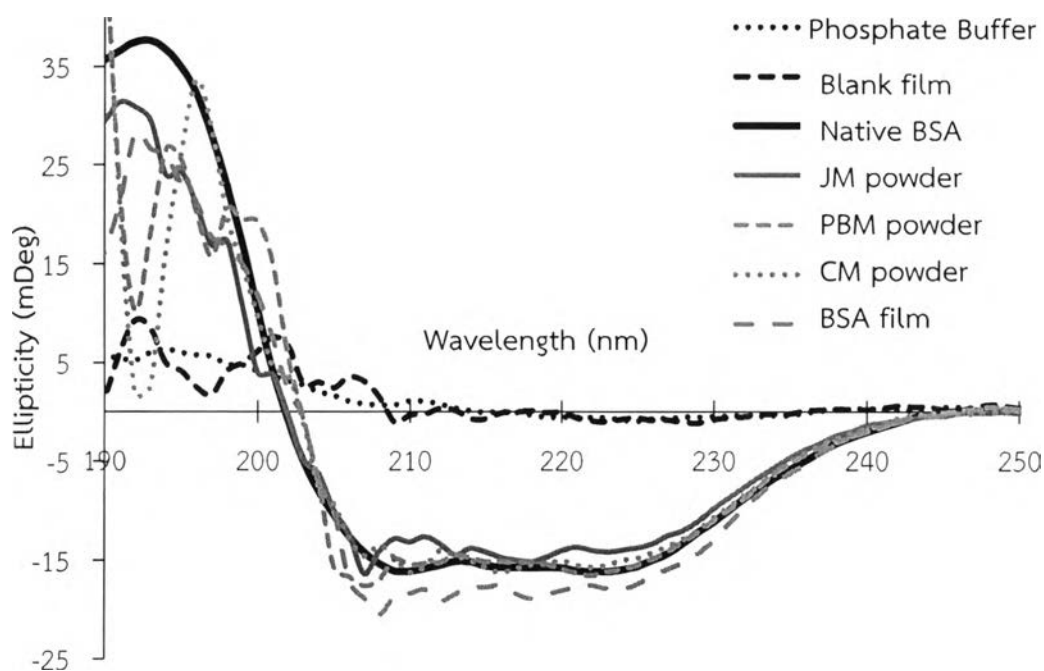


Figure IV-43 CD spectra of blank film, BSA film, native BSA and BSA incorporated S-6 formulations after JM, CM, and PBM processes.

7. BSA content determination

BSA content in powder formulations was examined by using bicinchoninic acid protein assay kit (BCA assay kit). As shown in **Figure IV-44**, S₇C₃-6 formulation and physical mixture of S₇C₃-6 formulation after JM exhibited low BSA content of 69.66±7.04% and 35.44±2.19%, respectively, as BSA content recovery in the other formulations was close to 100%. According to these results, there were two reasons for explaining such phenomena. First, high impaction force from micronization by JM may create insoluble fraction of protein (116) which have precluded use of colorimetric assays like BCA assay (217). Insoluble fraction of protein possibly resulted from heat creation during particle breakage, aggregate formation, and increased surface hydrophobicity of particle under JM (116). Second, an inappropriate formulation may not be able to preserve protein under such a condition resulting in insoluble fraction of protein, as can be seen in BSA content of pulverized film and pulverized physical mixture of S₇C₃-6 formulation.

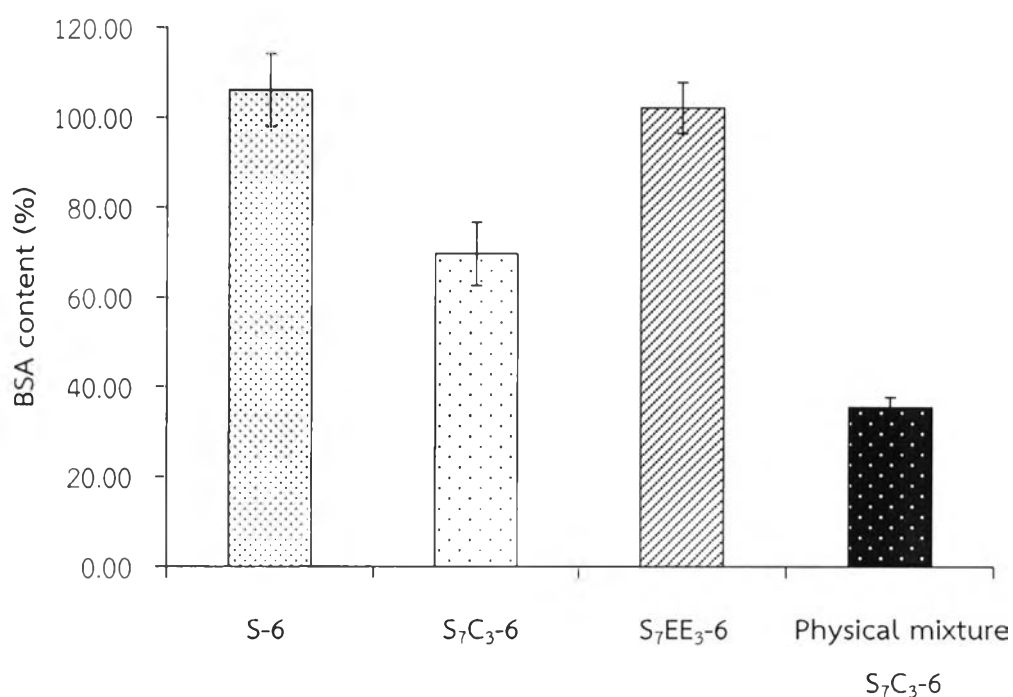


Figure IV-44 BSA content (%) in pulverized formulations after JM process (n=3).



Moreover, BSA content of film formulation and powder formulations obtaining from three milling processes were evaluated and the results are shown in **Figure IV-45**. The %BSA content in all formulations was within the range of 100%. It meant that in addition to JM, PBM and CM might not have any effect on the creation of insoluble fraction of protein during grinding processes of S-6 formulation. Moreover, the %BSA content of some processes was more than 100% which might result from not well homogeneous mixing of sample both before casting film and after milling as well as sampling. However, it was also found that there were differences in SD ranking from 32.08, 21.72, 17.69 and 7.26 of film, as well as powder from PBM, CM, and JM, respectively. The highest variation (SD=32.08) was observed in film formulation, while the lowest variation (SD=7.26) was obtained in JM formulation. From these results, it may be implied that although film preparation process was not uniformly mixed, micronization by JM enhanced homogenous mixing at the output (218).

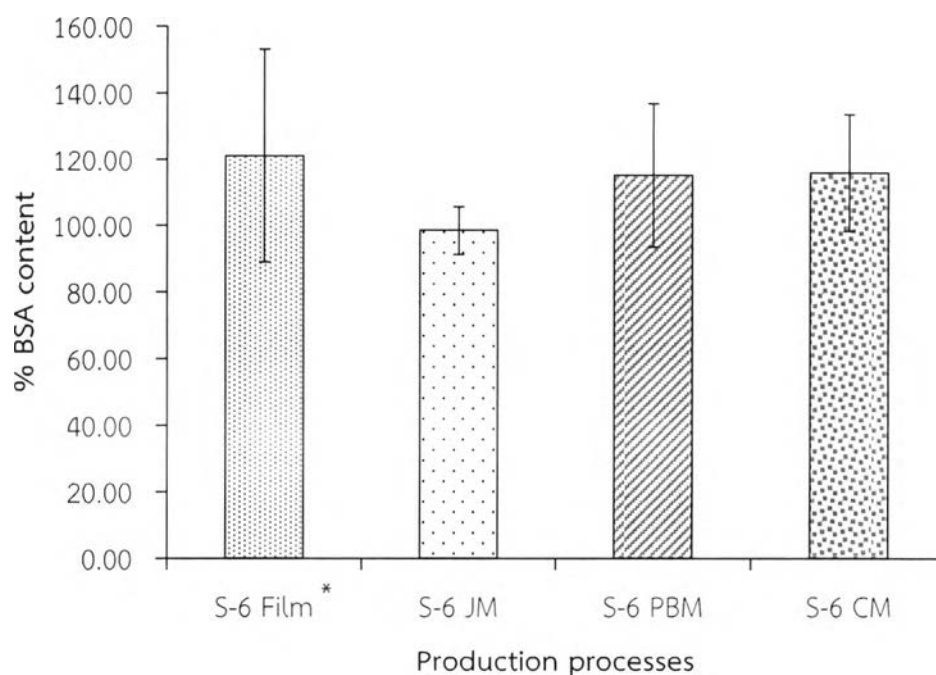


Figure IV-45 Percentage of BSA content in S-6 formulation with different production processes; film* (n=7), JM, PBM, and CM (n=5).

8. *In vitro* BSA release studies

The release of BSA from selected formulations (JM powder of S-6, S₇C₃-6, S₇EE₃-6, and physical mixed S₇C₃-6 formulations) was investigated using vertical Franz diffusion cells. A polyethersulfone membrane (Supor[®]) was selected as supporting membrane due to low albumin protein adsorption (153). The release profiles of different powder formulations through the membrane demonstrated non-linear release in **Figure IV-46**. The initial burst release was about 50% observed at 20 minutes, which might be because of small particle size and hydrophilic properties of excipients used. As clearance within nasal cavity normally is about 15-20 minutes (51), a fast release is necessary. For S-6 and S₇EE₃-6 formulations, approximately 70% of BSA released at 60 minutes, while both S₇C₃-6 formulations released up to 80% of available BSA in formulations at 30 minutes. For JM powder of physical mixed S₇C₃-6 formulations, this may be because BSA was not incorporated into a matrix resulting in spend shorter time diffusing through polymer matrix.

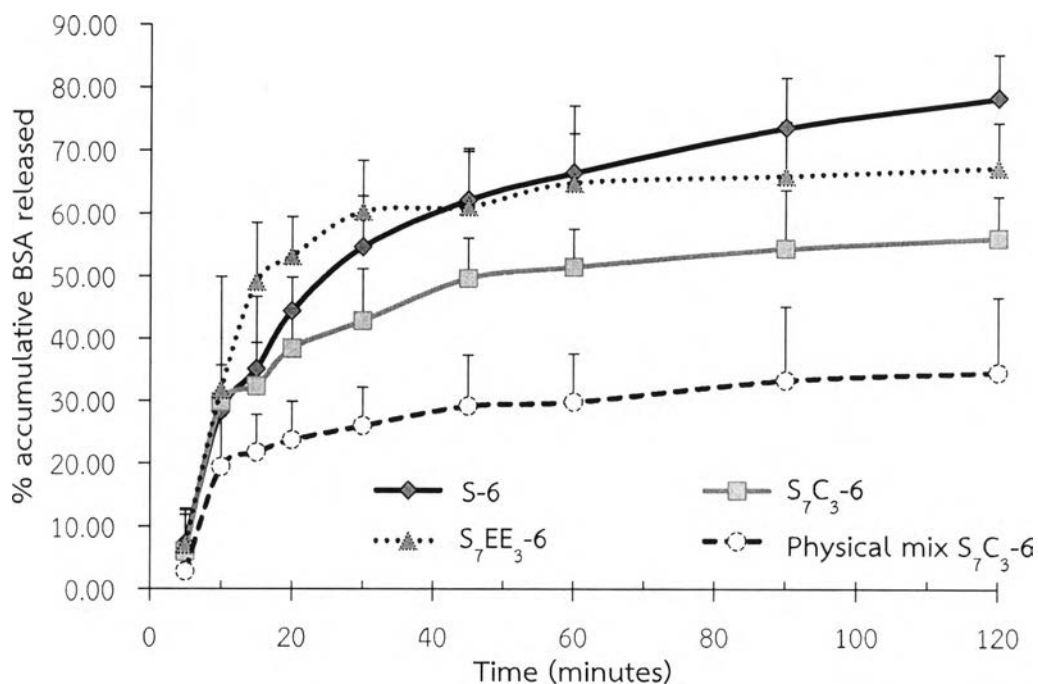


Figure IV-46 BSA release from the JM powder formulations (n=3).



Additionally, the release profiles of BSA formulations were fitted to various kinetic models including Zero order, First order, Higuchi, Korsmeyer-Peppas, Hixson-Crowell, and Weibull models. DDSolver program was used to calculate kinetic parameters of each model and a number of statistical criteria for determination the goodness of fit (154). The adjusted coefficient of determination (R^2_{adjusted}), Akaike Information Criterion (AIC), and Model Selection Criterion (MSC) were used to identify the goodness-of-fit. When comparing various models for the given data set, the model with the highest R^2_{adjusted} or MSC can be considered to be the better model, as the model with the smallest AIC value is the best fit (154, 219).

According to the calculated results in **Table IV-6**, when focusing on Franz cell no. 1 of S-6 formulation, R^2_{adjusted} ranking from highest to lowest was 0.9973, 0.8964, 0.8348, 0.8188, 0.6832, and -0.2166, of Weibull, Korsmeyer-Peppas, Higuchi, First order, Hixson-Crowell, and Zero order models, respectively, the similar results were observed in MSC. For AIC value, 25.3843, 57.5740, 60.9704, 61.8030, 66.8311, and 78.9426 of Weibull, Korsmeyer-Peppas, Higuchi, First order, Hixson-Crowell, and Zero order models, respectively, were observed. According to interpretation of three criteria, the release profile of S-6 formulation in Franz cell no.1 had the best goodness-of-fit with Weibull model. The same results were noted in Franz cell no. 2 and no.3 as well as others formulations as shown in **Table IV-6, IV-7, IV-8, and IV-9**. Therefore, the release data of all formulations had the best goodness-of-fit with Weibull model. There are several studies using Weibull model to compare the release profile of matrix type delivery system (220-222).

In addition, there are parameters presenting in Weibull equation. The location parameter, T_i , indicated the lag time before the onset of release which is about 4.4-7.1, 4.6-5.0, 4.8-8.9, and 4.7-9.9 minutes for JM powder of S-6, S_7C_3-6 , S_7EE_3-6 , and physical mixed S_7C_3-6 formulations, respectively. The shape parameter, β , described the release profiles as either exponential curve ($\beta=1$; case 1), sigmoidal curve with upward curvature following by a turning point ($\beta>1$; case 2), or parabolic curve with a steeper initial and then consistent with the exponential ($\beta<1$; case 3) (220).



Therefore, β values less than 1 for all formulations indicated that the release profiles were more pronounced parabolic shapes.

Moreover, to discern the drug release mechanism, the β value was used as an indicator for describing the mechanism of drug transport through the polymer matrix because this parameter was linearly relevant to the exponent n of power law (223). All formulations held the β value less than 0.75, which demonstrated Fickian diffusion (223). However, additional confirmation could be acquired from the diffusion component (n) in Korsmeyer-Peppas model with less than 0.5 indicating to Fickian diffusion (219).

In summary, release kinetic of BSA in all formulations was fitted to Weibull model with parabolic shape and their release mechanism was Fickian diffusion.



Table IV-6 *In vitro* release results of model fitting for S-6 formulation; k_0 = the release constant in zero-order model, k_1 = the release constant in first-order model, k_H = the release constant in Higuchi model, k_{KP} = the release constant in Korsmeyer-Peppas model, n = the diffusional exponent, k_{HC} = the release constant in Hixson-Crowell model, α = the scale parameter, β = the shape, T_i = the location parameter.

Models	Parameter	S-6 Formulation		
		No.1	No.2	No.3
Zero order	k_0	0.9460	0.9340	0.7580
	R^2	-0.2166	0.0247	0.4724
	$R^2_{adjusted}$	-0.2166	0.0247	0.4724
	AIC	78.9426	78.1304	71.2523
	MSC	-0.4183	-0.1972	0.4171
First order	k_1	0.0270	0.0260	0.0150
	R^2	0.8188	0.8902	0.8524
	$R^2_{adjusted}$	0.8188	0.8902	0.8524
	AIC	61.8030	58.4779	59.7886
	MSC	1.4861	1.9864	1.6909
Higuchi	k_H	8.8750	8.7180	6.9180
	R^2	0.8348	0.8604	0.9001
	$R^2_{adjusted}$	0.8348	0.8604	0.9001
	AIC	60.9704	60.6321	56.2744
	MSC	1.5786	1.7471	2.0814
Korsmeyer-Peppas	k_{KP}	14.8090	12.7840	7.0350
	n	0.3750	0.4070	0.4960
	R^2	0.9093	0.8958	0.9001
	$R^2_{adjusted}$	0.8964	0.8809	0.8859
	AIC	57.5740	60.0038	58.2703
	MSC	1.9560	1.8169	1.8596
Hixson-Crowell	k_{HC}	0.0080	0.0070	0.0040
	R^2	0.6832	0.7882	0.7686
	$R^2_{adjusted}$	0.6832	0.7882	0.7686
	AIC	66.8311	64.3867	63.8329
	MSC	0.9274	1.3299	1.2415
Weibull	α	4.9750	7.0430	7.9230
	β	0.4570	0.5430	0.4790
	T_i	4.7090	4.4700	7.1340
	R^2	0.9980	0.9870	0.9851
	$R^2_{adjusted}$	0.9973	0.9827	0.9801
	AIC	25.3843	43.2660	43.1619
	MSC	5.5326	3.6766	3.5383



Table IV-7 *In vitro* release results of model fitting for S₇C₃-6 formulation; k_0 = the release constant in zero-order model, k_1 = the release constant in first-order model, k_H = the release constant in Higuchi model, k_{kp} = the release constant in Korsmeyer-Peppas model, n = the diffusional exponent, k_{HC} = the release constant in Hixson-Crowell model, α = the scale parameter, β = the shape, T_i = the location parameter

Models	Parameter	S ₇ C ₃ -6 Formulation		
		No.1	No.2	No.3
Zero order	k_0	0.7520	0.6760	0.569
	R^2	-0.7219	-0.8683	-0.2556
	$R^2_{adjusted}$	-0.7219	-0.8683	-0.2556
	AIC	76.5388	76.5238	71.7507
	MSC	-0.7657	-0.8473	-1.3858
First order	k_1	0.0160	0.0130	0.0090
	R^2	0.3561	0.0361	0.2415
	$R^2_{adjusted}$	0.3561	0.0361	0.2415
	AIC	67.6858	70.5677	67.2149
	MSC	0.2180	-0.1855	-0.8819
Higuchi	k_H	7.1430	6.4880	5.3700
	R^2	0.7250	0.5540	0.6911
	$R^2_{adjusted}$	0.7250	0.5540	0.6911
	AIC	60.0298	63.6305	59.1301
	MSC	1.0687	0.5853	0.0165
Korsmeyer-Peppas	k_{p}	14.1860	14.0030	9.2840
	n	0.3320	0.3120	0.3660
	R^2	0.8938	0.7576	0.7667
	$R^2_{adjusted}$	0.8786	0.7230	0.7333
	AIC	53.4669	60.1437	58.6046
	MSC	1.7979	0.9727	0.0749
Hixson-Crowell	k_{HC}	0.0040	0.0040	0.0030
	R^2	0.0815	-0.2276	0.0928
	$R^2_{adjusted}$	0.0815	-0.2276	0.0928
	AIC	70.8829	72.7442	68.8258
	MSC	-0.1373	-0.4273	-1.0608
Weibull	α	4.8520	3.8100	5.4710
	β	0.3500	0.2520	0.2780
	T_i	4.6760	4.9990	5.0000
	R^2	0.9834	0.9873	0.9610
	$R^2_{adjusted}$	0.9778	0.9831	0.9480
	AIC	38.7741	35.5953	44.5003
	MSC	3.4304	3.7003	1.6420



1515806291

Table IV-8 *In vitro* release results of model fitting for S₇EE₃₋₆ formulation; k_0 = the release constant in zero-order model, k_1 = the release constant in first-order model, k_H = the release constant in Higuchi model, k_{kp} = the release constant in Korsmeyer-Peppas model, n = the diffusional exponent, k_{HC} = the release constant in Hixson-Crowell model, α = the scale parameter, β = the shape, T_i = the location parameter.

Models	Parameter	S ₇ EE ₃₋₆ Formulation		
		No.1	No.2	No.3
Zero order	k_0	0.9360	0.8050	0.7390
	R^2	-1.7846	-0.8649	-0.3865
	$R^2_{adjusted}$	-1.7846	-0.8649	-0.3865
	AIC	84.5210	80.3223	77.9214
	MSC	-1.2463	-0.8454	-0.5490
First order	k_1	0.0380	0.0210	0.0160
	R^2	0.4127	0.2310	0.4050
	$R^2_{adjusted}$	0.4127	0.2310	0.4050
	AIC	70.5133	72.3492	70.3069
	MSC	0.3101	0.0405	0.2970
Higuchi	k_H	9.1450	7.7360	7.0430
	R^2	0.2307	0.4792	0.6136
	$R^2_{adjusted}$	0.2307	0.4792	0.6136
	AIC	72.9430	68.8423	66.4233
	MSC	0.0401	0.4301	0.7285
Korsmeyer-Peppas	k_{kp}	24.6160	17.1770	12.9570
	n	0.2570	0.3050	0.3510
	R^2	0.6717	0.6851	0.7087
	$R^2_{adjusted}$	0.6248	0.6401	0.6671
	AIC	67.2795	66.3142	65.8798
	MSC	0.6694	0.7110	0.7889
Hixson-Crowell	k_{HC}	0.0100	0.0050	0.0040
	R^2	0.1817	-0.0440	0.1982
	$R^2_{adjusted}$	0.1817	-0.0440	0.1982
	AIC	73.4986	75.1012	72.9924
	MSC	-0.0216	-0.2653	-0.0014
Weibull	α	2.1030	2.0940	5.4370
	β	0.2470	0.1750	0.3800
	T_i	4.9970	8.9890	4.8680
	R^2	0.9760	0.9878	0.8405
	$R^2_{adjusted}$	0.9680	0.9837	0.7873
	AIC	45.7461	39.0777	62.4597
	MSC	3.0620	3.7373	1.1689



1515806291

Table IV-9 *In vitro* release results of model fitting for S₇C₃-6 physical mixture; k_0 = the release constant in zero-order model, k_1 = the release constant in first-order model, k_H = the release constant in Higuchi model, k_{KP} = the release constant in Korsmeyer-Peppas model, n = the diffusional exponent, k_{HC} = the release constant in Hixson-Crowell model, α = the scale parameter, β = the shape, T_i = the location parameter.

Models	Parameter	S ₇ C ₃ -6 physical mixture Formulation		
		No.1	No.2	No.3
Zero order	k_0	0.5180	0.4140	0.2810
	R^2	0.3835	-1.7511	-1.6134
	$R^2_{adjusted}$	0.3835	-1.7511	-1.6134
	AIC	64.7273	70.2617	65.3463
	MSC	0.2614	-1.2342	-1.1829
First order	k_1	0.0080	0.0060	0.0030
	R^2	0.6726	-1.1661	-1.3447
	$R^2_{adjusted}$	0.6726	-1.1661	-1.3447
	AIC	59.0314	68.1099	64.3696
	MSC	0.8943	-0.9951	-1.0744
Higuchi	k_H	4.7500	4.0530	2.7590
	R^2	0.9183	0.1688	-0.1027
	$R^2_{adjusted}$	0.9183	0.1688	-0.1027
	AIC	46.5432	59.4901	57.5802
	MSC	2.2819	-0.0374	-0.3200
Korsmeyer-Peppas	k_{KP}	5.3800	11.1930	8.8340
	n	0.4700	0.2500	0.2130
	R^2	0.9211	0.6109	0.3384
	$R^2_{adjusted}$	0.9098	0.5554	0.2439
	AIC	48.2244	54.6574	54.9818
	MSC	2.0951	0.4996	-0.0313
Hixson-Crowell	k_{HC}	0.0020	0.0020	0.0010
	R^2	0.5891	-1.3578	-1.4336
	$R^2_{adjusted}$	0.5891	-1.3578	-1.4336
	AIC	61.0753	68.8731	64.7047
	MSC	0.6672	-1.0799	-1.1116
Weibull	α	12.7310	3.4500	4.6320
	β	0.4520	0.0700	0.0200
	T_i	4.7630	9.9440	5.0000
	R^2	0.9759	0.9837	0.8095
	$R^2_{adjusted}$	0.9679	0.9783	0.7460
	AIC	39.5332	28.1098	45.7779
	MSC	3.0608	3.4493	0.9914



9. *In vitro* permeation studies

9.1. *In vitro* permeation

Powder formulations obtained from JM process were used because of low variability of BSA content comparing to the others and availability of equipment. Moreover, all JM formulations were in appropriate particle size range for intranasal preparation and exhibited no physicochemical interactions. Although S-6 formulation did not have the best mucoadhesive properties, it was easily prepared as matrix film due to quite good flowability of polymer blend showing passable to poor flowability of pulverized formulation, and importantly, was able to maintain secondary structure of BSA. Therefore, S-6 powder formulation, which incorporated with FITC-BSA as an indicator and was pulverized by JM, was selected as a test powder sample, and native FITC-BSA solution used as a control sample.

The permeation profiles in olfactory tissue (OLF) were demonstrated in **Figure IV-47**. FITC-BSA in solution formulation revealed better permeation than powder formulation with the increasing time. At the end of experiment of 120 minutes, %accumulative amounts permeated were $13.75 \pm 0.41\%$ and $9.70 \pm 1.52\%$, from solution and powder formulations, respectively ($p < 0.05$). However, amounts permeated in both samples were not significantly different at time 0-90 minutes ($p > 0.05$).



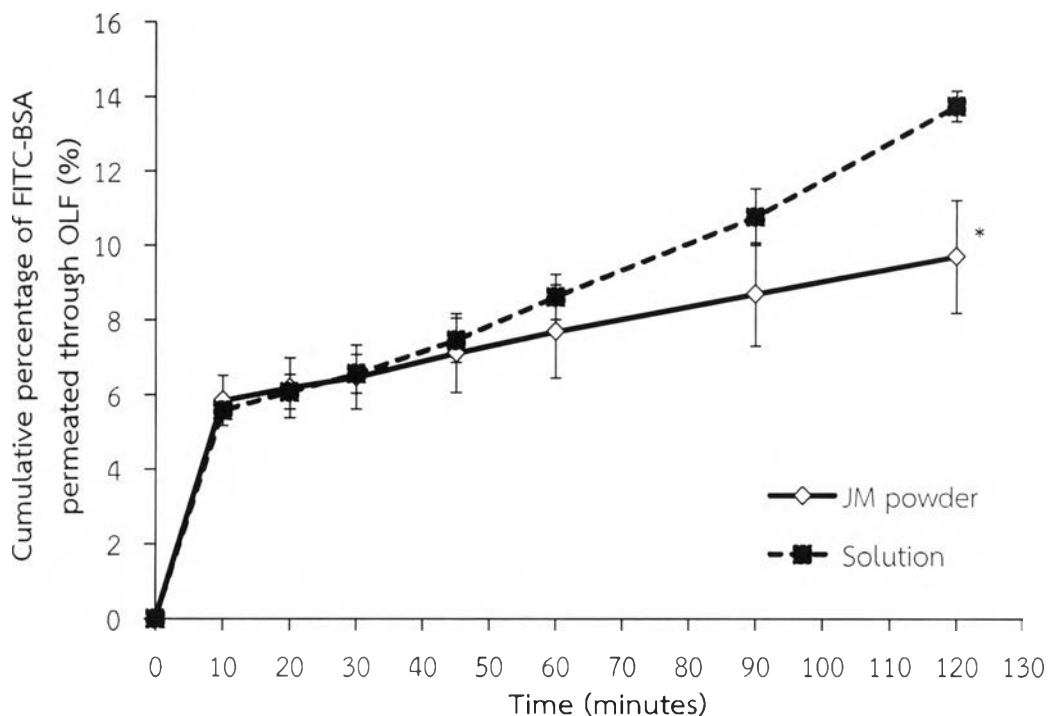


Figure IV-47 Cumulative percentage of FITC-BSA permeated through OLF (n=3). (* = statistically significant difference at $p < 0.05$ compared to solution formulation).

In respiratory mucosae (RES) as illustrated in **Figure IV-48**, FITC-BSA permeation profiles were quite similar to both powder and solution formulations with accumulative percent permeated of $10.46 \pm 0.98\%$ and $9.75 \pm 0.58\%$ at 120 minutes, respectively. There was no statistically significant difference between %accumulative amount of permeant of powder and solution formulations ($p > 0.05$), except the results at first 10 minutes.

In summary, permeability of BSA across both OLF and RES of powder formulation was quite the same as solution formulation conducting by Franz diffusion cell. However, nasal solution preparation generally could maintain on the mucosa for only about 15-20 minutes due to MCC (51), while according to the previous results from mucoadhesive property determination, powder formulation could retain on the mucosa for about 60 minutes. Therefore, it may be assumed that more protein from powder formulation practically permeated compared to solution upon application.

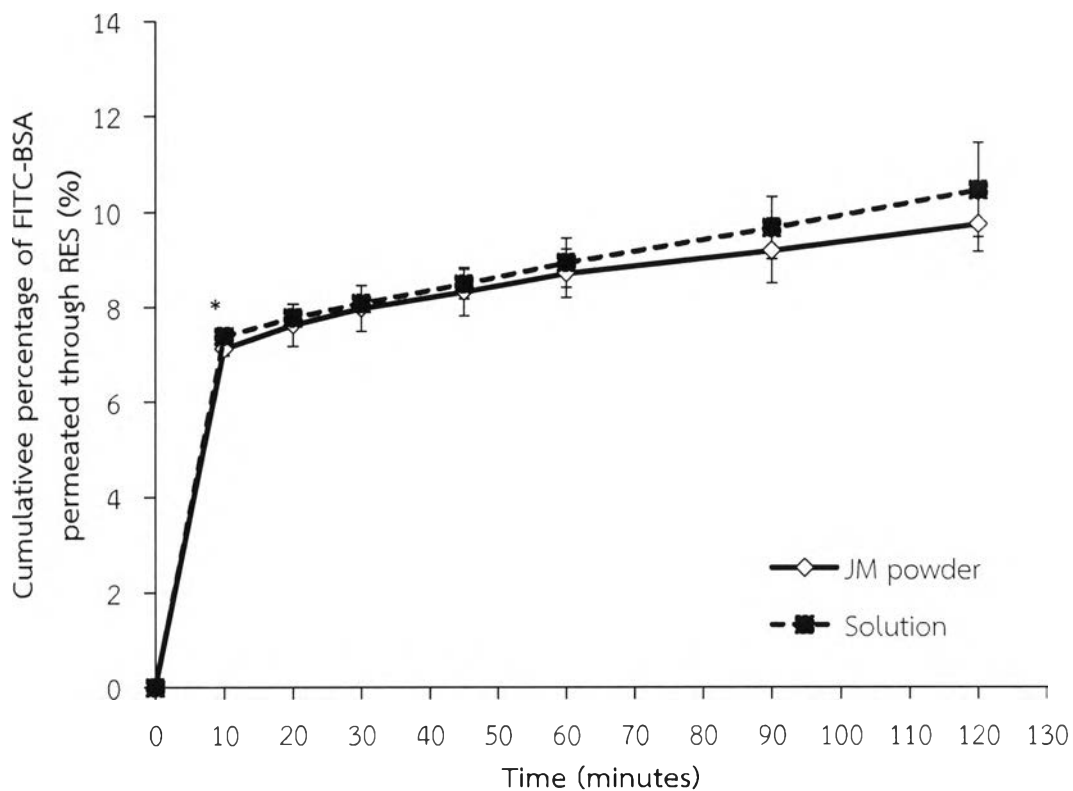


Figure IV-48 Cumulative percentage of FITC-BSA permeated through RES (n=5). (* = statistically significant difference at $p < 0.05$ compared to solution formulation).

Furthermore, the recovery amounts of FITC-BSA which were still on the mucosae in the donor compartments of Franz diffusion cells and did not permeate were evaluated after ending permeation study. Figure IV-49 showed the %FITC-BSA recovered of $92.15 \pm 4.53\%$ and $88.43 \pm 4.05\%$ from powder and solution formulations in OLF, respectively, which was no statistical significance ($p > 0.05$). When amounts of FITC-BSA recovered and amounts in the permeant were combined, the results were close to 100% in both formulations.

While the recovery amounts in RES were $72.92 \pm 7.87\%$ and $93.04 \pm 4.06\%$ of S-6 powder and solution formulations, respectively, as shown in Figure IV-50. Significant difference of those values was observed at $p < 0.05$.

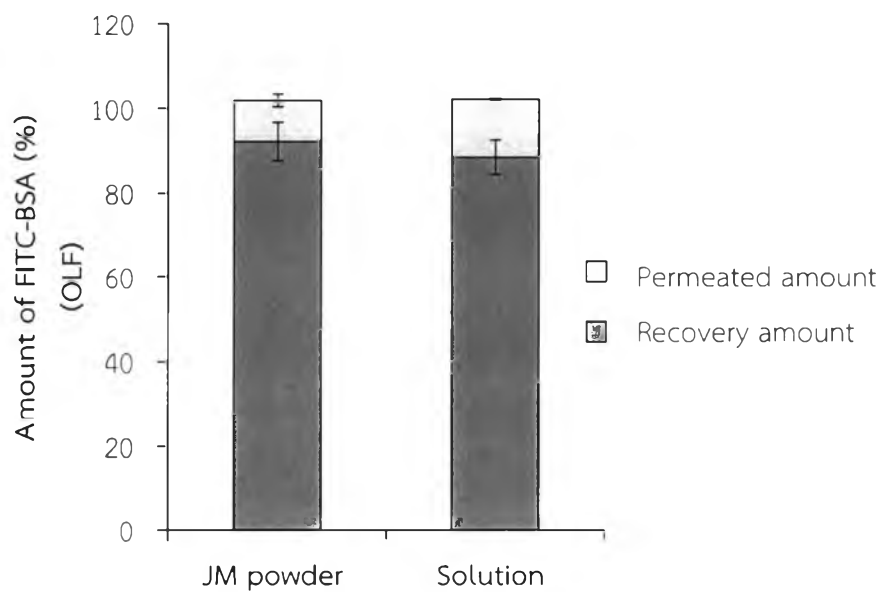


Figure IV-49 Permeated and recovery amount of FITC-BSA in permeation study through OLF (n=3).

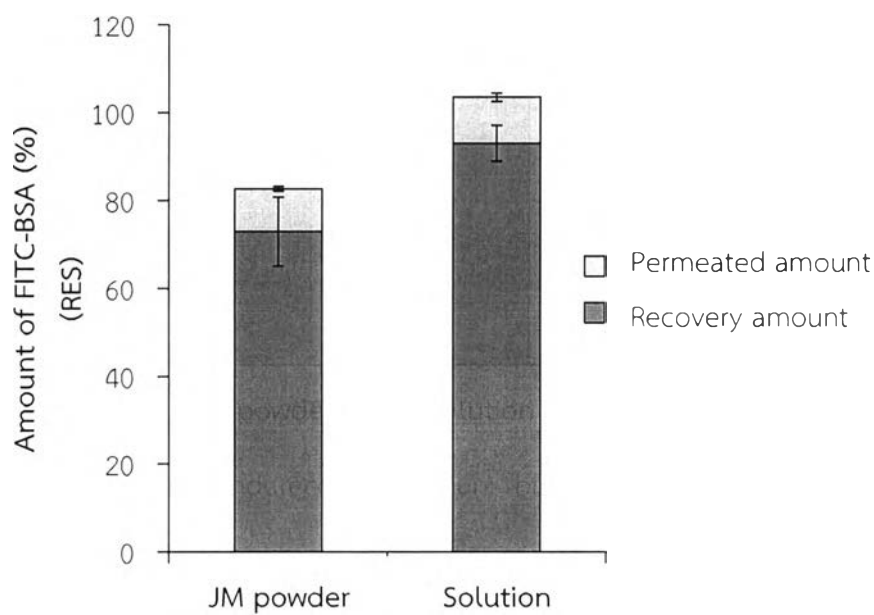


Figure IV-50 Permeated and recovery amount of FITC-BSA in permeation study through RES (n=5).



9.2. Tissue integrity by trans-epithelial electrical resistance (TEER) measurement

The mucosal tissues can be evaluated for their integrity during the experiment by several methods. One of the methods used was trans-epithelial electrical resistance (TEER) measurement (159). TEER value obtained from measuring the electrical resistance across the mucosal membrane. If TEER value decreased greater than 20% of the initial value, the tissue was identified to be poor integrity tissue (156) or TEER value is lower than $40 \Omega \cdot \text{cm}^2$, it was excluded (155).

In this study, two types of mucosal tissues were investigated the integrity of tissue during the whole process of permeation study by TEER measurement. As can be seen in **Figure IV-51** and **Figure IV-52**, it was found that both types of tissues still had strong integrity of during whole permeation process with TEER value reduction of 9-15% and 4-17% in OLF and RES, respectively, after ending the experiments. Moreover, TEER values which measured in both test sample (powder formulation) and control sample (solution formulation) were not statistically significant at all measuring time interval ($p > 0.05$). Additionally, there was a report that porcine nasal mucosa could remain viable for up to 8 hours after excision (155).



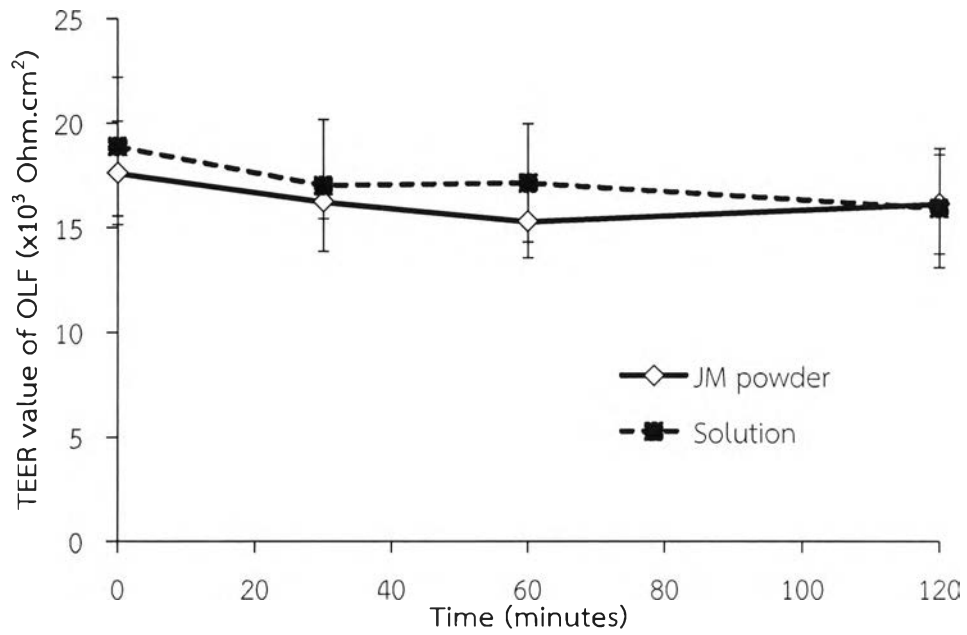


Figure IV-51 TEER value of OLF during permeation studies (n=3).

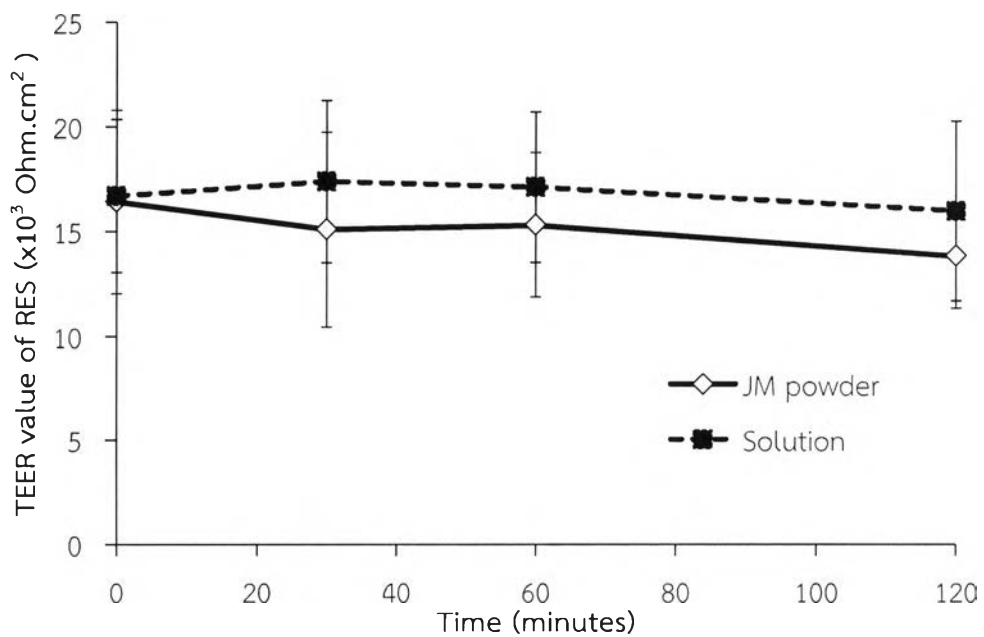


Figure IV-52 TEER value of RES during permeation studies (n=5).



1515806291

9.3. Histomicroscopic examination

Histomicroscopic analysis was examined morphological changes of mucosae after contact with formulations for 120 minutes, and hematoxylin and eosin (H&E) staining technique was utilized. As can be seen in **Figure IV-53 (C-F)**, the overall structure of the OLF of both solution and powder formulations were well preserved, without evident of ulceration, hemorrhage, and necrosis of mucosa comparing to a control group (**Figure IV-53 (A-B)**) and the similar results were observed in RES, as shown in **Figure IV-54**. Moreover, these results were also in consistent with TEER measurement. Thus, it can be concluded that powder formulation would be safe to nasal mucosa.

Furthermore, H&E sections of the mucosae were also observed under fluorescent light microscope. The results demonstrated that there were some FITC-BSA staying in the tissue after finishing an experiment of both JM powder and solution formulation, as shown in **Figure IV-55 (C-F)** and **Figure IV-56 (C-F)**, respectively. The results also revealed that FITC-BSA moved from epithelial tissue and then passed to lamina propria which high amount of FITC-BSA would accumulate around vessels supplying the mucosae before entering to buffer solution in receptor compartment. In OLF, fluorescent light intensity from JM powder formulation was comparable to that from solution, while in RES, higher fluorescent intensity was examined from powder formulation (**Figure IV-56 (C-D)**) when comparing to solution formulation (**Figure IV-56 (E-F)**). Although in OLF, the summation of FITC-BSA amount in permeant and recovery amount in donor compartment was close to 100%, there was some FITC-BSA observed in the tissue. Because thickness of OLF was only about 300-400 micron, amount of FITC-BSA in that mucosa was not much enough to have an effect on such a summation. On the contrary, while RES was about 1000 micron in thickness, high amount of FITC-BSA that revealed by high intensity of florescent light in the tissue may result in obvious difference in the recovery amount of FITC-BSA in the tissues like the result from powder formulation in **Figure IV-56**. Therefore, it may be the reason for making an



explanation about loss of recovery amounts of FITC-BSA which were still on RES in donor compartment of powder formulation (Figure IV-50).

For possible permeation mechanism, polar drugs such as peptide and protein require paracellular transport for delivery via nasal route as described in literatures (67, 224). According to the all permeation results, although TEER values obtained from S-6 powder formulation were likely to lower than that obtained from solution formulation, it could not draw a definite conclusion that there was transient paracellular or tight junction opening occurring due to shrinkage of cell or cell dehydration by water absorption of powder formulation itself, like several literatures reported (46, 225). However, a study about S conducting in Caco-2 cell found that S may not have any effect on tight junction due to TEER value staying constant (226). In addition to paracellular route, transports via endocytosis and transcytosis processes were reported for peptides and proteins in respiratory epithelium (227). Zhang et al. (228) reported that mechanism of permeation through rabbit nasal epithelial of Hirudin-2, an acidic polypeptide, could be related to endocytosis and passive diffusion.

Furthermore, in Linn's dissertation (226) it was found that S with 10% concentration had a slight effect on trypsin inhibition. For S-6 formulation (S+60% w/w of PEG) containing S about 60% may have an influence on inhibition to proteolytic enzyme on nasal mucosa which probably resulted in peptide delivery enhancement.

Finally, it is possible that FITC-BSA from S-6 powder formulation might mainly be delivered through nasal mucosa via passive diffusion along the concentration gradient additional with other mechanisms and enhanced with proteolytic enzyme inhibition by S.



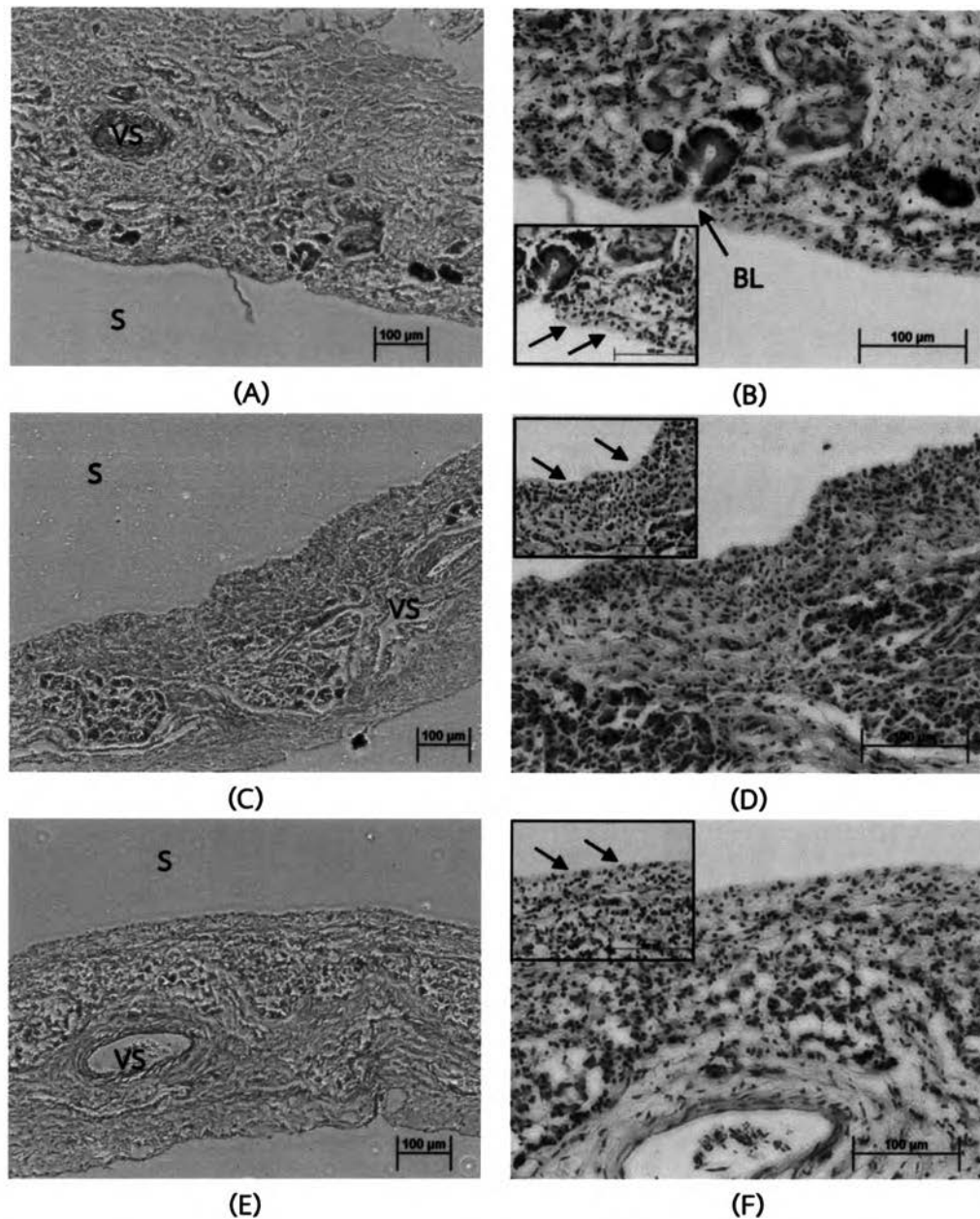


Figure IV-53 Porcine OLF after 120 minutes of *in vitro* permeation study (H&E staining) under inverse light microscope. Figure A, C, and E indicated a control group (untreated tissue), JM powder formulation, and solution formulation, respectively (magnification: x100) and figure B, D, and F indicated a control group (untreated tissue), JM powder formulation, and solution formulation, respectively (magnification: x200). Insert pictures were higher magnification (x400) of the superficial layers of epithelial layer indicated by arrows. Mucosal surface (S), vessel (VS), serous gland (G), and Bowman's gland (BL) were illustrated.

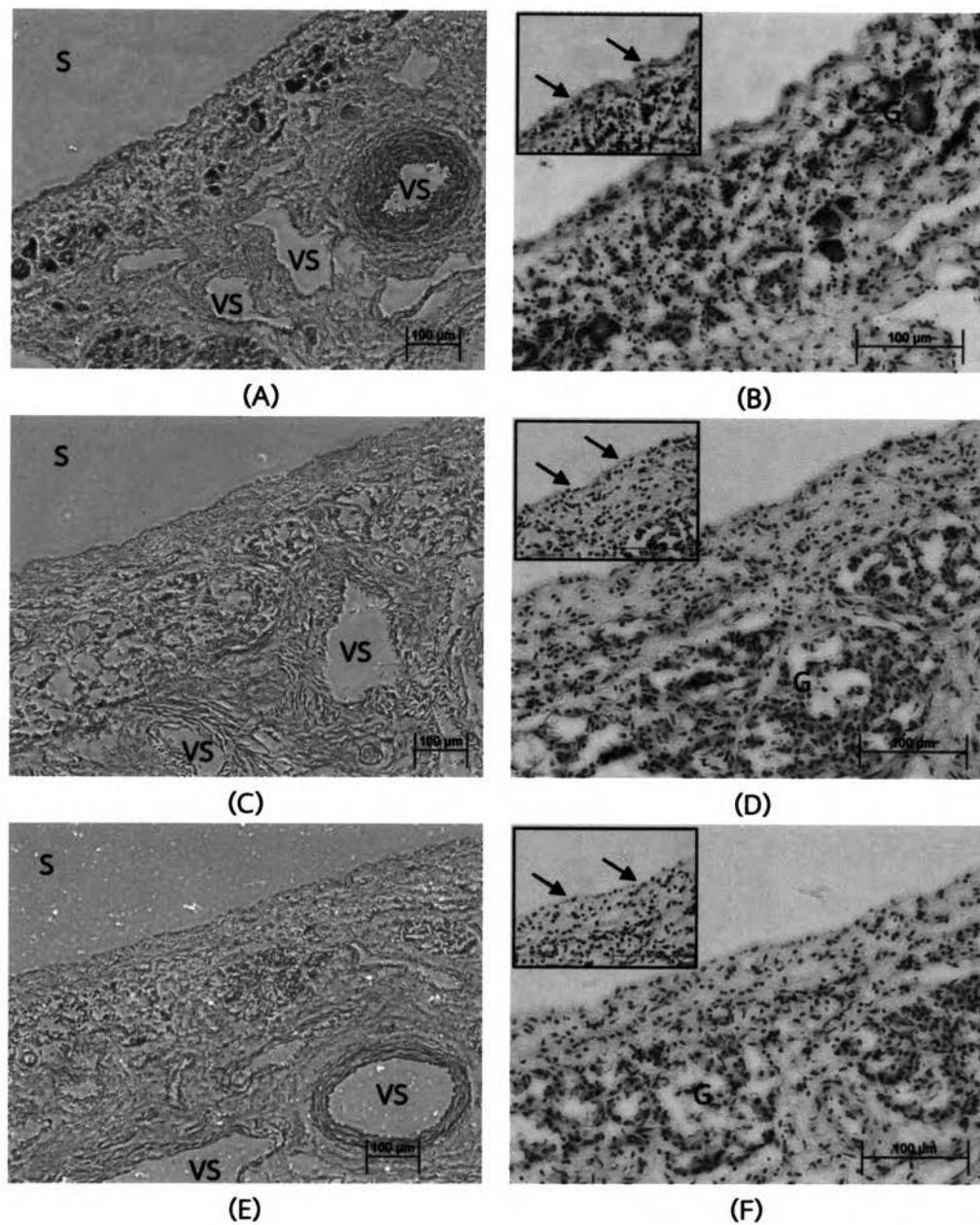


Figure IV-54 Porcine RES after 120 minutes of *in vitro* permeation study (H&E staining) under inverse light microscope. Figure A, C, and E indicated a control group (untreated tissue), JM powder formulation, and solution formulation, respectively (magnification: x100) and figure B, D, and F indicated a control group (untreated tissue), JM powder formulation, and solution formulation, respectively (magnification: x200). Insert pictures were higher magnification (x400) of the superficial layers of epithelial layer indicated by arrows. Mucosal surface (S), vessel (VS), and serous gland (G) were illustrated.

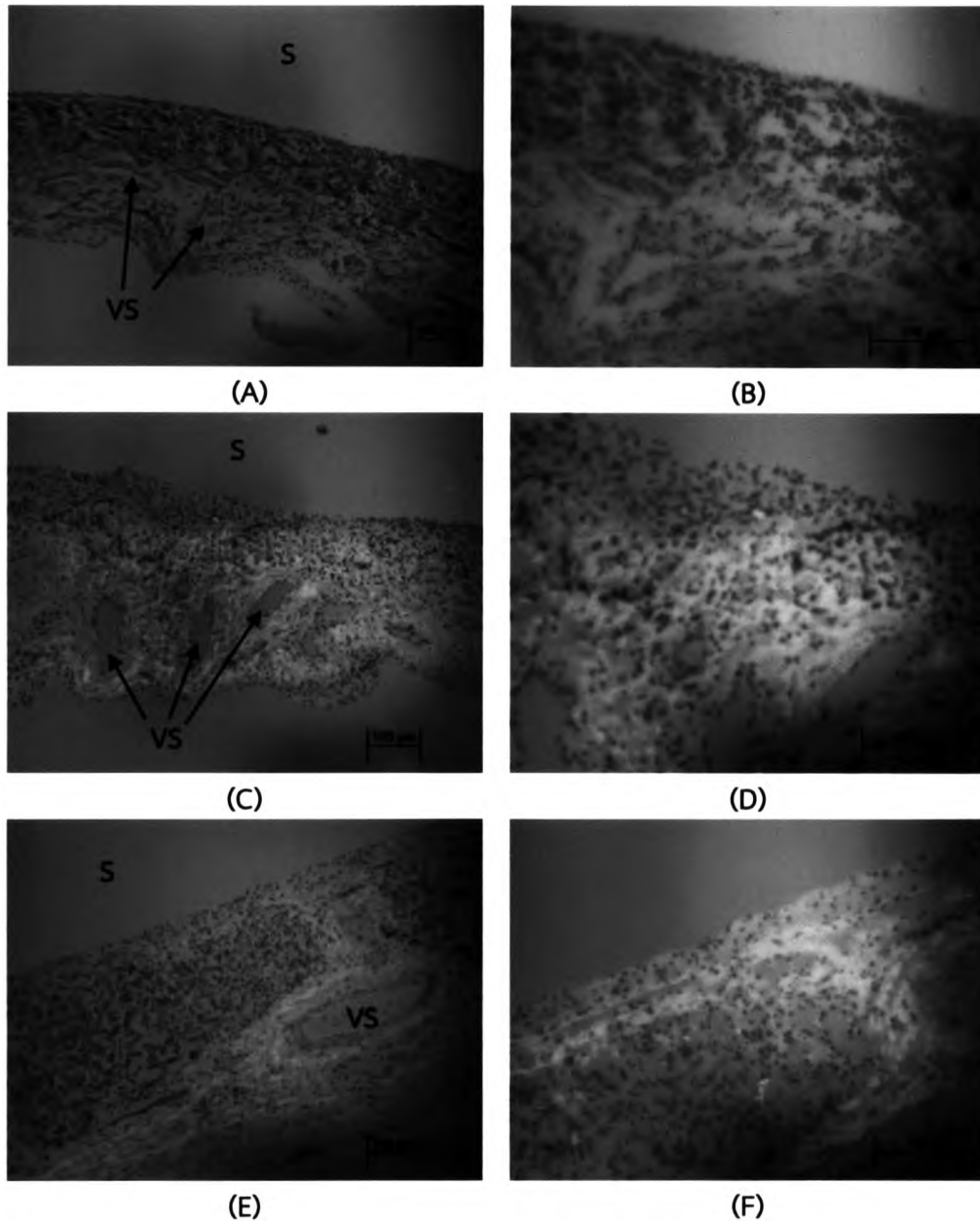


Figure IV-55 Porcine OLF after 120 minutes of *in vitro* permeation study (H&E staining) under fluorescent light microscope. Figure A, C, and E indicated a control group (untreated tissue), JM powder formulation, and solution formulation, respectively (magnification: x100) and figure B, D, and F indicated a control group (untreated tissue), JM powder formulation, and solution formulation, respectively (magnification: x200). Mucosal surface (S) and vessel (VS) were illustrated.

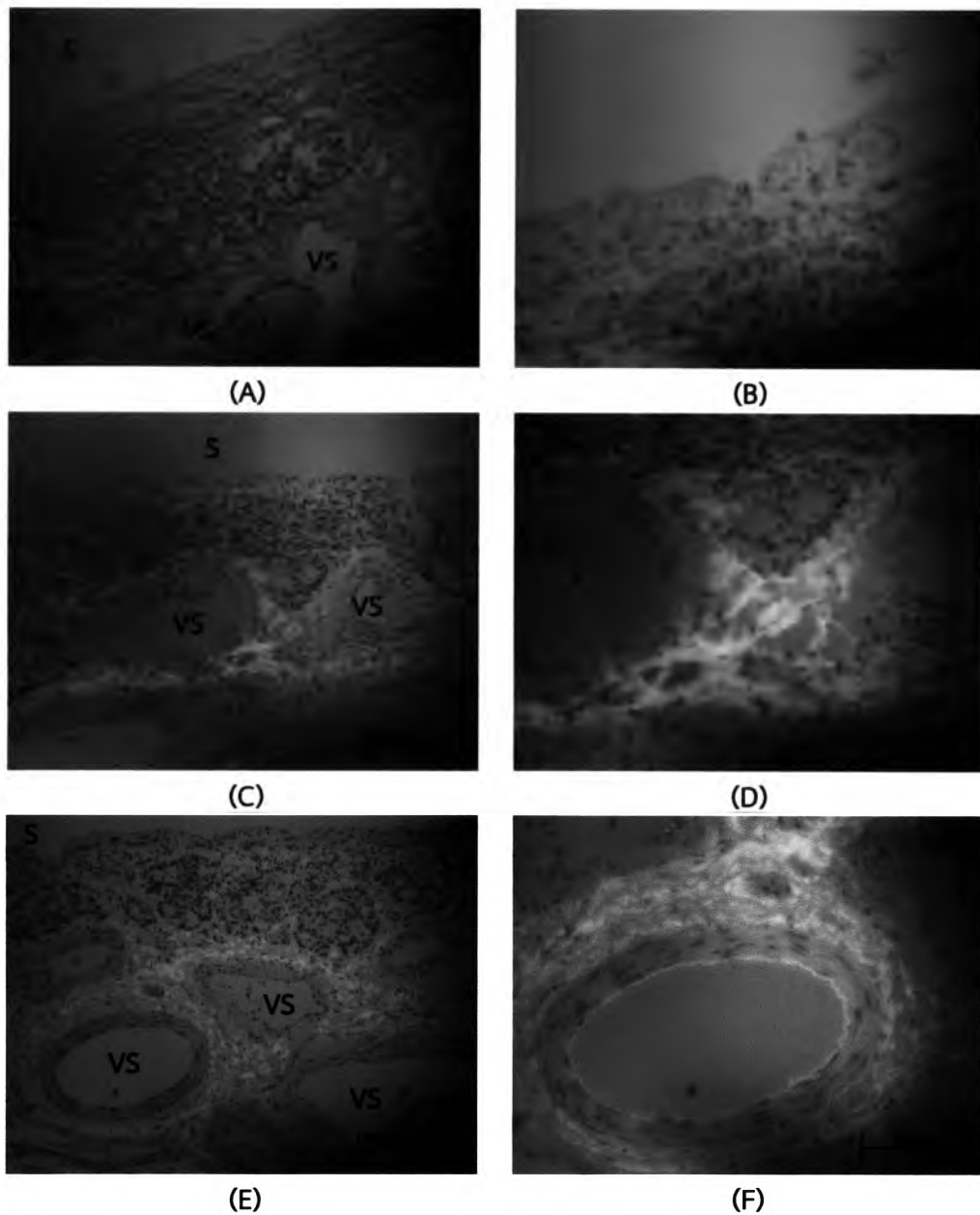


Figure IV-56 Porcine RES after 120 minutes of *in vitro* permeation study (H&E staining) under fluorescent light microscope . Figure A, C, and E indicated a control group (untreated tissue), JM powder formulation, and solution formulation, respectively (magnification: x100) and figure B, D, and F indicated a control group (untreated tissue), JM powder formulation, and solution formulation, respectively (magnification: x200). Mucosal surface (S), vessel (VS), serous gland (G) and Bowman's gland (BL) were illustrated.